JOINT INSTITUTE FOR NUCLEAR RESEARCH
INSTITUTE OF NUCLEAR PHYSICS

A manuscript
UDC 621.3.082.782

KHUSHVAKTOV JURABEK HATAMOVICH

STUDY OF SECONDARY NEUTRON INTERACTIONS WITH ^{232}Th, ^{129}I, AND ^{127}I NUCLEI AT THE URANIUM ASSEMBLY QUINTA IRRADIATED BY 2, 4, 6, AND 8 GeV DEUTERONS

01.04.08 - Physics of atomic nuclei and elementary particles, accelerator technics

DISSERTATION
on the scientific degree competition of the doctor of philosophy (PhD)
of physical and mathematical sciences

Scientific supervisor: Yuldashev Bekhzod Sadykovich
doctor of sciences in physics and mathematics,
professor, academician of the Academy of
sciences of the Republic of Uzbekistan

Tashkent – 2019

CONTENTS

INTRODUCTION

Topicality and demand of the theme of dissertation. The accelerator-driven system (ADS) is recognized as a promising system for the purpose of nuclear waste transmutation and minimization of spent fuel radiotoxicity. The main reason is related to their work in sub-critical mode, based on the use of an accelerator as an external source. The presence of an external source allows such setup to operate in the subcritical mode, thereby providing safer conditions for transmutation or burning out of long-lived fission products and minor actinides. Natural uranium and thorium can be used as fuel materials for accelerator-driven system.

For many years there has been interest in utilizing ^{232}Th as a nuclear fuel since it is three to five times as abundant in the Earth's crust as uranium. A thorium reactor can be work due to the fission of ^{233}U, which is formed as a result of neutron capture by the ^{232}Th nucleus. The problem is that at the use of natural thorium produces an insufficient neutrons to sustain the fission reaction, and therefore enriched fuel is needed (by adding plutonium or ^{235}U). The same situation with natural uranium. In the last two decades, scientific efforts at Joint Institute for Nuclear Research (Dubna) have been concentrated on investigation of an original concept of deep sub-critical accelerator-driven systems. The Relativistic Nuclear Technology (RNT) with a core made of natural uranium or thorium is intended for nuclear energy production and transmutation of spent nuclear fuel employing spallation neutron field with a substantial contribution of fast neutrons.

In our republic, much attention is paid to fundamental and applied research in the field of such priority areas of nuclear science as the introduction of nuclear technologies in science and production, safe nuclear energy and the problem of radioactive waste disposal. The directions of these fundamental research and design, which are of great importance for the development of science in our country and their practical application, are reflected in the strategy of further

development of the Republic of Uzbekistan in 2017-2021[1].

The studies conducted in this dissertation work correspond to the tasks stipulated in the Decrees of the President of the Republic of Uzbekistan DP-4947 of February 2, 2017 "The strategy of further development of the Republic of Uzbekistan in 2017-2021", DP-5484 of July 19, 2018 "On measures for the development of nuclear energy in the Republic of Uzbekistan", in the Resolutions of the President RP-3855 of July 14, 2018 "About additional measures to increase the efficiency of commercialization of the results of scientific and scientific-technical activities" and RP-3365 of November 1, 2017 "On measures to further strengthen the infrastructure of scientific-research institutions and the development of innovation", as well as other legal acts adopted in this field.

Conformity of research to priority directions of development of science and technologies of the Republic of Uzbekistan. The dissertation research was carried out in accordance with the priority areas of science and technology development of the Republic of Uzbekistan: II. "Power, energy and resource saving".

Degree of study of the problem. To date, the leading international researchers conducted a number of experimental studies in the field of accelerator-driven subcritical systems and in the field of radioactive waste transmutation. Czech (Adam J. et al.) and Russian (Pronskikh V.S., Solnyshkin A.A., Tsoupko-Sitnikov V.M.) scientists studied the interaction of secondary neutrons with the ^{129}I and ^{127}I nuclei on the massive lead target "GENERATOR" (17 kg lead) irradiated with 0.66 GeV protons. At the following work, Czech (Adam J., Katovsky K.) and Russian (Krivopustov M.I., Solnyshkin A.A., Tsoupko-Sitnikov V.M.) scientists have investigated the possibility of transmuting the radionuclide ^{129}I on a massive lead target surrounded by a uranium blanket "Energy plus transmutation" (28.7 kg lead, 206.4 kg uranium) irradiated with 0.7, 1, 1.5 and 2 GeV protons. The same group of scientists studied the interaction of secondary neutrons with ^{232}Th nuclei

[1] The Decrees of the President of the Republic of Uzbekistan DP-4947 of February 2, 2017 "The strategy of further development of the Republic of Uzbekistan"

on the “Energy plus transmutation” target irradiated with 1.6 GeV deuterons.

With a group of scientists from Czech Republic (Adam J., Katovsky K.), India (Bhatia Ch., Kumar V.), Belarus (Khilmanovich A.M., Marcinkevich B.A., Zhuk I.V., Potapenko A.S.) and Russia (Pronskikh V.S., Solnyshkin A.A., Tyutyunnikov S.I., Tsoupko-Sitnikov V.M.) were measured the rates of (n,f), (n,γ) and (n,2n) reactions in ^{232}Th on the lead-graphite target “GAMMA-3” (34 kg lead, 1230 kg graphite) irradiated with 2.33 GeV deuterons. Australian researchers (Hashemi-Nezhad R.S., Asquith N.L.) measured the rates of ^{232}Th(n,γ) and ^{232}Th(n,f) reactions on the target “GAMMA-3” irradiated with 1.6 GeV deuterons.

Beginning in 2011, experiments with the 512 kg subcritical natural uranium assembly QUINTA were conducted for the first time. It was found that upon irradiation of above targets, the energy spectrum and the flux of generated neutrons substantially differ from the subcritical assembly QUINTA and in the above experiments have not been determined the fast neutron fluences using the threshold ^{127}I(n,xn) reactions.

Connection of dissertational research with the plans of scientific-research works. The dissertational work was carried out within the framework of problem-thematic plans and international cooperation of the Joint Institute for Nuclear Research on the topic 02-1-1107-2011/2019 “Development and creation of the prototype of a complex for radiotherapy and applied researches on beams of heavy ion on the Nuclotron-M” and the research project of the Institute of Nuclear Physics ASRU on the theme of FA-Atech-2018-166 “Development of the fundamentals of a subcritical reactor based on the NG-150 neutron generator of INP”.

The aim of the research is the determination of reaction rate for residual nuclei in the interaction of secondary neutrons with ^{232}Th, ^{129}I, and ^{127}I nuclei on the natural uranium assembly QUINTA irradiated with 2, 4, 6, and 8 GeV deuteron beams of Nuclotron accelerator.

The tasks of the research:

to describe both past and state-of-the-art research projects on accelerator-

driven systems;

to take part in preparation and realization of an experiment with a spallation target and the beam of deuterons with an energies 2, 4, 6 and 8 GeV;

to carry out measurements of irradiated samples employing methods of gamma-ray spectrometry with HPGe detectors;

to analyze the acquired spectra, determine of reaction rate for the identified radionuclides;

to learn and perform Monte Carlo simulations using FLUKA and Geant4 codes for determine the fluence of secondary particles, the number of fission reactions, and the number of produced isotopes in the spallation target, and in the measuring samples;

to determine the fluence of neutrons using the threshold (n,xn) reactions in the ^{127}I samples;

to experimentally assess the possibility of transmutation of the long lived radionuclide ^{129}I;

to compare the experimental results with the results of Monte Carlo simulations.

The objects of the research are the natural uranium assembly QUINTA, thorium and iodine samples.

The subjects of the research are interactions of relativistic deuterons with ^{238}U nuclei and neutrons with ^{232}Th, ^{129}I and ^{127}I nuclei.

The methods of the research. Neutron-activation method of analysis, gamma-ray spectrometry, Monte Carlo simulations.

The scientific novelty of the research is the follows:

a method to determine of neutron fluences using the threshold ^{127}I(n,xn) reactions was developed;

for the first time, the fluences of neutrons with energies from 10 to 120 MeV were determined using the threshold (n,xn) reactions in the ^{127}I samples;

at the results of Monte Carlo simulations are taken detailed information about the number of fission reactions in the each 298 natural uranium cylinders of

QUINTA setup;

the ratio of the mass of the produced ^{130}I to the mass of ^{129}I was determined, in order to experimentally assess the possibility of transmutation by means of the ^{129}I(n,γ) reaction in the QUINTA setup.

Practical results of the research are as follows:

for the first time, experimental studies have been carried out on the irradiation of deep subcritical assembly QUINTA by deuteron beams with energies of 2, 4, 6, and 8 GeV. The subcritical assembly QUINTA consists of 298 cylinders of natural uranium;

the spectra of gamma rays emitted by the activated ^{232}Th, ^{129}I, and ^{127}I samples have been analyzed. For each of identified residual nuclei, reaction rates have been determined;

obtained experimental results for ^{232}Th samples were compared with the results of simulations. On comparisons were found of good agreements for residual nuclei ^{233}Pa, ^{231}Th and for several products of fission reactions such as ^{87}Kr, ^{88}Kr, ^{91}Sr, ^{92}Sr, ^{92}Y, ^{93}Y, ^{97}Zr, ^{99}Mo, ^{103}Ru, ^{105}Ru, ^{105}Rh, ^{115}Cd, ^{128}Sb, ^{132}Te, ^{131}I, ^{132}I, ^{133}I, ^{135}I, ^{135}Xe, ^{140}Ba, ^{142}La, ^{143}Ce.

Reliability of the research results is justified by the high experimental level of performance, using reliable methods to measurement and processing experimental data, using modern codes to Monte Carlo simulation, such as FLUKA, MCNPX-2.7, MARS-15 and Geant4, good agreement between the simulation results and obtained experimental data.

Scientific and practical significance of the research results. The scientific significance of the research results is determined by the ability of method to determine the fluence of neutrons using ^{127}I(n,xn) threshold reactions to use to determine the fluence of fast neutrons in the future accelerator driven systems and fast reactors.

The practical significance of the results of research lies in the fact that the results of experimentally assess the possibility of transmutation of long lived radionuclide ^{129}I and yield of residual nuclei ^{233}Pa, ^{231}Th and of several products of

fission reactions such as ^{87}Kr, ^{88}Kr, ^{91}Sr, ^{92}Sr, ^{92}Y, ^{93}Y, ^{97}Zr, ^{99}Mo, ^{103}Ru, ^{105}Ru, ^{105}Rh, ^{115}Cd, ^{128}Sb, ^{132}Te, ^{131}I, ^{132}I, ^{133}I, ^{135}I, ^{135}Xe, ^{140}Ba, ^{142}La, ^{143}Ce can be used in the design of industrial accelerator driven systems for the transmutation of radioactive waste.

Application of the research results. Based on the results of studing of secondary neutron interactions with ^{232}Th, ^{129}I, and ^{127}I nuclei at the uranium assembly QUINTA irradiated by 2, 4, 6, and 8 GeV deuterons:

developed method to determine fluence of neutrons using ^{127}I(n,xn) threshold reactions, has been used in the experiments of international collaboration Energy and Transmutation of Radioactive Waste, wich were held at the Joint Institute for Nuclear Research (Dubna, Russia) in 2012-2015 (letter from the Laboratory of High Energy Physics of JINR No. 100-26/83 dated March 5, 2019). Using this method allowed to determine of neutron fluences with energies from 10 to 120 MeV and to benchmark the results of Monte Carlo simulations;

measured rate of ^{129}I(n,γ)^{130}I reaction in the QUINTA setup allowed to preliminary assess the possibility of transmutation of the long lived radionuclide ^{129}I for experiments on irradiating a massive lead target with 660 MeV protons, which were carried out at the Phasotron JINR.

Approbation of the work. The research results were reported in the form of reports and tested at 7 international scientific conferences, in particular: XVII Conference of Young Scientists and Specialists (AYSS'13) (Dubna, 2013), XIX International Scientific Conference of Young Scientists and Specialists (AYSS-2015) (Dubna, 2015), IV Annual Conference of Young Scientists and Specialists "Neutron and Neutrinos: Fundamental Properties, Experiments and Applied Research" (Alushta, 2015), 22nd International Seminar on Interaction of Neutrons with Nuclei (ISINN-22): "Fundamental Interactions & Neutrons, Nuclear Structure, Ultracold Neutrons, Related Topics" (Dubna, 2014), ISINN-23 (Dubna, 2015), ISINN-24 (Dubna, 2016), ISINN-25 (Dubna, 2017).

The main results of the study were tested at the scientific seminars of the Institute of Nuclear Physics (2015-2017), Joint Institute for Nuclear Research

(Dubna, 2012-2017).

Publication of results. On the dissertation theme there were published 12 scientific works, including 5 scientific papers in international scientific journals recommended by the Supreme Attestation Commission of the Republic of Uzbekistan for publishing basic scientific results of dissertation theses.

Structure and volume of dissertation. The dissertation consists of an introduction, four chapters, conclusion, two appendixes and a bibliography. The size of the dissertation is 108 pages.

Acknowledgements

I would like to express my gratitude to the Dr. Adam J., Prof. Tsoupko-Sitnikov V.M., Dr. Solnyshkin A.A. and Academician Yuldashev B.S. for their helps and valuable advices in carrying out dissertation work. I also thank Prof. Brudanin V.B. and Prof. Tyutyunnikov S.I. for their support and to other colleagues and members of the “Energy and Transmutation of Radioactive Waste” collaboration.

List of published papers [1-12]:

1. Balabekyan A.R., Demekhina N.A., Karapetyan G.S., Drnoyan D.R., Zhemenik V.I., Adam J., Zavorka L., Solnyshkin A.A., Tsoupko-Sitnikov V.M., Khushvaktov J., Karayan L., Guimarães V., Deppman A., Garcia F. Target residues formed in the 4.4 GeV deuteron-induced reaction on gold //Physical Review C. - American Physical Society (USA), 2014. - vol. 90. - id. 054612 (№3, Scopus, IF=3.30)
2. Adam J., Baldin A.A., Chilap V., Furman W., Katovsky K., Khushvaktov J., Kumar V., Pronskikh V., Mar’in I., Solnyshkin A., Suchopar M., Tsupko-Sitnikov V., Tyutyunnikov S., Vrzalova J., Wagner V., Zavorka L. Measurement of the high energy neutron flux on the surface of the natural uranium target assembly QUINTA irradiated by deuterons of 4 and 8 GeV energy //Physics Procedia.- Elsevier, 2015. - vol.80. - pp. 94-97 (№3, Scopus, IF=0.64)
3. Khushvaktov J., Adam J., Baldin A.A., Chilap V.V., Furman V.I., Sagimbaeva F., Solnyshkin A.A., Stegailov V.I., Tichy P., Tsoupko-Sitnikov V.M., Tyutyunnikov

S.I., Vespalec R., Vrzalova J., Yuldashev B.S., Wagner V., Zavorka L., Zeman M. Interactions of secondary particles with thorium samples in the setup QUINTA irradiated with 6 GeV deuterons //Nuclear Instruments and Methods in Physics Research B. - Elsevier, 2016. - vol.381. - pp. 84-89 (№3, Scopus, IF=1.32)

4. Adam J., Chilap V.V., Furman V.I., Kadykov M.G., Khushvaktov J., Pronskikh V.S., Solnyshkin A.A., Stegailov V.I., Suchopar M., Tsoupko-Sitnikov V.M., Tyutyunnikov S.I., Vrzalova J., Wagner V., Zavorka L. Study of secondary neutron interactions with ^{232}Th, ^{129}I, and ^{127}I nuclei with the uranium assembly "QUINTA" at 2, 4, and 8 GeV deuteron beams of the JINR Nuclotron accelerator //Applied Radiation and Isotopes. - Elsevier, 2016. - vol.107. - pp. 225-233 (№3, Scopus, IF=1.12)
5. Khushvaktov J.H., Adam J., Baldin A.A., Furman W.I., Gustov S.A., Kish Yu.V., Solnyshkin A.A., Stegailov V.I., Svoboda J., Tichy P., Tsoupko-Sitnikov V.M., Tyutyunnikov S.I., Vespalec R., Vrzalova J., Wagner V., Yuldashev B.S., Zavorka L., Zeman M. Monte Carlo simulations and experimental results on neutron production in the uranium spallation target QUINTA irradiated with 660 MeV protons //Applied Radiation and Isotopes. - Elsevier, 2018. - vol.137. - pp. 102-107 (№3, Scopus, IF=1.12)
6. Адам И., Врзалова И., Гайсак И., Заворка Л., Киш Ю., Корнеев С.В., Максим М., Марцынкевич Б.А., Мухаммедов С., Солнышкин А.А., Стегайлов В.И., Хильманович А.М., Хушвактов Ж.Х., Цупко-Ситников В.М. Восстановление спектра вторичных нейтронов на свинцовой мишени при облучении её протонами 660 МэВ //XVII молодежная научная конференция Объединения молодых ученых и специалистов (ОМУС). - Дубна (Россия), 2013.- С. 149-154
7. Adam J., Chilap V.V., Furman V.I., Khushvaktov J., Pronskikh V.S., Solnyshkin A.A., Stegailov V.I., Suchopar M., Tsoupko-Sitnikov V.M., Tyutyunnikov S.I., Vrzalova J., Wagner V., Zavorka L. Study of secondary neutron interactions with nuclei ^{232}Th, ^{129}I, ^{127}I on the uranium assembly "QUINTA" Nuclotron JINR on deuterons beam with energy 2, 4, 8 GeV //22nd International Seminar on

Interaction of Neutrons with Nuclei (ISINN-22): "Fundamental Interactions & Neutrons, Nuclear Structure, Ultracold Neutrons, Related Topics". - Dubna (Russia), 2014. - pp. 22

8. Adam J., Chilap V.V., Furman V.I., Khushvaktov J., Kish Yu., Pronskikh V.S., Solnyshkin A.A., Stegailov V.I., Suchopar M., Tsoupko-Sitnikov V.M., Tyutyunnikov S.I., Vespalec R., Vrzalova J., Wagner V., Yuldashev B.S., Zavorka L., Zeman M. Study of secondary neutron interactions with ^{232}Th, ^{129}I, and ^{127}I nuclei with the uranium assembly “QUINTA” at 2, 4, and 8 GeV deuteron beams of the JINR Nuclotron accelerator //23rd International Seminar on Interaction of Neutrons with Nuclei (ISINN-23): "Fundamental Interactions & Neutrons, Nuclear Structure, Ultracold Neutrons, Related Topics". - Dubna (Russia), 2015. - pp. 19
9. Adam J., Chilap V.V., Furman V.I., Khushvaktov J., Kish Yu., Pronskikh V.S., Solnyshkin A.A., Stegailov V.I., Suchopar M., Tsoupko-Sitnikov V.M., Tyutyunnikov S.I., Vespalec R., Vrzalova J., Wagner V., Yuldashev B.S., Zavorka L., Zeman M. Study of secondary neutron interactions with ^{232}Th, ^{129}I, and ^{127}I nuclei with the uranium assembly “QUINTA” at 2, 4, and 8 GeV deuteron beams of the JINR Nuclotron accelerator //The XIX International Scientific Conference of Young Scientists and Specialists (AYSS-2015). - Dubna (Russia), 2015. - pp. 23
10. Adam J., Chilap V.V., Furman V.I., Khushvaktov J., Kish Yu., Pronskikh V.S., Solnyshkin A.A., Stegailov V.I., Suchopar M., Tsoupko-Sitnikov V.M., Tyutyunnikov S.I., Vespalec R., Vrzalova J., Wagner V., Yuldashev B.S., Zavorka L., Zeman M. Study of secondary neutron interactions with ^{232}Th, ^{129}I, and ^{127}I nuclei with the uranium assembly “QUINTA” at 2, 4, and 8 GeV deuteron beams of the JINR Nuclotron accelerator //IV Annual Conference of Young Scientists and Specialists "Neutron and Neutrinos: Fundamental Properties, Experiments and Applied Research" (Alushta, 2015). - Alushta (Russia), 2015.- pp. 25
11. Khushvaktov J., Adam J., Baldin A.A., Chilap V.V., Furman V.I., Khabipov N., Sagimbaeva F., Solnyshkin A.A., Stegailov V.I., Tichy P., Tsoupko-Sitnikov V.M., Tyutyunnikov S.I., Vespalec R., Vrzalova J., Yuldashev B.S., Wagner V., Zavorka L., Zeman M. Interaction of secondary particles with the thorium samples

in the QUINTA setup irradiated with 6 GeV deuterons //24th International Seminar on Interaction of Neutrons with Nuclei (ISINN-24): "Fundamental Interactions & Neutrons, Nuclear Structure, Ultracold Neutrons, Related Topics". - Dubna (Russia), 2016. - pp. 57

12. Khushvaktov J.H., Adam J., Baldin A.A., Furman W.I., Gustov S.A., Kish Yu.V., Solnyshkin A.A., Stegailov V.I., Svoboda J., Tichy P., Tsoupko-Sitnikov V.M., Tyutyunnikov S.I., Vespalec R., Vrzalova J., Wagner V., Yuldashev B.S., Zavorka L., Zeman M. Monte Carlo simulations and experimental results on neutron production in the spallation target QUINTA irradiated with 660 MeV protons //25th International Seminar on Interaction of Neutrons with Nuclei (ISINN-25): "Fundamental Interactions & Neutrons, Nuclear Structure, Ultracold Neutrons, Related Topics". - Dubna (Russia), 2017. - pp. 65

CHAPTER I. ACCELERATOR-DRIVEN SYSTEMS

§ 1.1. Introduction

§ 1.1.1. General principles

An important feature of the fission reaction is that it generates neutrons that can cause further fission. If the fission reaction repeats itself the process that occurs is called a "chain reaction". The fission chain-reaction is general to all nuclear reactors. If the neutrons from one fission cause on the average one more fission a "self-sustained chain reaction" is accomplished and the reactor is called "critical". The neutrons in the first fission are belong to the first generation and the neutrons from the second fission which they caused belong to the next generation and so on. The effective multiplication factor, k_{eff}, gives the ratio of the number of neutrons of one generation to the previous generation (taking all losses into account):

$$k_{eff} = \frac{\text{number of neutrons in one generation}}{\text{number of neutrons in the previous generation}}$$

It is obvious that a self-sustained reactor will continue to operate at a constant fission rate as long as the effective multiplication factor remains equal to unity. If k_{eff} is smaller than one, there are produced fewer neutrons in each generation than in the previous generation and the reactor is called subcritical. Without any support from an outside source of neutrons the chain-reaction will eventually extinguish. In contrast, if k_{eff} is greater than 1, the neutron population will increase with or without the presence of an external source, and the reactor is supercritical. It should be understood that the value of k_{eff} depends only on the properties of the reactor core (size, shape, material composition, and temperature) not on the characteristics of the external source. The material composition consists of a mixture of nuclear fuel, coolant, structural, and control material. To establish a self-sustained chain-reaction the material must be arranged in a suitable

configuration of sufficient size and right shape.

§ 1.1.2. Source multiplication in a subcritical reactor

In operator formulation, the steady-state Boltzmann neutron balance equation for a subcritical reactor including a neutron source reads [8; p.34]:

$$(M - F) \cdot \Phi_s(r, E, \Omega) = S(r, E, \Omega) \tag{1.1}$$

Where F is the fission operator, M is the migration and loss operator, $\Phi_s(r, E, \Omega)$ is the angle-dependent inhomogeneous neutron flux, and $S(r, E, \Omega)$ is the independent neutron source. From the above neutron balance formulation, it is seen that in a subcritical reactor, fewer neutrons are produced through fission $F \cdot \Phi_s(r, E, \Omega)$ than lost $M \cdot \Phi_s(r, E, \Omega)$, and the difference is compensated by neutrons from the outside source, $S(r, E, \Omega)$. The fundamental mode flux is defined as:

$$\left(M - \frac{1}{k_{eff}} \cdot F\right) \cdot \Phi_s(r, E, \Omega) = 0 \tag{1.1a}$$

The subcritical multiplication factor, k_s, is defined as the ratio of the fission neutrons to the total neutron source as:

$$k_s = \frac{\langle F \cdot \Phi_s(r,E,\Omega) \rangle}{\langle M \cdot \Phi_s(r,E,\Omega) \rangle + \langle S(r,E,\Omega) \rangle} \tag{1.2}$$

where < > denotes phase-space integration. Unlike the effective multiplication factor, k_{eff}, which is a characteristic of the core, the subcritical multiplication factor depends on the characteristics of the external source neutrons (spatial position, energy, angular distribution). It is a local multiplication factor in that sense that it describes the multiplication of source neutrons from the point of where they are

inserted. Using the inhomogeneous flux in Eq. (1.1), the fission neutrons per external source neutron can be related according to:

$$\frac{1}{k_s} = \frac{\langle M \cdot \Phi_s(r,E,\Omega)\rangle + \langle S(r,E,\Omega)\rangle}{\langle F \cdot \Phi_s(r,E,\Omega)\rangle} = 1 + \frac{\langle S(r,E,\Omega)\rangle}{\langle F \cdot \Phi_s(r,E,\Omega)\rangle},$$

$$\frac{1}{k_s} - 1 = \frac{\langle S(r,E,\Omega)\rangle}{\langle F \cdot \Phi_s(r,E,\Omega)\rangle},$$

$$\frac{\langle F \cdot \Phi_s(r,E,\Omega)\rangle}{\langle S(r,E,\Omega)\rangle} = \frac{1}{1/k_s - 1} \tag{1.3}$$

The fission power of the inhomogeneous system can be represented as

$$P_{fission} = E_f \langle \Sigma_f \cdot \Phi_s(r,E,\Omega)\rangle \tag{1.4}$$

Where E_f is the energy recovered per fission. If we now combine Eq. (1.3) and (1.4), the fission power can be written as:

$$\mathrm{P}_{fission} = \frac{E_f}{\bar{\nu}} \frac{k_s}{1-k_s} \langle S(r,E,\Omega)\rangle \tag{1.4}$$

Where the average number of neutrons per fission is defined as

$$\bar{\nu} = \frac{\langle F \cdot \Phi_s(r,E,\Omega)\rangle}{\langle \Sigma_f \cdot \Phi_s(r,E,\Omega)\rangle} \tag{1.5}$$

§ 1.1.3. External neutron source intensity

Conventional power reactors generally do not require external neutron sources for normal operation. These reactors are based on the self-multiplication of neutrons in a critical state. In a critical reactor, the fission reactions alone are able to maintain a steady-state. In contrast, the accelerator-driven system (ADS) is a subcritical reactor driven by an external neutron source. The external source is

maintained by a spallation neutron target driven by a high power proton accelerator thereby the leading adjective “accelerator-driven”. Taken by itself, critical or near-critical reactor operation would seem like the optimum solution, since it eliminates the need for an external source. But safety and controllability are the main issues for the ADS. The main purpose is to minimize the risk for uncontrolled reactivity excursions. Among the advantages of subcritical operation is the stable nature of operation, increased reserve for prompt criticality, and reduced influence of reactivity feedbacks.

Spallation is a nuclear reaction that may occur when a high energy particle strikes a heavy element, in which the nucleons struck by the incoming particle may collide with other nucleons inside the nucleus causing an “intra-nuclear cascade”. In the process, the incoming particle may “spall” the target nucleus, breaking it into smaller pieces, releasing protons, neutrons and other nuclear fragments. The incoming particle may be a proton, and the target material may, for example, be tungsten, lead or lead-bismuth. High-energy secondary particles (neutron, protons, or pions) may be knocked out in the initial collision. The remaining nucleus is left in an excited state. In the de-excitation process (evaporation stage) the nucleus may emit additional nucleons or it may fission. Most of the particles emitted in the de-excitation process are neutrons which are emitted isotropically. The neutron yield depends on the energy of the incident proton for Lead Bismuth Eutectic (LBE) spallation target, as shown in Fig.1.1. The yield increases almost linearly in the range 1-3 GeV [8; p.35].

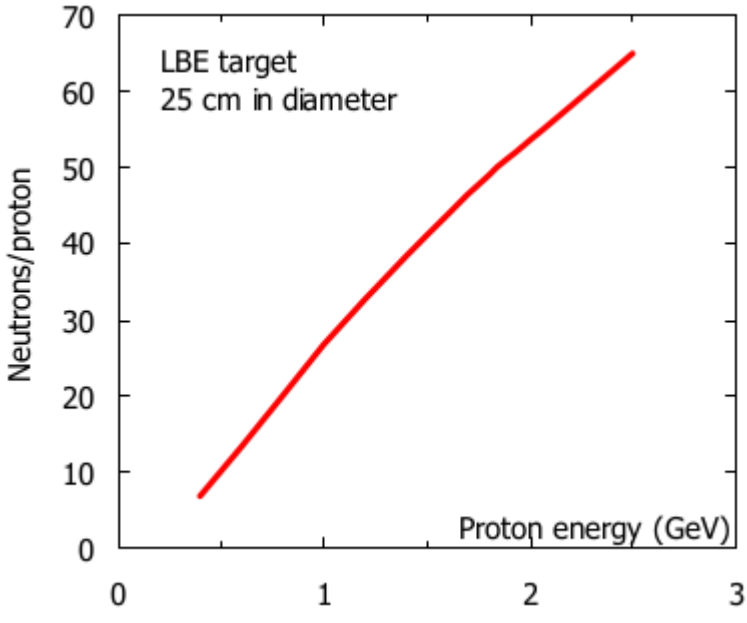

Fig.1.1. Spallation neutron yield as function of incident proton energy.

In order to produce a spallation neutron source of sufficient intensity, the accelerator must be capable of delivering energetic protons at high current. However, the total power of the system depends both on the intensity of the source and on the multiplication factor. Increasing the power of the system requires either reduced subcriticality or high intensity source. To reduce the cost of the source it may seem desirable to increase the multiplication factor. This will, on the other hand, reduce reactivity safety reserves. The degree of criticality offset is a fundamental design parameter of the ADS systems. The choice of multiplication factor involves a trade-off between various design goals such as reactor safety, core characteristics, and desired power rating, and at the same time remain consistent with current accelerator performance and cost goals. For typical industrial ADS designs, it is envisioned that the thermal power would be of the order of 500 MW to 1500 MW and employ k_{eff} values in the range 0.95-0.98 [8; p.35]. If consider a subcritical reactor operating at steady-state at 800 MW with a k_{eff} =0.95. The required source intensity to maintain a fission power of 800 MW is given by the source multiplication formula (1.4):

$$S = \frac{800 \cdot 10^6[\mathrm{W}] \cdot 2.5 \left[\frac{\text{neutron}}{\text{fission}}\right]}{0.35 \cdot 10^{-10} \left[\mathrm{W} \cdot \frac{\mathrm{s}}{\text{fission}}\right]} \left(\frac{1 - 0.95}{0.95}\right) \approx 3 \cdot 10^{18} \text{ neutrons released per second}$$

Whether an accelerator can produce a spallation neutron source of this intensity, the required source intensity seems tremendous, considering that the neutron production rate in ^{252}Cf is $2.3 \cdot 10^{12}$ neutrons/sec·g. As we saw in Fig.1.1, the spallation neutron yield depends on the incoming proton energy and the yield curve increases almost linearly in the range 1-3 GeV. However, most studies

suggest optimum proton energy for an industrial ADS plant, somewhere in the range 0.8-1 GeV, in terms of cost and system efficiency. At 1 GeV each proton will on the average produce 25 neutrons, according to Fig.1.1. Thus, the required proton intensity will be approximately $1.2 \cdot 10^{17}$ protons/sec, which equals a beam current of about 20 mA ($1.2 \cdot 10^{17}$ protons/sec*$1.6 \cdot 10^{-19}$ C/proton) or expressed in different units, 20 MW of beam power ($1 \cdot 10^{9}$*$1.6 \cdot 10^{-19}$ J/proton*$1.2 \cdot 10^{17}$ protons/sec). Although a beam power of 20 MW is an ambitious goal (such powerful accelerators do not exist today), it is not without reach with existing accelerator technology. Recent advances in accelerator technology have confirmed that a linear accelerator capable of delivering up to 100 MW power at 1 GeV energy is a relatively direct extension of existing technology. Well-supported designs for this class of accelerator were completed at Los Alamos National Lab [1; p.6] and high power proton accelerators can be built and they can be used to produce neutron sources of very high intensities, sufficient to drive an industrial sized ADS. The beam power required will be in the range 10-30 MW.

§ 1.2. Transmutation of radioactive waste

§ 1.2.1. Physics of transmutation

The term “transmutation” is used in reference to nuclear transformation processes in which one nuclide is converted into another. Transmutation of atomic nuclei can be artificially induced by collisions with neutrons, protons, alpha particles, and gamma quantum, or by natural disintegration processes such as α- and β-decay, and spontaneous fission decay resulting in changes in the nuclear composition. In all cases, transmutation involves a change in the structure of the atomic nuclei, i.e., change to the number of protons and/or neutrons, and is accompanied with a change to its properties.

Partitioning and transmutation is the general term for methods related to the conversion process of long-lived radiotoxic isotopes into shorter-lived nuclides. Partitioning refers to chemical operations used to separation and extraction of

selected elements from the spent nuclear fuel. It is closely related to the traditional methods of reprocessing spent fuel, but includes additional separation operations to extract the minor actinides and the fission products. Partitioning is a necessary operation for preparation of the spent nuclear fuel to realize further transmutation steps.

The goal of partitioning and transmutation is to achieve a hundredfold reduction of the radiotoxicity beyond a few hundreds of years, which would significantly reduce the requirements for the performance of underground storage. Most likely, an underground storage can provide a retention for at least 1000 years, during which the most radiotoxic fission products have decayed. The conditions of a hundredfold reduction require the control of both plutonium and minor actinides. In addition a few long-lived fission products as ^{99}Tc and ^{129}I are being considered for transmutation.

§ 1.2.2. Transmutation of minor actinides

The minor actinides, which are considered for transmutation are americium, curium, and neptunium. Americium is responsible for the second highest contribution to the radiotoxicity in the spent fuel, after plutonium. It dominates the radiotoxicity during the first 2000 years after discharge and it is produced in large quantities during multi recycling of plutonium [8; p.28]. Different types of reactors can be considered for transmutation of minor actinides, such as light-water reactors, fast reactors, and dedicated critical or subcritical reactors (accelerator driven systems), either in homogeneous or heterogeneous mode. In a homogeneous mode, the minor actinides are diluted at a low concentration in a standard fuel material. In a heterogeneous mode, the minor actinides are separated from conventional fuel and concentrated in special fuel elements known as “targets”.

However, the transmutation of americium targets by thermal neutrons leads to the production of ^{242}Cm and ^{244}Cm due to neutron capture in ^{241}Am and ^{243}Am, see Fig.1.2. Since ^{242}Cm decays rapidly ($T_{1/2}$=162 days) into ^{238}Pu, the proportion of

^{238}Pu and ^{244}Cm increases during consecutive recycles. Reprocessing and recycling of fuels containing high amounts of ^{238}Pu and ^{244}Cm is problematic due to their strong alpha activity and neutron emission intensity.

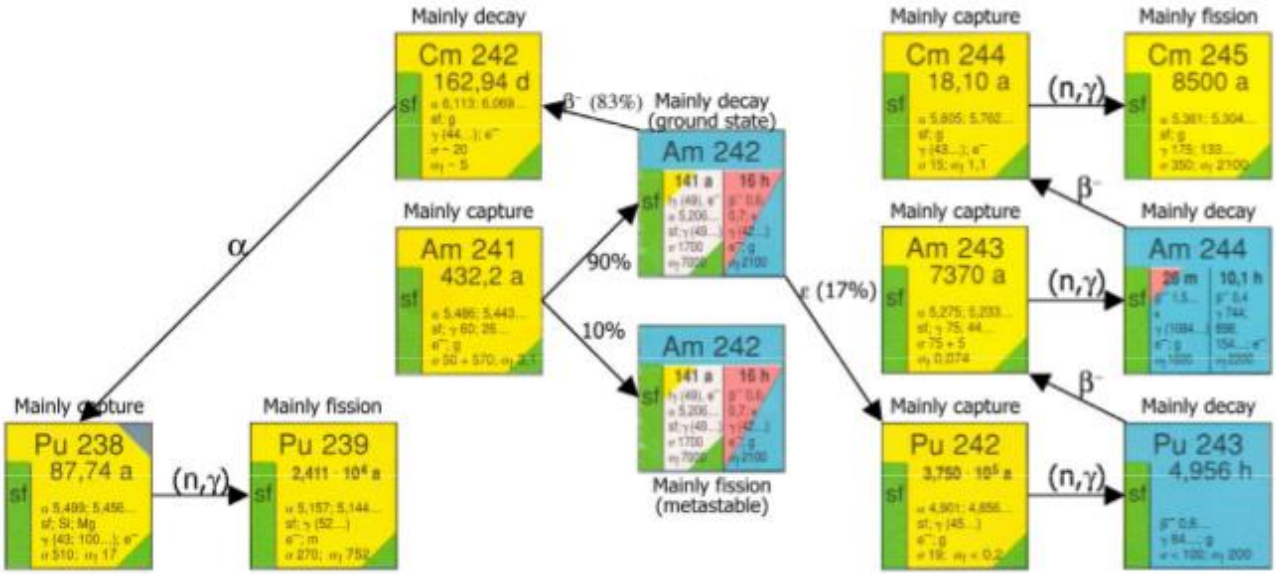

Fig.1.2. Reaction path of ^{241}Am and ^{243}Am under thermal neutron irradiation. Of importance is the production of ^{238}Pu and ^{244}Cm which increases the radioactivity and decay heat of the fuel. The alpha-decay of ^{242}Cm is a source for helium production and swelling of the fuel during irradiation. (Reaction path data from [2; p.156-162]).

To overcome the safety problems associated with highly enriched minor actinide cores, accelerator-driven systems with a fast neutrons have been proposed. Since these systems will operate in a sub-critical mode they can more easily eliminate the adverse safety characteristics of fuels based on minor actinides. While a critical system requires a significant fraction of the fertile materials in the fuel to provide acceptable core safety characteristics, accelerator-driven systems provide more flexibility in fuel composition. In an extreme case, accelerator-driven systems may allow the use of fuel with a pure minor actinide mixed with some plutonium.

§ 1.2.3. Transmutation of fission products

The fission products are small contributors to the radiotoxicity contained in the spent fuel, being several orders of magnitude lower than the transuranic elements after a few hundreds of years. Thus, in terms of reducing radiotoxicity, transmuting of fission products seems to be uninteresting. However, some fission products are mobile in groundwater and therefore can significantly affect the dose rate on the surface under certain leakage conditions from the storage, i.e. scenarios for the release of groundwater. The fission products that are relevant in this respect are primarily ^{99}Tc, ^{129}I, ^{135}Cs, ^{79}Se, and possibly ^{126}Sn, depending on the type of storage. It is theoretically possible to transmute fission products into shorter-lived or stable nuclides by capturing neutrons. But, taking into account the small neutron capture cross-section for many of the long-lived fission products, it takes quite a long time to irradiate. Transmutation of fission products is reasonable only if the neutron capture cross section of the target isotope is sufficiently high to allow transmutation rates [3; p.263-269]. This immediately eliminates ^{90}Sr and ^{137}Cs for potential transmutation purposes due to their short half-life ($T_{1/2}$ ~30 years). ^{135}Cs is long-lived ($T_{1/2}$ ~$2.3 \cdot 10^6$ years) and has moderate capture cross section of thermal neutrons, but Cs occurs in many isotopic forms in the radioactive wastes and would require isotopic separation to isolate ^{135}Cs in order to prevent the capture of neutrons in ^{133}Cs and ^{134}Cs [4; p.100]. The isotopes that have received the highest transmutation priorities, considering both their practical ability to transmute and in terms of their potential impact on the long-term radiological risk, are ^{99}Tc ($T_{1/2}$ ~$2.1 \cdot 10^5$ years) and ^{129}I ($T_{1/2}$ ~$1.6 \cdot 10^7$ years). ^{99}Tc is present as single isotopic species and can be transmuted into ^{100}Tc, which rapidly ($T_{1/2}$ ~16 seconds) transforming into a stable ^{100}Ru with beta decays. Iodine, separated from spent fuel, is a mixture of ^{127}I and ^{129}I, but the former is present within 16 %, which is permissible [5; p.175]. Hence, ^{129}I can be transformed to ^{130}I, which decays with a half-life of 12 h to stable ^{130}Xe. It should be noted that reactions involving successive neutron capture in ^{99}Tc and ^{129}I will yield stable nuclides after beta decay. Although the lower neutron flux in a thermal system is partly compensated by high capture cross sections, requirements for the neutron economy favor the use

of fast systems. It should be borne in mind that fission products act as poisons without compensation for the production of neutrons. Fast systems provide the best neutron economy that can be used for transmutation while the LWR system will require a higher enrichment [5; p.175]. An optimal strategy, for transmutation of ^{99}Tc and ^{129}I, is the use of moderated target assemblies of fast reactors, which could then combine the high neutron flux of a fast system with the high capture cross-sections in a thermal system [6; p.291-318].

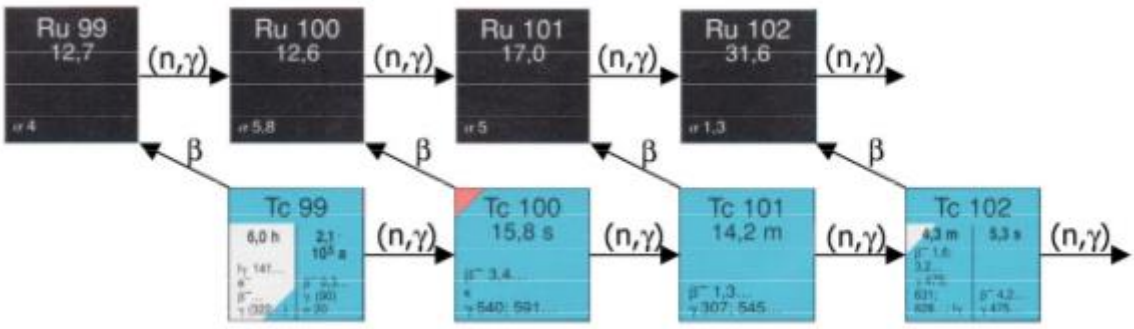

Fig.1.3. Transmutation path of ^{99}Tc.

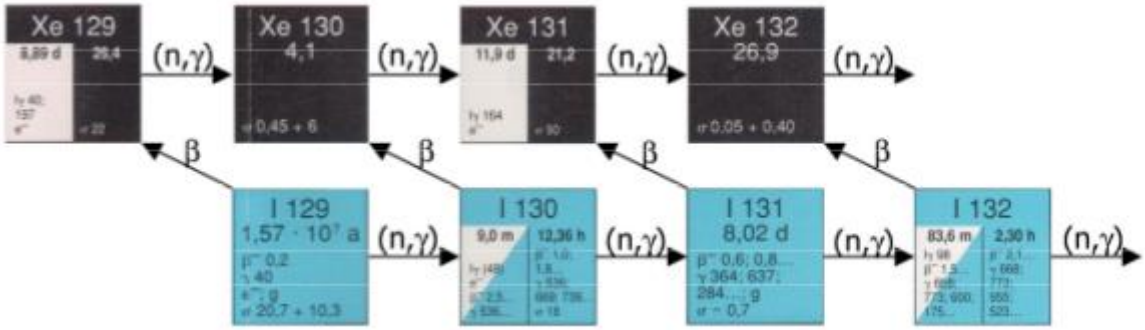

Fig.1.4. Transmutation path of ^{129}I.

§ 1.3. ADS research at Dubna

Joint Institute for Nuclear Research in Dubna, is the research organization that possesses a wide instrumental basement for ADS studies [11; p.38]. Cross sections and transmutation rates of the long-lived fission products as well as actinides, generation of neutrons in the spallation targets, spatial distribution, and the spectral characteristics of secondary fast and thermal neutrons have been systematically

investigated at the JINR accelerator fleet since the last two decades [7; p.475]. Phasotron, Synchrophasotron, and Nuclotron accelerators provided the relativistic proton beams of energy up to 8 GeV and deuteron or even carbon beams up to 4 GeV per nucleon (AGeV), which makes JINR particularly unique for the purposes of ADS research among other research centers worldwide. Due to the well-defined geometry of solid heavy-metal cuprum, lead, and uranium targets, a wide series of performed experiments has served as the benchmark test of different physics models provided by various Monte Carlo transport codes.

§ 1.3.1. Phasotron experiments

The main aims of the ADS-related experiments at the JINR Phasotron accelerator that provides 1 μA beam of 660 MeV protons are the measurements of cross sections in thin actinide spallation targets and the experimental investigation of production of neutrons in thick heavy-metal spallation targets. The results of the cross section measurements were submitted to the nuclear data library Experimental Nuclear Reaction Data (EXFOR), e.g. [9; p.201, 10; p.1814].

The basic physics principles of neutron production in the spallation target were examined during the experiments with the cylindrical lead target of 80 mm in diameter and 480 mm long and the 660 MeV proton beam [12; p.110]. Properties of the secondary neutron field were investigated with Au, Al, and Bi activation detectors using the methods of gamma-ray spectrometry. The experimental results were compared to those simulated with the MCNPX 2.5.0 radiation transport code. The experimental study [13; p.23, 122; p.102-107] was focused on the investigation of the (n,xn) reactions – particularly important for fast-spectrum ADS – in the samples of natural thorium and uranium irradiated with spallation neutrons generated in the thick lead target.

Besides a series of experimental studies performed with the use of high-intensity Phasotron proton beam, the accelerator should have represented the key component of the ADS demonstration facility designed in the framework of a wide

international collaboration at JINR.

§ 1.3.2. The GAMMA-2 target

In order to investigate the basic physics principles of neutron production in a spallation target as well as transport through the surrounding moderator, the spallation target GAMMA-2 [14; p.239] was designed and commissioned for experimental purposes at JINR. The target setup consists of a 200 mm long lead target – assembled from a 10 mm thick disks of 80 mm in diameter – and a 60 mm thick paraffin moderator. The target was irradiated with proton beams of energy from 0.65 GeV up to 7.4 GeV at Synchrophasotron and Nuclotron accelerators.

A maximum neutron production at a distance of about 100 mm from the front end of the target was determined with the copper foils measured with the use of gamma-ray spectrometry. The distance was discovered to be independent of energy of incident protons [14; p.239]. Another study [15; p.61] with a set of the following activation threshold detectors: ^{59}Co, ^{115}In, ^{197}Au, ^{209}Bi, and ^{232}Th irradiated at the GAMMA-2 target revealed that the neutron production determined experimentally and the results of the simulation performed with the CASCADE [16; p.28] code were not in agreement within experimental uncertainties (underestimation of the simulated neutron production up to energy of 10 MeV; above this value, conversely, simulations overestimated the measured neutron production). Finally, the (n,γ) transmutation rates in ^{129}I and ^{237}Np were investigated in the moderated flux of neutrons from the GAMMA-2 target [17; p.634]. The experimental neutron flux was found larger than the flux simulated with the LAHET [18] computer code.

§ 1.3.3. The GAMMA-3 setup

A spallation lead target surrounded by a large graphite moderator was developed at JINR for the purpose of research on transmutation of actinides in the field of moderated neutrons. The experimental setup referred to as GAMMA-3 [19; p.26] is composed of the 600 mm long cylindrical spallation lead target of 80 mm in diameter installed in a central part of the large block of graphite of dimensions 1100 × 1100 × 600 mm^3. The large graphite moderator consists of 25 blocks of different size, some of which are perforated and serve as the experimental channels for various activation samples. The target was designed for irradiation with relativistic beams of JINR Nuclotron accelerator.

The process of neutron generation in the spallation lead target and moderation in graphite at different radial distances from the target were experimentally investigated using the (n,f), (n,γ), and (n,2n) reaction rates in the natural uranium and thorium samples [20; p.85]. The experimental results were in reasonably good agreement with the results of simulations performed with the MCNPX 2.6c code. Good agreement was also reached when comparing the experimental spatial distribution of thermal and epithermal neutrons in the graphite moderator to the results of simulations carried out with the MCNPX 2.7 code [21; p.15].

§ 1.3.4. The Energy plus Transmutation assembly

A wide series of experiments focused on physics research of fast spallation and fission neutron field were carried out at a spallation lead target surrounded by a uranium blanket, referred to as the “Energy plus Transmutation” target-blanket assembly [22; p.517]. The setup was irradiated with the beams of protons and deuterons provided by the JINR Nuclotron accelerator till 2012.

The target is composed of four identical hexagonal sections. The central part of each section is formed by a 114 mm long cylindrical lead target of 84 mm in diameter. Each target section is surrounded by the uranium blanket that consists of 30 natural uranium cylinders of 104 mm in length and 36 mm in diameter. An 8 mm thick air gap separates the sections one from another. Simultaneously, the gaps provide a space where the experimental samples can be placed during the

irradiation. The whole target-blanket assembly was mounted on a wooden plate and surrounded by a 300 mm thick shielding of granulated polyethylene. The inner side of the polyethylene shielding was covered by a 1 mm thick layer of cadmium to avoid the backscattered thermal neutrons entering the target. However, the backscattered neutrons above the energy of 1 eV can influence the fast neutron spectrum inside the target.

The experimental study [23; p.159] on transmutation of natural uranium and thorium samples situated at the surface of the uranium blanket revealed a substantial contribution of the (n,2n) reaction rate to the total transmutation rate of thorium. A calculation of neutron production with the MCNPX 2.6c code shows a considerably high contribution of neutrons with energy higher than 20 MeV to the total fission rate in the ^{232}Th (58%) and ^{nat}U (38%) samples.

Another work [24; p.1765] revealed good agreement between the experimental reaction rates for the ^{209}Bi(n,4n)^{206}Bi reaction, which is a suitable indicator of the high-energy neutrons due to the energy threshold 22.6 MeV, and predictions of the MCNPX 2.5.0 code employing the INCL4-ABLA physics models.

The study of neutron production inside the “Energy plus Transmutation” setup proved that the neutron cost saturates at the energy about 1 GeV, although the exact value could not have been specified [25; p.70]. The setup was irradiated with proton and deuteron beams in the energy range from 0.7 GeV up to 2.5 GeV and the ^{27}Al and ^{197}Au activation detectors were used.

Apart from the gamma-ray spectrometry, the fission track technique [26; p.204], solid state nuclear track detectors [27; p.103], and nuclear emulsions [28; p.917] were used to investigate the characteristics of the spallation and fission neutron field in the “Energy plus Transmutation” assembly.

In general, the INCL4-ABLA intranuclear cascade and fission-evaporation physics models used when performing simulations of neutron production and transport with the MCNPX code provided the results close to those obtained in experiment, in some cases within one standard deviation. For this reason, these

models will also be employed in the Monte Carlo simulations of neutron production further in this work.

§ 1.3.5. The subcritical natural uranium assembly QUINTA

On the QUINTA setup since 2011 conducted extensive researches:

to assess the possibility of transmutation using ^{129}I, ^{237}Np, ^{238}Pu, ^{239}Pu, and ^{241}Am samples [121; p.225-233];

to study the spallation and fission reactions using ^{232}Th, ^{233}U, ^{235}U, ^{236}U, and ^{nat}U samples [120; p.84-89];

to measure of neutrons fluence using threshold reactions in the ^{27}Al, ^{55}Mn, ^{59}Co, ^{89}Y, ^{115}In, ^{127}I, ^{197}Au, ^{nat}Pb, and ^{209}Bi samples [122-124]. In some experiments fluence of neutrons around of the setup was measured on-line, using the liquid scintillator neutron multidetector DEMON and diamond neutron detector. However, at high intensity of neutron flux, deteriorates work of neutron detectors due to the radiation stability of the detectors. The most reliable method for measuring of neutron flux is using of threshold detectors, although require more time for careful analysis and processing of the results;

to monitor the relativistic beam of deuterons and protons using the ^{27}Al and ^{nat}Cu foils, to additionally to the ionizing chamber;

to measure of cross sections for the formation of nuclei in fission and spallation reactions using the ^{232}Th and ^{nat}U samples at the irradiating with relativistic proton and deuteron beam [124];

to measure of releasing heat inside of the assembly using thermocouples to determine energy production, number of fission reactions and neutrons flux.

In this dissertation given the results of assess the possibility of transmutation using ^{129}I samples, of study the spallation and fission reactions using ^{232}Th samples, and of measurements of the neutrons fluence using threshold reactions in the ^{127}I samples.

§ 1.4. Conclusions

ADS is a subcritical reactor controlled by an external neutron source, whose kinetics characteristics differ significantly from conventional (critical) nuclear reactors. The critical operating state represents a sensitive balance between the production rate of neutrons through fission and the neutron loss rate and a relatively small off-balance in these two quantities can lead to large deviations in power. In contrast, a subcritical reactor is inherently stable to reactivity changes within the subcritical range or changes in the external neutron source.

The ADS can be used to destroy heavy isotopes contained in the used fuel from a conventional nuclear reactor – particularly actinides. ADSs could also be used to destroy longer-lived fission products, such as ^{99}Tc and ^{129}I (213,000 and 16 million years half-lives, respectively). These isotopes can acquire a neutron to become ^{100}Tc and ^{130}I respectively, which are very short-lived, and beta decay to ^{100}Ru and ^{130}Xe, which are stable.

CHAPTER II. MONTE CARLO SIMULATIONS

§ 2.1. Introduction

Monte Carlo simulations of particle transport is mainly performed step by step. A true step length for a next physics interaction is randomly sampled using the mean free path of the interaction or by various step limitations established by different components of Monte Carlo simulation codes [42; p.8]. The smallest step limit defines the new true step length. Computation of mean free path of a particle in a media is performed using cross section of a particular physics process and density of atoms. In a simple material the number of atoms per volume is:

$$n = \frac{N\rho}{A}, \tag{2.1}$$

where N is Avogadro's number, ρ is density of the medium, and A is mass of a mole.

In a compound material the number of atoms per volume of the i^{th} element is:

$$n_i = \frac{N\rho w_i}{A_i}, \tag{2.2}$$

where w_i is proportion by mass of the i^{th} element, and A_i is mass of a mole i^{th} element.

The mean free path of a process λ also called the interaction length, can be given in terms of the total cross section:

$$\lambda(E) = (\sum_i [n_i \cdot \sigma(Z_i, E)])^{-1}, \tag{2.3}$$

where $\sigma(Z, E)$ is the total cross section per atom of the process and Σ_i runs over all elements composing the material. $\sum_i [n_i \cdot \sigma(Z_i, E)]$ is also called the macroscopic cross section. The mean free path is the inverse of the macroscopic cross section.

The mean free path λ of a particle for a given process depends on the medium and cannot be used directly to sample the probability of an interaction in a heterogeneous detector. The number of mean free paths which a particle travels is:

$$n_\lambda = \int_{x_1}^{x_2} \frac{dx}{\lambda(x)}\,, \tag{2.4}$$

which is independent of the material traversed. If n_r is a random variable denoting the number of mean free paths from a given point to the point of interaction, it can be shown that n_r has the distribution function:

$$P(n_r < n_\lambda) = 1 - e^{-n_\lambda}, \tag{2.5}$$

The total number of mean free paths the particle travels before reaching the interaction point n_λ is sampled at the beginning of the trajectory as:

$$n_\lambda = -\log(\eta)\,, \tag{2.6}$$

where η is a random number uniformly distributed in the range (0, 1). n_λ is updated after each step Δx according the formula:

$$n'_\lambda = n_\lambda - \frac{\Delta x}{\lambda(x)}\,, \tag{2.7}$$

until the step originating from $s(x) = n_\lambda \cdot \lambda(x)$ is the shortest and this triggers the specific process.

The short description given above is the differential approach to particle transport. In this approach besides the other discrete processes the continuous energy loss imposes a limit on the step-size too, because the cross section of different processes depend on the energy of the particle. Then it is assumed that the step is small enough so that the particle cross sections remain approximately constant during the step. In principle one must use very small steps in order to insure an accurate simulation, but computing time increases as the step-size decreases. A good compromise depends on required accuracy of a concrete simulation.

The laboratory time of a particle should be updated after each step:

$$\Delta t_{lab} = 0.5\Delta x \left(\frac{1}{v_1} + \frac{1}{v_2}\right), \tag{2.8}$$

where Δx is a true step length traveled by the particle, v_1 and v_2 are particle velocities at the beginning and at the end of the step correspondingly.

§ 2.2 FLUKA simulations

§ 2.2.1 Hadron-nucleon interaction models

A complete understanding of hadron–nucleon (h–N) interactions over a wide energy range is, of course, a main ingredient for the qualitative description of hadron–nuclear processes. Elastic, charge exchange and strangeness exchange reactions are described, as far as possible, by the phase–shift analysis and the fits of experimental differential data [31; p.1-10]. Standard eikonal approximations are often used at high energies.

At the low energy end (below 100 MeV) the p–p and p–n cross sections are rapidly increasing with decreasing energy. The n–p and the p–p cross sections differ approximately three-fold three at the lowest energies, as expected on the basis of symmetry and isospin considerations, while at high energies they tend to be the same. The total cross section for the two isospin components present in the nucleon–nucleon amplitude is determined as follows:

$$\sigma_1 = \sigma_{pp}$$

$$\sigma_0 = 2\sigma_{np} - \sigma_{pp}$$

The cross section for pion–nucleon scattering is dominated by the existence of several direct resonances, the most notable of which is Δ(1232). Given the pion isotopic spin (T = 1), the three π charge states correspond to the three values of T_z. Thus, in the pion-nucleon system two values of T are allowed: $T = 1/2$ and $T = 3/2$, and two independent scattering amplitudes, $A_{1/2}$ and $A_{3/2}$, enter in the cross

sections. Using Clebsch-Gordan coefficients all differential cross sections can be derived from the three measured ones: $\sigma(\pi^+ p \rightarrow \pi^+ p)$, $\sigma(\pi^- p \rightarrow \pi^- p)$, and $\sigma(\pi^- p \rightarrow \pi^0 n)$. In inelastic hadron-nucleon interactions as soon as particle production is concerned, the description becomes more complex at once. Two families of models are adopted, depending on the projectile energy: those based on individual resonance production and decays, which cover the energy range up to 3–5 GeV, and those based on dual parton and quark gluon string models, which can provide reliable results up to several tens of TeV.

The channel of inelastic collision with the lowest threshold, single pion production, opens already around 290 MeV in nucleon-nucleon interactions, and becomes important above 700 MeV. In pion-nucleon interactions the production threshold is as low as 170 MeV. Both reactions are usually described in the framework of the isobar model: all reactions proceed through an intermediate state containing at least one resonance. There are two main classes of reactions that form a resonant intermediate state and those that contain two particles in the intermediate state. The former demonstrates bumps in the cross sections corresponding to the energy of the formed resonance. Examples are given below:

$$N_1 + N_2 \rightarrow N'_1 + \Delta(1232) \rightarrow N'_1 + N'_2 + \pi$$
$$\pi + N \rightarrow \Delta(1600) \rightarrow \pi' + \Delta(1232) \rightarrow \pi' + \pi'' + N'$$
$$N_1 + N_2 \rightarrow \Delta_1(1232) + \Delta_2(1232) \rightarrow N'_1 + \pi_1 + N'_2 + \pi_2$$

Partial cross sections can be obtained from one-boson-exchange theories and folding of Breit-Wigner with matrix elements fixed by N–N scattering or experimental data. Resonance energies, widths, cross sections, and branching ratios are taken from the data, and conservation laws are used for spin and isospin ratios.

As soon as the projectile energy exceeds several GeV, the description in terms of resonance production and decay becomes more and more difficult. The number of resonances that need to be considered exponentially increases and their properties are often poorly known. The features of low-p_T interactions cannot be

derived from the quantum chromodynamics Lagrangian, because the large value taken by the running coupling constant prevents the use of perturbation theory. Models based on interacting strings have become a powerful tool in understanding quantum chromodynamics in the soft hadronic scale, that is, in the non-perturbative regime. An interacting string theory naturally leads to a topological expansion [31; p.1-10]. The dual parton model [29; p.225] is one of these models and it is built introducing partonic ideas into a topological expansion which explicitly incorporates the constraints of duality and unitarity, typical of Regge's theory. In the dual parton model, hadrons are considered as open strings with quarks, antiquarks or diquarks sitting at the ends; mesons are strings with their valence quark and antiquark at the ends. The chains produced in an interaction are then hadronized. Dual parton model gives no prescriptions on this stage of the reaction. All the available chain hadronization models, however, rely on the same basic assumptions, the most important one being chain universality, that is chain hadronization does not depend on the particular process which originated the chain, and until the chain energy is much larger than the mass of the hadrons to be produced, the fragmentation functions (which describe the momentum fraction carried by each hadron) are the same. As a consequence, fragmentation functions can in principle be derived from hard processes and e^+e^- data and the same functions and parameters should be valid for all reactions and energies; actually mass and threshold effects are non-negligible at the typical chain energies involved in hadron-nucleus reactions.

§ 2.2.2 Main steps of hadron-nucleus interactions

High energy hadron–nucleus (h–A) interactions can be schematically described as a sequence of the following steps:

• Glauber–Gribov cascade

• (Generalized) IntraNuclear cascade ((G)INC)

• Preequilibrium emission

• Evaporation/Fragmentation/Fission and final deexcitation.

The Glauber formalism [30; p.135] provides a powerful and elegant method to derive elastic, quasi-elastic and absorption h–A cross sections from the free h–N cross section and the nuclear ground state only. Inelastic interactions are equivalent to multiple interactions of the projectile with *ν* target nucleons. The number of such "primary" interactions follows a binomial distribution (at a given impact parameter, b):

$$P_{r\nu}(b) \equiv \binom{A}{\nu} P_r^{\nu}(b)[1 - P_r(b)]^{A-\nu}, \tag{2.9}$$

where $P_r(b) \equiv \sigma_{hNr} T_r(b)$, and $T_r(b)$ is the profile function (folding of nuclear density and scattering profiles along the path). On average:

$$< \nu > = \frac{Z\sigma_{hpr} + N\sigma_{hnr}}{\sigma_{hA\ abs}},$$

$$\sigma_{hA\ abs}(s) = \int d^2\vec{b}\,[1 - (1 - \sigma_{hNr}(s) T_r(b))^A].$$

The Glauber-Gribov model [32; p.709, 33; p.45] represents the diagram interpretation of the Glauber cascade. The *ν* interactions of the projectile originate *2ν* chains, out of which 2 chains (valence-valence chains) struck between the projectile and target valence (di)quarks, $2(\nu - 1)$ chains (sea-valence chains) between projectile sea $q - \bar{q}$ and target valence (di)quarks.

At energies high enough to consider coherent effects as corrections, a h–A reaction can be described as a cascade of two-body interactions, concerning the projectile and the reaction products. This is the mechanism called IntraNuclear Cascade (INC). INC models were developed already at the infancy of the computer era with great success in describing the basic features of nuclear interactions in the 0.2-2 GeV range. Modern INC models had to incorporate many more ideas and effects in order to describe in a reasonable way reactions at higher and lower energies. Despite particle trajectories are described classically, many quantistic effects have to be incorporated in these (G)INC models, like Pauli blocking,

formation time, coherence length, nucleon antisymmetrization, hard core nucleon correlations.

At energies lower than the π production threshold a variety of preequilibrium models have been developed [34] following two leading approaches: the quantum-mechanical multistep model and the exciton model. The former has a very good theoretical background but is quite complex, while the latter relies on statistical assumptions, and it is simple and fast. Exciton-based models are often used in Monte Carlo codes to join the INC stage of the reaction to the equilibrium one.

In the FLUKA implementation the INC step goes on until all nucleons are below a smooth threshold around 50 MeV, and all particles but nucleons (typically pions) have been emitted or absorbed. At the end of the INC stage a few particles may have been emitted and the input configuration for the preequilibrium stage is characterized by the total number of protons and neutrons, by the number of particle-like excitons (nucleons excited above the Fermi level), and of hole-like excitons (holes created in the Fermi sea by the INC interactions), and by the nuclear excitation energy and momentum. All the above quantities can be derived by properly recording what occurred during the INC stage.

At the end of the reaction chain, the nucleus is a thermally equilibrated system, characterized by its excitation energy. This system can "evaporate" nucleons, fragments, or γ rays, or can even fission, to dissipate the residual excitation.

Neutron emission is favored over charged particle emission, due to the Coulomb barrier, especially for medium-heavy nuclei. Moreover, the excitation energy is higher in heavier nuclei due to the larger cascading chances and to the larger number of primary collisions in the Glauber cascade at high energies. The level density parameter $a \approx A/8$ MeV^{-1} is higher too, thus the average neutron energy is smaller. Therefore, the neutron multiplicity is higher for heavy nuclei than for light ones.

The FLUKA evaporation module is based on the standard Weisskopf-Ewing formalism [35; p.295]. The evaporation/fission/break-up processes represent the

last stage of a nuclear interaction and are responsible for the exact nature of the residuals left after the interactions. However, for a coherent self-consistent model, the mass spectrum of residuals is highly constrained by the excitation energy distribution found in the slow stages, which in turn is directly related to the amount of primary collisions and following cascading which has taken place in the fast stages.

§ 2.3 Geant4 simulations

§ 2.3.1 Bertini intranuclear cascade model in Geant4

This cascade model is a re-engineered version of the INUCL code [44] and includes the Bertini intra-nuclear cascade model with excitons, a pre-equilibrium model, a nucleus explosion model, a fission model, and an evaporation model [42; p.414]. It considers nuclear reactions initiated by long-lived hadrons (p, n, π, K, Λ, Σ, Ξ, Ω) and γ-rays with energies between 0 and 10 GeV. The intra-nuclear cascade model (INC) was first proposed by Serber in 1947 [36; p.1114]. He noticed that in particle-nuclear collisions the deBroglie wavelength of the incident particle is comparable (or shorter) than the average intra-nucleon distance. Hence, a description of interactions in terms of particle-particle collisions is justified. The INC has been used successfully in Monte Carlo simulations at intermediate energies since Goldberger made the first hand-calculations in 1947 [37; p.1269]. The first computer simulations were done by Metropolis et al. in 1958 [38; p.185]. Standard methods in INC implementations were developed when Bertini published his results in 1968 [39; p.29]. An important addition to INC was the exciton model introduced by Griffin in 1966 [40; p.478-481].

In the next part will describes the implementation of the Bertini INC model within the Geant4 hadronic physics framework [41; p.250]. This framework is flexible and allows for the modular implementation of various kinds of hadronic interactions. Inelastic particle-nucleus collisions are characterized by both fast and slow components. The fast (10^{-23} – 10^{-22} s) intra-nuclear cascade results in a

highly excited nucleus which may decay by fission or pre-equilibrium emission. The slower (10^{-18} – 10^{-16} s) compound nucleus phase follows with evaporation. The intra-nuclear cascade (INC) model developed by Bertini [39; p.29] solves the Boltzmann equation on average. This model has been implemented in several codes such as HETC [43; p.337-343].

The target nucleus is modeled by up to six concentric shells of constant density as an approximation to the continuously changing density distribution of nuclear matter within nuclei [42; p.415]. The cascade begins when an incident particle strikes a nucleon in the target nucleus and produces secondary particles. The secondary particles may in turn interact with other nucleons or be absorbed. The cascade ends when all particles that can be kinematically capable leave the nucleus. At this point, the conservation of energy is checked. Relativistic kinematics is applied throughout the cascade. The necessary condition of validity of the INC model is $\lambda_B/v << \tau_c << \Delta t$, where λ_B is the de Broglie wavelength of the nucleons, v is the average relative velocity between two nucleons and Δt is the time interval between collisions. At energies below 200 MeV, this condition is no longer strictly valid, and a pre-quilibrium model must be invoked. At energies higher than ≈ 10 GeV) the INC picture breaks down. This model has been tested against experimental data at incident kinetic energies between 100 MeV and 10 GeV [42; p.415]. The basic steps of the INC model are summarized as follows:

- the space point at which the incident particle enters the nucleus is selected uniformly over the projected area of the nucleus,
- the total particle-particle cross sections and region-dependent nucleon densities are used to select a path length for the projectile particle,
- the momentum of the struck nucleon, the type of reaction and the four-momenta of the reaction products are determined, and
- the exciton model is updated as the cascade proceeds.
- If the Pauli exclusion principle allows and $E_{particle} > E_{cutoff} = 2$ MeV, second step is performed to transport the products.

After the intra-nuclear cascade, the residual excitation energy of the producing nucleus is used as input for non-equilibrium model. Some of the basic features of the nuclear model are:

• the nucleons are assumed to have a Fermi gas momentum distribution. The Fermi energy is calculated in a local density approximation i.e. the Fermi energy is made radius-dependent with Fermi momentum $p_F(r) = (\frac{3\pi^2 p(r)}{2})^{\frac{1}{3}}$.

• Nuclear binding energies are calculated using the semi-empirical mass formula.

The initialization phase fixes the nuclear radius and momentum according to the Fermi gas model. If the target is hydrogen (A = 1) a direct particle-particle collision is performed, and no nuclear modeling is required. If 1 < A < 4, a nuclear model consisting of one layer with a radius of 8.0 fm is created. For 4 < A < 11, the nuclear model is composed of three concentric spheres i = {1, 2, 3} with radius

$$r_i(\alpha_i) = \sqrt{C_1^2\left(1 - \frac{1}{A}\right) + 6.4\sqrt{-log(\alpha_i)}}\,. \tag{2.10}$$

Here α_i = {0.01, 0.3, 0.7} and C_1 = $3.3836A^{1/3}$. If A > 11, a nuclear model with three concentric spheres is also used. The sphere radius is now defined as

$$r_i(\alpha_i) = C_2 log\left(\frac{1+e^{-\frac{C_1}{C_2}}}{\alpha_i} - 1\right) + C_1\,, \tag{2.11}$$

where C_2 = 1.7234. The potential energy V for nucleon N is

$$V_N = \frac{p_F^2}{2m_N} + BE_N(A,Z)\,, \tag{2.12}$$

where p_F is the Fermi momentum and BE is the binding energy. The momentum distribution in each region follows the Fermi distribution with zero temperature.

$$f(p) = cp^2\,, \tag{2.13}$$

where

$$\int_0^{p_F} f(p)dp = n_p \text{ or } n_n \,,$$

where n_p and n_n are the number of protons or neutrons in the region. P_f is the momentum corresponding to the Fermi energy

$$E_f = \frac{p_F^2}{2m_N} = \frac{\hbar^2}{2m_N}\left(\frac{3\pi^2}{v}\right)^{\frac{2}{3}}, \tag{2.14}$$

which depends on the density n/v of particles, and which is different for each particle and each region.

The exclusion principle of Pauli prohibits interaction in which products will be in occupied states. Following the assumption of a completely degenerate Fermi gas, the levels are filled from the lowest level. The minimum energy allowed for the products of a collision correspond to the lowest unfilled level of the system, which is the Fermi energy in the region. So in practice, the exclusion principle of Pauli is taken into account by accepting only secondary nucleons which have $E_N > E_f$. Path lengths of nucleons in the nucleus are sampled according to the local density and the free $N - N$ cross sections. Angles after the collision are sampled from experimental differential cross sections. Tabulated total reaction cross sections are calculated by Letaw's formulation [45-47]. For $N - N$ cross sections the parameterizations are based on the experimental energy and isospin dependent data. The parameterization described in [48] is used.

For pions the intra-nuclear cross sections are provided to consider elastic collisions and the following inelastic channels: $\pi^- p \rightarrow \pi^0 n$, $\pi^0 p \rightarrow \pi^+ n$, $\pi^0 n \rightarrow \pi^- p$, and $\pi^+ n \rightarrow \pi^0 p$. Multiple particle production is also implemented. The pion absorption channels are $\pi^+ nn \rightarrow pn$, $\pi^+ pn \rightarrow pp$, $\pi^0 nn \rightarrow nn$, $\pi^0 pn \rightarrow pn$, $\pi^0 pp \rightarrow pp$, $\pi^- pn \rightarrow nn$, and $\pi^- pp \rightarrow pn$.

The Geant4 cascade model implements the exciton model proposed by Griffin [40; p.478-481, 49; p.5-7]. In this model, nucleon states are characterized by the number of excited particles and holes (the excitons). Intra-nuclear cascade

collisions give rise to a sequence of states characterized by increasing exciton number, eventually leading to an equilibrated nucleus. For a practical implementation of the exciton model used parameters from [50; p.545-560], (level densities) and [51; p.319-322] (matrix elements). In the exciton model the possible selection rules for particle-hole configurations in the source of the cascade are: $\Delta p = 0, \pm 1$ $\Delta h = 0, \pm 1$ $\Delta n = 0, \pm 2$, where p is the number of particles, h is number of holes and $n = p + h$ is the number of excitons. In the cascade pre-equilibrium model, the target excitation data and the exciton configurations for neutrons and protons are used to produce non-equilibrium evaporation. The angular distribution is isotropic in the rest frame of the exciton system.

The fission model is phenomenological, using potential minimization. A binding energy parametrization is used and some features of the fission statistical model are included [52]. A statistical theory for particle emission of the excited nucleus remaining after the intra-nuclear cascade was originally developed by Weisskopf [35; p.295]. This model assumes complete energy equilibration before particle emission, and re-equilibration of excitation energies between successive evaporations. As a result the angular distribution of emitted particles is isotropic. The Geant4 evaporation model for the cascade implementation adapts the often-used computational method developed by Dostrowski [53; p.683-702, 54; p.791]. The emission of particles is computed until the excitation energy falls below some specific cutoff. If a light nucleus is highly excited, the Fermi break-up model is executed. Also, fission is performed if that channel is open. The main chain of evaporation is followed until $E_{excitation}$ falls below E_{cutoff} = 0.1 MeV. The evaporation model ends with an emission chain which is followed until $E_{excitation} < E^{\gamma}_{cutoff} = 10^{-15}$ MeV.

§ 2.3.2 The geant4 binary cascade

The Geant4 Binary Cascade is an intranuclear cascade propagating primary and secondary particles in a nucleus. The name Binary Cascade leads from the

interactions between the primary or secondary particle and the individual nucleon of the nucleus. Cross section data are used to select collisions and in the presence of experimental cross sections are used in the simulation. The propagation of particles in a nuclear field is accomplished by numerically solving the equation of motion. The cascade terminates when the average and maximum energy of secondary particles is below threshold. The remaining fragment is treated by precompound and de-excitation models.

The nucleus is constructed from A nucleons and Z protons with nucleon coordinates r_i and momenta p_i, with i = 1, 2, ..., A. Used a common initialization Monte Carlo procedure, which is realized in the most of the high energy nuclear interaction models:

• Nucleon coordinates r_i are selected randomly in the nucleus rest frame according to nucleon density $\rho(r_i)$. For heavy nuclei with $A > 16$ [55; p.1093] nucleon density is

$$\rho(r_i) = \frac{\rho_0}{1+\exp[(r_i - R)/a]}\ , \qquad (2.15)$$

where

$$\rho_0 \approx \frac{3}{4\pi R^3}\left(1 + \frac{a^2\pi^2}{R^2}\right)^{-1}.$$

Here $R = r_0 A^{1/3}$ fm and $r_0 = 1.16(1 - 1.16A^{-2/3})$ fm and $a \approx 0.545$ fm. For light nuclei with A < 17 nucleon density is given by a harmonic oscillator shell model [56], e. g.

$$\rho(r_i) = \pi R^{2^{-3/2}} \exp\left(-r_i^2/R^2\right), \qquad (2.16)$$

where $R^2 = 2/3 < r^2 >= 0.8133A^{2/3}$ fm^2. To take into account nucleon repulsive core it is assumed that internucleon distance $d > 0.8$ fm;

• The initial momenta of the nucleons p_i are randomly chosen between 0 and $p_F^{max}(r)$, where the maximal momenta of nucleons (in the local Thomas-Fermi approximation [57]) depends from the proton or neutron density ρ according to

$$p_F^{max}(r) = \hbar c(3\pi^2\rho(r))^{1/3}. \quad (2.17)$$

In the calculation of the total, inelastic and elastic cross-section are used available experimental data. For the case of proton-proton (pp) and proton-neutron (pn) collisions, as well as π^+ and π^- nucleon collisions, experimental data are used from the Particle Data Group (PDG) for both elastic and inelastic collisions. These experimental data are used for energies below 3 GeV. For higher energies, parametrizations from the CERN-HERA collection are included. The angular distributions for the elastic scattering of nucleons are taken from the available experimental data. Final states are derived by sampling from tables of the cumulative distribution function of the center-of-mass scattering angle, tabulated for kinetic energies from 10 MeV to 1200 MeV.

In simulating light ion reactions, the initial state of the cascade is prepared in the form of two nuclei. The lighter of the collision partners is selected to be the projectile. The nucleons in the projectile are then entered, with position and momenta, into the initial state of the cascade. The nucleon distribution inside the projectile nucleus is taken to be a representative distribution of its nucleons in configuration space.

§ 2.3.3 INCL++: the liège intranuclear cascade model

There is an increased interest in the study of spallation reactions. This is basically due to the new technological applications, such as Accelerator-Driven Systems, consisting of sub-critical nuclear reactor coupled to a particle accelerator. These applications require optimized targets as spallation sources. This type of problem typically involves a large number of parameters and it is necessary to rely on simulations. Above ∼200 MeV incident energy it is necessary to use reliable models due to the prohibitive number of open channels. The most appropriate modeling technique in this energy region is intranuclear cascade (INC) combined with evaporation model. One such pair of models is the Liège cascade model

INCL++ [58, 59] coupled with the G4ExcitationHandler statistical de-excitation model. The INCL++ model is available through dedicated physics lists. The *HP variants of the physics lists use the NeutronHP model for neutron interactions at low energy; the QGSP* and FTFP* variants respectively use the QGSP and FTFP model at high energy. Figure 2.1 shows a schematic model map of the INCL++-based physics lists.

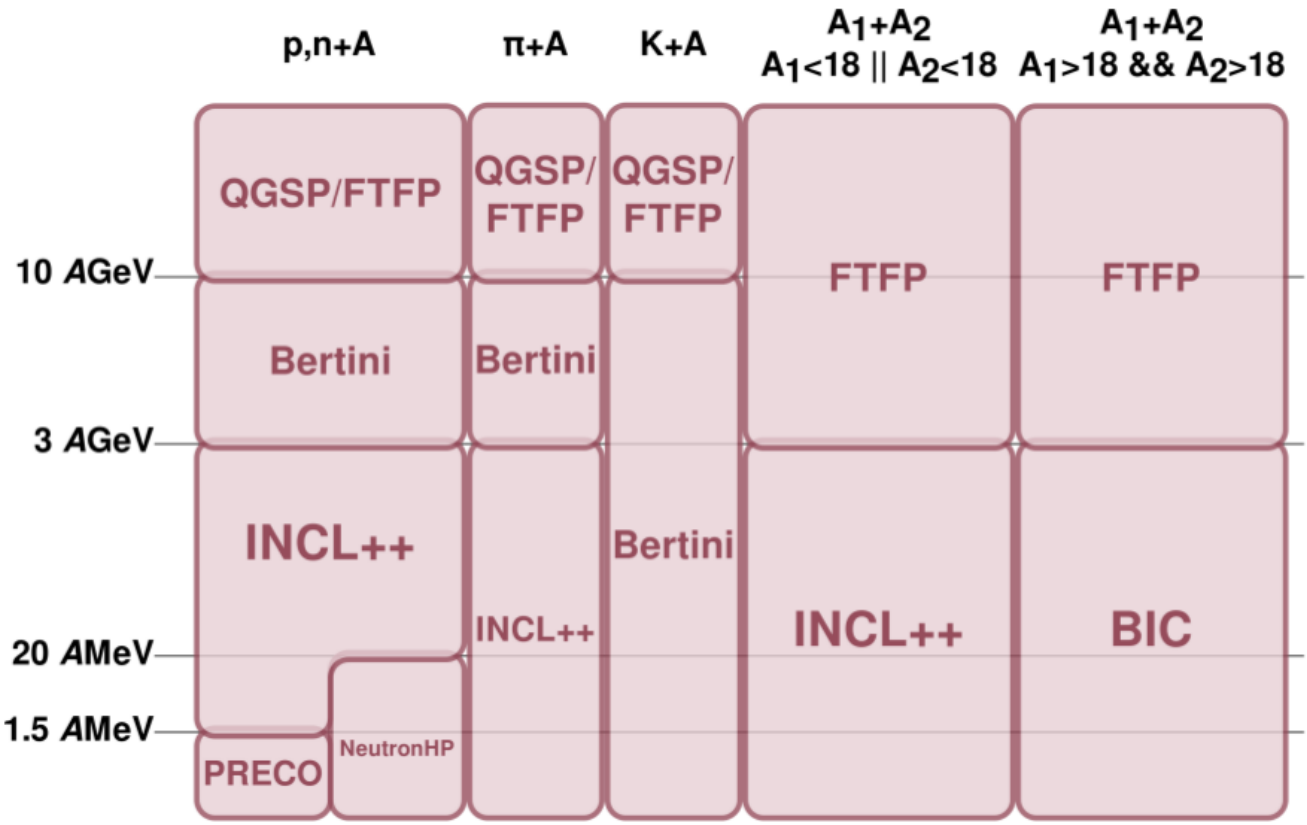

Figure 2.1. Model map for the INCL++ based physics lists [42; p.494]. The first two columns represent nucleon- and pion-induced reactions. The fourth column represents nucleus-nucleus reactions where at least one of the partners is below A = 18. The fifth column represents other nucleus-nucleus reactions.

The INCL++ cascade model can be used to simulate the collisions between bullet particles and nuclei. The momenta and positions of the nucleons inside the nuclei are determined at the beginning of the simulation run by modeling the nucleus as a free Fermi gas in a static potential well with a realistic density. The cascade is modeled by tracking the nucleons and their collisions. The possible

reactions inside the nucleus are

• $N\,N \rightarrow N\,N$ (elastic scattering)

• $N\,N \rightarrow N\,\Delta$ and $N\,\Delta \rightarrow N\,N$

• $\Delta \rightarrow \pi N$ and $\pi N \rightarrow \Delta$

• $N\,N \rightarrow N\,N\,x\pi$ (multiple pion production)

• $\pi N \rightarrow \pi N$ (elastic scattering and charge exchange)

• $\pi N \rightarrow N\,(x + 1)\pi$ (multiple pion production)

• $N\,N \rightarrow N\,N\,M$ ($M = \eta$ or ω)

• $N\,N \rightarrow N\,N\,M\,x\pi$ (inclusive production, $M = \eta$ or ω)

• $\pi N \rightarrow M\,N$ ($M = \eta$ or ω)

• $M\,N \rightarrow \pi N$, $\pi\pi N$ ($M = \eta$ or ω)

• $M\,N \rightarrow M\,N$ ($M = \eta$ or ω; elastic scattering)

The INCL++ cascade model also has certain limitations with respect to the bullet particle energy and type, and target-nucleus type. The supported energy range for incident nucleons and pions is 1 MeV–20 GeV. Any target nucleus starting with deuterium (^{2}H) is almost acceptable.

§ 2.3.4 Low energy neutron interactions

The neutron transport class library simulates the interactions of neutrons with kinetic energies from 0.025 eV up to 20 MeV. The upper limit of energy is set by the multipurpose evaluated neutron scattering data libraries that the simulation is based on. The interactions of neutrons at low energies are divided into four parts in a similarity with other hadronic processes in Geant4 code. Radiative capture, elastic scattering, fission, and inelastic scattering are considered as separate models. All cross-section data are taken from the ENDF/B-VI [60] evaluated data library.

The final state of elastic scattering is described by sampling the differential scattering cross-sections $\frac{d\sigma}{d\Omega}$ [42; p.507]. Two representations are supported for the normalized differential cross-section for elastic scattering. The first is a tabulation

of the differential cross-section, as a function of the cosine of the scattering angle θ and the kinetic energy E of the incoming neutron.

$$\frac{d\sigma}{d\Omega} = \frac{d\sigma}{d\Omega}(cos\theta, E) \tag{2.20}$$

In the second representation, the normalized cross-section are represented as a series of legendre polynomials $P_l(cos\theta)$, and the legendre coefficients a_l are tabulated as a function of the incoming energy of neutron.

$$\frac{2\pi}{\sigma(E)}\frac{d\sigma}{d\Omega}(cos\theta, E) = \sum_{l=0}^{n_l}\frac{2l+1}{2}a_l(E)P_l(cos\theta) \tag{2.21}$$

The final state of radiative capture is described by either photon multiplicities, or photon production cross-sections, and the discrete and continuous contributions to the photon energy spectra, along with the angular distributions of the emitted photons [42; p.509]. The photon energies E_γ are associated to the multiplicities or the cross-sections for all discrete photon emissions. For the continuum contribution, the normalized emission probability f is broken down into a weighted sum of normalized distributions g.

$$f\left(E \to E_\gamma\right) = \sum_i p_i(E) g_i\left(E \to E_\gamma\right) \tag{2.22}$$

The weights p_i are tabulated as a function of the energy E of the incoming neutron. For each neutron energy, the distributions g are tabulated as a function of the photon energy.

For neutron induced fission, taken first chance, second chance, third chance and forth chance fission into account [42; p.510]. Neutron yields are tabulated as a function of both the incoming and outgoing neutron energy. The neutron angular distributions are either tabulated, or represented in terms of an expansion in legendre polynomials, similar to the angular distributions for neutron elastic scattering.

For inelastic scattering, the currently supported final states are (nA→) nγ, np, nd, nt, n 3 He, nα, nd2α, nt2α, n2p, n2α, npα, n3α, 2n, 2np, 2nd, 2nα, 2n2α, nX, 3n, 3np, 3nα, 4n, p, pd, pα, 2p d, dα, d2α, dt, t, t2α, 3 He, α, 2α, and 3α [42; p.513].

§ 2.5 Conclusions

FLUKA is a code for calculations the transport of particles in the matter and their interactions. The program covering an extended range of applications like as accelerator physics, calorimetry, activation analysis, dosimetry, Accelerator Driven Systems, cosmic rays, neutrino physics and radiotherapy. The program can simulate with high accuracy the interaction of several tens different particles with matter, including photons and electrons from 1 keV to 1 PeV, neutrinos, muons, hadrons of energies up to 20 TeV and their antiparticles, neutrons down to 0.025 eV and heavy ions. The simulation code can also transport of polarized and optical photons, and using Combinatorial Geometry (CG) package can handle complex geometries.

Geant4 is a Monte Carlo simulation code for modelling the passage of particles through matter. It consist a full set of features including tracking, geometry, physics models and hits. The proposed physical processes cover a wide range, including hadronic, electromagnetic and optical processes, a kit of long-lived particles, elements and materials, in a wide energy range from 250 eV to several TeV. The code is developed within the framework of worldwide cooperation of physicists and software engineers. It is used in applications in nuclear physics, particle physics, accelerator design and medical physics.

The physical meanings of the following terms which using in the simulations using the Geant4 code are listed. A *track* is a snapshot of a particle at a particular point along its path. The *G4Track* class provides information about the particle's current energy, momentum, position, time and so on, as well as its mass, charge, lifetime and other quantities. A *trajectory* is a collection of track snapshots along the particle path. A *step* consists of the two endpoints which connect the

fundamental unit of propagation in space or time. The *G4Step* stores the information about the change in track properties between the two endpoints. The *process* is the implementation class of physical or navigational interaction. In the simulations the *process* is categorized by when the interaction occurs, either at the end of the step (*PostStep*) or during the step (*AlongStep*). An *event* consists of the decay or interaction of a primary particle with the target, and all subsequent interactions with the secondary particles. The *G4Event* class contain information about hits, digitization and trajectories. The *run* consists of a series of events.

CHAPTER III. EXPERIMENT ON THE NATURAL URANIUM ASSEMBLY

§ 3.1. Introduction

Accelerator Driven Systems (ADS) are suggested as a means for safe, cost-effective energy production and nuclear waste transmutation [61-64]. An ADS consists of a high current, high energy accelerator coupled with a sub-critical nuclear assembly. During the past several years, such studies have been conducted with accelerated particle beams at Nuclotron of Joint Institute for Nuclear Research (JINR) in the framework of the international collaboration "Energy plus Transmutation of Radioactive Waste". This program has carried out a large number of experiments with the subcritical uranium target QUINTA [65-72, 120-123], as well as the lead-graphite target GAMMA-3 [20; p.85, 73; p.51-58]. Several experiments were conducted using a solid lead target GENERATOR [74-76] at the proton beam of the JINR Phasotron accelerator.

^{232}Th is a fissionable material by fast neutrons, but neutron capture reaction is also important in order to study the breeding efficiency of fissile ^{233}U in a thermal-spectrum ADS. In this chapter we present experimental data and a comparison with the calculations by the FLUKA [77; p.211-214, 78] code. For thorium samples, located at the central axis of the setup QUINTA the reaction rates for generated radionuclides were measured and are presented in this chapter.

§ 3.2. Structure of the setup QUINTA

Uranium assembly "QUINTA" is presented in Fig.3.1. It consists of five sections of hexagonal shaped aluminum containers with an inscribed circular hole of diameter 28.4 cm. The containers are filled with cylindrical rods of natural uranium, having a sealed aluminum shell (external dimensions: 3.6 cm diameter, 10.4 cm in length, and 1.72 kg uranium mass). The containers are made of 5 mm thick aluminum. The first section, facing the deuteron beam contains 54 uranium rods and has a central beam window, 80 mm in diameter, installed in order to

reduce its albedo and reduce the leakage of neutrons from the target. Four subsequent sections are structurally identical and contain 61 uranium rods. The mass of the natural uranium in each of these sections is 104.92 kg, and the total mass of uranium in the entire target is 512.56 kg. The filling factor of the 2nd, 3rd, 4th, and 5th uranium sections is about 0.8, and is ~ 0.6 of the entire assembly.

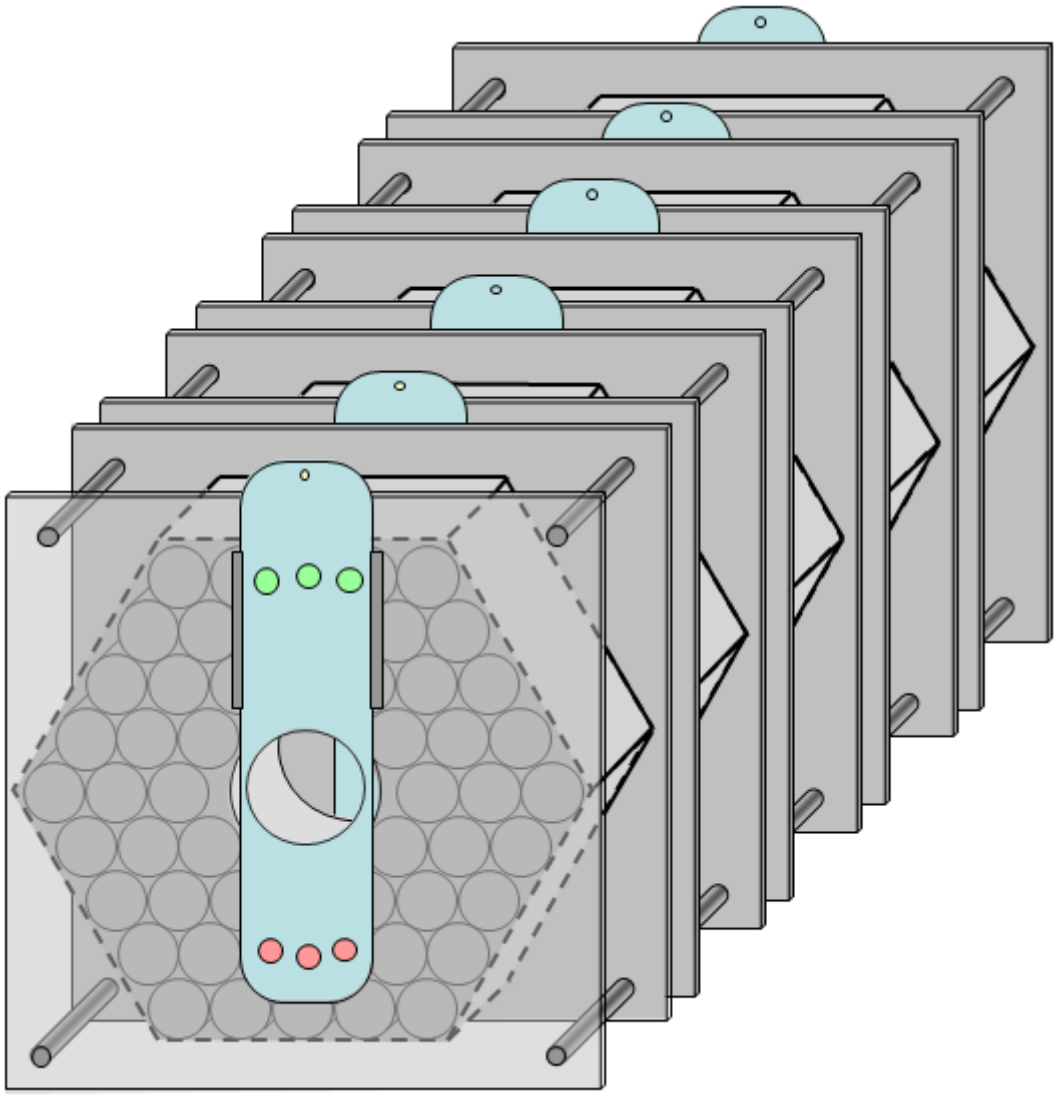

Fig.3.1. General view of the QUINTA setup.

§ 3.3. Processing of experimental data

During the experiment, the ^{232}Th samples were conventionally marked as a 9Th, 10Th, 11Th and 12Th, masses of the samples are respectively 0.1236 g,

0.1242 g, 0.1355 g and 0.1402 g. The 9Th sample was placed on the central axis of the setup QUINTA, between the first and the second section at a distance of 12.1 cm, the 10Th sample between the third and the fourth section at a distance of 25.2 cm, the 11Th sample between the third and the fourth section at a distance of 38.3 cm and 12Th sample between the fourth and the fifth section at a distance of 51.4 cm from the front end. The total number of incident deuterons colliding with the target was determined by standard method of activation of aluminum foil by reaction $^{27}Al(d,x)^{24}Na$. After an irradiation for 975 min the total number of incident deuterons to the target was 1.93(2)E+13. The technique used to determine the total number of incident deuterons on target is described in detail in Ref. [65; p.20]. The γ-ray spectra of the samples were measured with three HPGe detectors manufactured by ORTEC (two detectors with relative efficiencies of 28% and 33% and the energy resolutions of 1.9 keV and 1.8 keV, respectively, at the 1.33 MeV ^{60}Co line) and CANBERRA (one detector with a relative efficiency of 19%, and an energy resolution of 1.8 keV at the 1.33 MeV ^{60}Co line). For each sample, from 8 to 13 γ-ray spectra were measured with different time intervals and the cooling time of the first spectrum ranged from 120 to 160 min. Energy and efficiency calibrations of the detectors were performed using a set of the γ-ray standards (^{54}Mn, ^{57}Co, ^{60}Co, ^{88}Y, ^{113}Sn, ^{133}Ba, ^{137}Cs, ^{139}Ce, ^{152}Eu, ^{228}Th, ^{241}Am).

The primary analysis of the measured γ-ray spectra was performed using the DEIMOS32 code [79; p.583-587]. The program allows determining the areas under the peaks and their positions (channel number). After that, using a software package [80; p.57-61] the spectra were calibrated for energy, corrected for the detector efficiency and separate γ-ray lines of the product nuclei were identified as formed in the samples as a result of interactions with secondary neutrons, protons or deuterons. Experimental count rates of the individual γ-ray transitions were corrected for the nuclear decay during the irradiation as well as for the self-absorption for the γ-rays measured, for the geometric dimensions of the samples, for the true coincidence summing [81; p.37-48], for the beam interruptions during irradiation and the variations in intensity of the deuteron beam (based on the on-

line measurements with fast ionization chambers). All these procedures are described in detail in Refs. [23; p.159, 80; p.57-61, 82; p.53-64].

For determining the experimental reaction rates the following equation was used [23; p.159]:

$$R(A_r, Z_r) = \frac{Q(A_r, Z_r)}{N_t N_d} \quad , \tag{3.1}$$

where, $Q(A_r, Z_r)$ is the production rate of the radioactive nucleus (A_r, Z_r), N_t the number of atoms in the sample, and N_d the number of incident deuterons on the target.

§ 3.4. Experimental results and comparisons with Monte Carlo simulations

The FLUKA hadron-nucleon interaction models are based on resonance production and decay at energies below a few GeV, and on the Dual Parton model at energies above. Two models are used also in hadron-nucleus interactions. At momenta below 3-5 GeV/c the PEANUT package [83; p.277-288, 84] includes a very detailed Generalized Intra-Nuclear Cascade (GINC) and a preequilibrium stage, while at high energies the Gribov-Glauber multiple collision mechanism is included in a less refined GINC. Both modules are followed by equilibrium processes: evaporation, fission, Fermi break-up, γ-ray de-excitation [85; p.75-86, 86; p.413-426]. Inelastic cross sections for hadron-hadron interactions are represented by parameterized fits based on available experimental data [87]. For hadron-nucleus interactions, a mixture of tabulated data and parameterized fits is used [48, 88-91]. Elastic and charge exchange reactions are described by phase-shift analyses and eikonal approximation. Ion-induced nuclear interactions described for energy between 0.1 and 5 GeV/nucleon with modified Relativistic Quantum Molecular Dynamics (RQMD) model [92-94] and for energy below 0.1 GeV/nucleon with Boltzmann Master Equation (BME) theory [95-97].

In Fig.3.2, there are shown (a) the total fluence of secondary neutrons, (b) the total fluence of secondary protons and (c) the total fluence of primary and

secondary deuterons in the QUINTA setup (cut geometry from the center by Z axis is shown conditionally). By Y and Z axis shown size of the setup. Fluence was produced by one 6-GeV deuteron and averaged by axis X. In Fig.3.3, there is presented a calculated double differential fluence of secondary neutrons for the position of the thorium samples. As can be seen from the picture, biggest fluence of neutrons for sample 10Th and the smallest fluence for samples 9Th and 12Th at energies below 10 MeV and at energies above 10 MeV smallest fluence only for sample 9Th. The deuteron beam parameters used in the simulations were determined experimentally in Ref. [65; p.20]. Coordinates of center of the beam (X_C = 2.0, Y_C = -0.1) cm and FWHM-distribution ($FWHM_X$ = 3.9, $FWHM_Y$ = 3.1) cm. The dependence of reaction rate on mass of the residual isotopes for samples 9Th, 10Th, 11Th and 12Th is shown in Fig.3.4, in units of nuclei/cm^3·deuteron. The products of evaporation, fragmentation, fission (with low and high energy particles), spallation and quasi-elastic reactions in the thorium samples can be seen on the Fig.3.4.

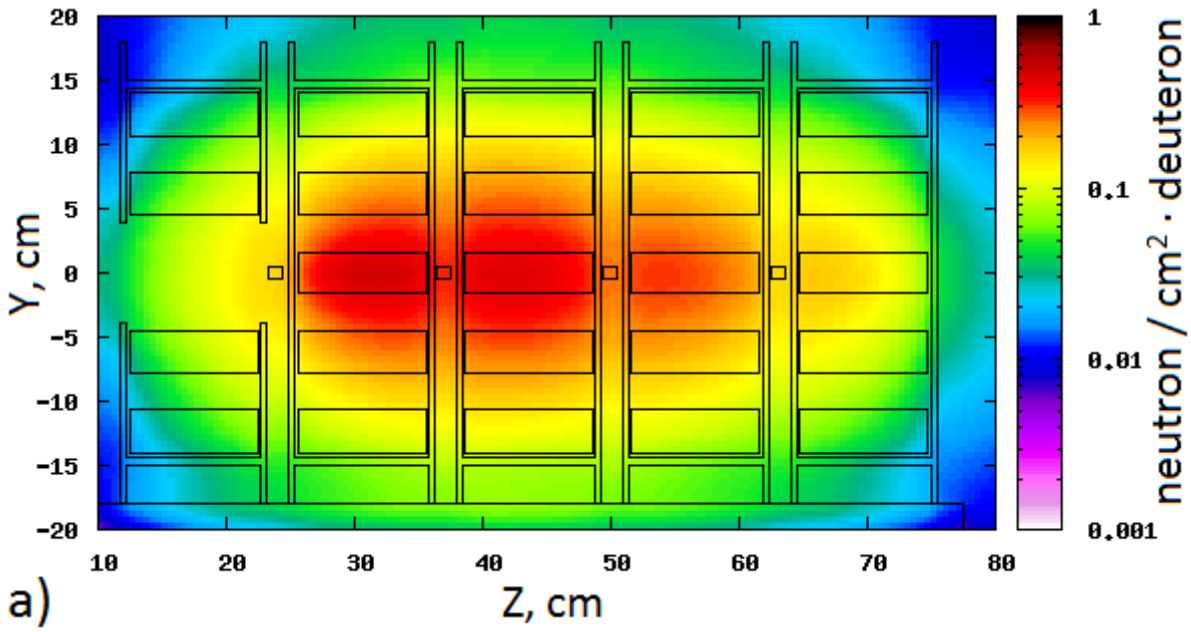

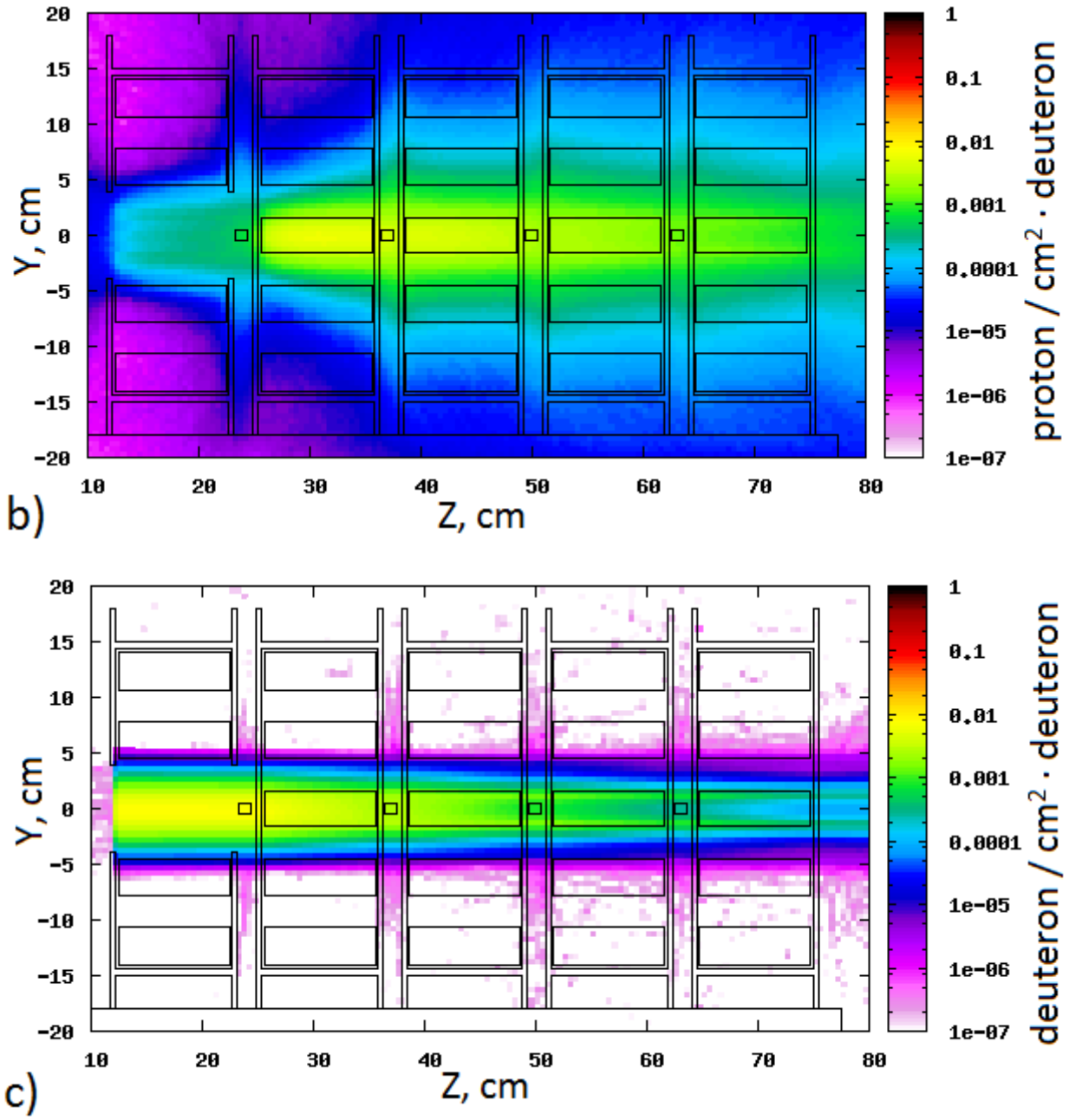

Fig.3.2. (a) total fluence of secondary neutrons, (b) total fluence of secondary protons and (c) total fluence of primary and secondary deuterons in the setup QUINTA. Shown side view of the setup geometry and cut from the center by Z axis.

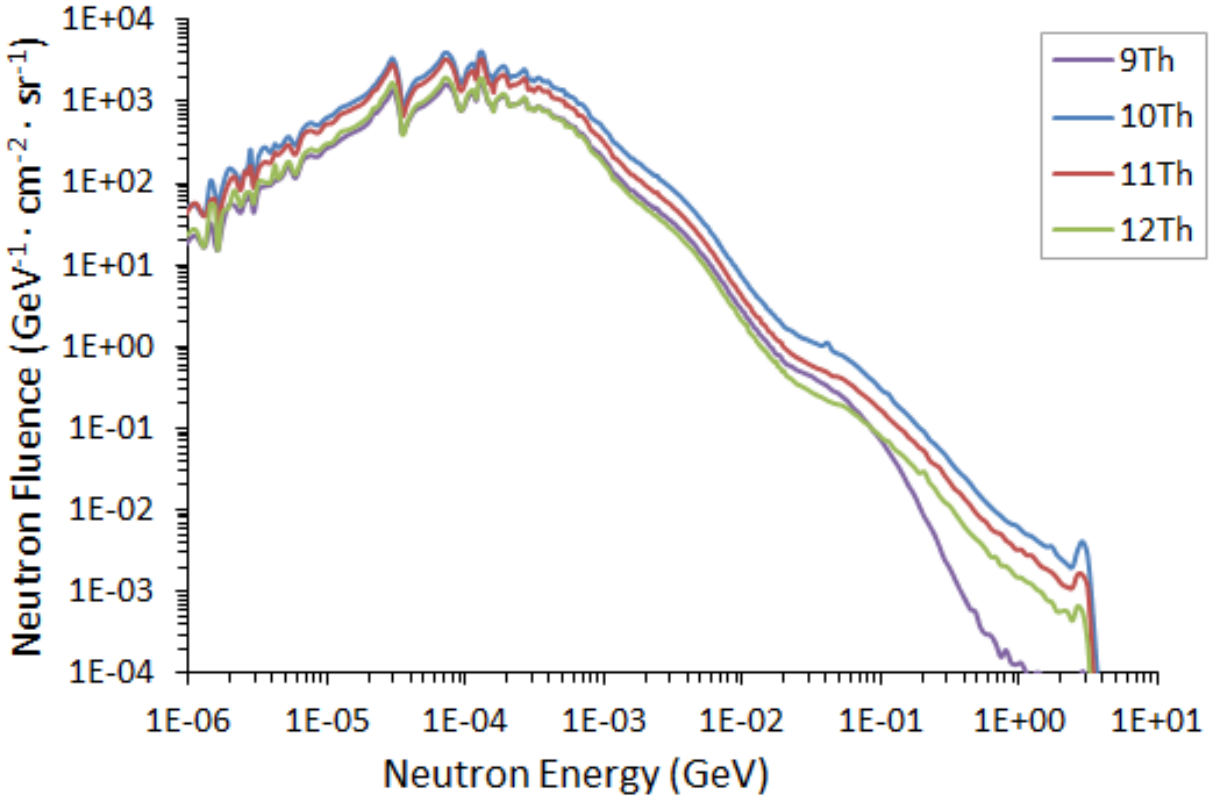

Fig.3.3. Double differential fluence of secondary neutrons for the position of the samples 9Th, 10Th, 11Th and 12Th.

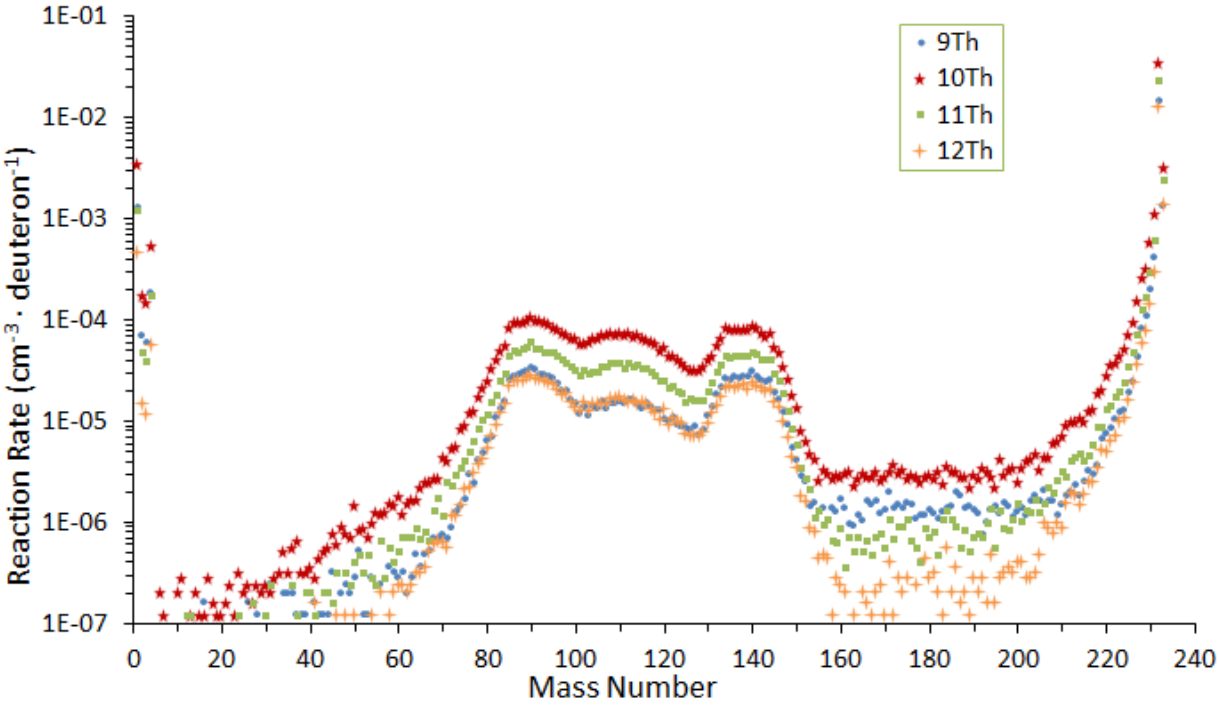

Fig.3.4. Dependence of reaction rate on mass of the residual isotopes for samples 9Th, 10Th, 11Th and 12Th.

At the results of simulations is taken detailed information about number of fission reactions in the each natural uranium cylinders of QUINTA setup. Table 3.1 gives the number of fission reactions for natural uranium cylinders per one deuteron with an energy of 6 GeV, and the cylinders were marked, as shown in Fig.3.5. The total number of fission reactions in the setup, generated by one 6 GeV deuteron is 51.3 and 14.9 fission of them generated with high energy (E > 20 MeV) particles. From the fission reactions with high energy (E > 20 MeV) particles, 0.34 fission is generated by deuterons, 1.7 fission is generated by protons, 11.3 fission is generated by neutrons, 0.37 fission is generated by positive pions and 1.22 fission is generated by negative pions. Total number of fission reactions in the 1st section is 2.7, in the 2nd section is 16.4, in the 3rd section is 16.0, in the 4th section is 10.7 and in the 5th section is 5.6. The number of fission reactions with high energy (E > 20 MeV) particles in the 1st section is 0.52, in the 2nd section is 4.96, in the 3rd section is 4.66, in the 4th section is 3.08 and in the 5th section is 1.72.

Table 3.1. Number of fission reactions for natural uranium cylinders per one deuteron with an energy of 6 GeV.

№ of cylinders	**1st section**	**2nd section**	**3rd section**	**4th section**	**5th section**
U01	1.94E-02	4.43E-02	5.63E-02	4.38E-02	2.49E-02
U02	2.56E-02	6.40E-02	8.09E-02	6.19E-02	3.50E-02
U03	3.06E-02	8.21E-02	1.03E-01	7.88E-02	4.46E-02
U04	3.18E-02	8.73E-02	1.12E-01	8.68E-02	4.98E-02
U05	2.75E-02	7.46E-02	9.84E-02	7.84E-02	4.63E-02
U06	2.30E-02	5.26E-02	6.54E-02	4.96E-02	2.79E-02
U07	3.42E-02	8.81E-02	1.07E-01	7.92E-02	4.38E-02
U08	4.39E-02	1.30E-01	1.54E-01	1.12E-01	6.15E-02
U09	5.09E-02	1.65E-01	1.97E-01	1.43E-01	7.79E-02
U10	4.85E-02	1.58E-01	1.97E-01	1.48E-01	8.44E-02

U11	3.72E-02	1.12E-01	1.47E-01	1.16E-01	6.90E-02
U12	2.33E-02	5.30E-02	6.56E-02	4.94E-02	2.76E-02
U13	4.01E-02	9.87E-02	1.16E-01	8.42E-02	4.59E-02
U14	6.23E-02	1.76E-01	1.96E-01	1.35E-01	7.12E-02
U15	7.79E-02	2.90E-01	3.06E-01	2.02E-01	1.05E-01
U16	8.35E-02	3.54E-01	3.86E-01	2.63E-01	1.39E-01
U17	6.82E-02	2.57E-01	3.13E-01	2.34E-01	1.33E-01
U18	4.49E-02	1.45E-01	1.91E-01	1.52E-01	9.09E-02
U19	2.08E-02	4.58E-02	5.65E-02	4.29E-02	2.41E-02
U20	3.66E-02	9.08E-02	1.06E-01	7.68E-02	4.16E-02
U21	6.47E-02	1.82E-01	1.95E-01	1.31E-01	6.86E-02
U22		4.22E-01	3.79E-01	2.32E-01	1.14E-01
U23		1.02E+00	7.84E-01	4.33E-01	1.99E-01
U24	1.79E-01	8.10E-01	8.28E-01	5.51E-01	2.83E-01
U25	8.23E-02	3.30E-01	4.06E-01	3.14E-01	1.87E-01
U26	4.42E-02	1.43E-01	1.91E-01	1.56E-01	9.64E-02
U27	1.59E-02	3.34E-02	4.17E-02	3.25E-02	1.87E-02
U28	2.96E-02	6.82E-02	8.23E-02	6.10E-02	3.37E-02
U29	5.54E-02	1.36E-01	1.52E-01	1.05E-01	5.59E-02
U30		3.19E-01	2.97E-01	1.86E-01	9.31E-02
U31		1.29E+00	7.75E-01	3.87E-01	1.72E-01
U32		2.71E+00	1.81E+00	8.96E-01	3.68E-01
U33	1.74E-01	7.95E-01	9.03E-01	6.56E-01	3.62E-01
U34	6.66E-02	2.46E-01	3.19E-01	2.56E-01	1.58E-01
U35	3.36E-02	1.02E-01	1.40E-01	1.18E-01	7.37E-02
U36	2.04E-02	4.52E-02	5.58E-02	4.26E-02	2.38E-02
U37	3.63E-02	8.92E-02	1.05E-01	7.62E-02	4.14E-02
U38	6.39E-02	1.79E-01	1.91E-01	1.30E-01	6.73E-02
U39		4.06E-01	3.70E-01	2.27E-01	1.12E-01
U40		9.38E-01	7.39E-01	4.16E-01	1.91E-01
U41	1.61E-01	7.59E-01	7.80E-01	5.21E-01	2.67E-01
U42	7.98E-02	3.22E-01	3.97E-01	3.06E-01	1.82E-01

U43	4.31E-02	1.40E-01	1.88E-01	1.54E-01	9.51E-02
U44	2.29E-02	5.16E-02	6.37E-02	4.81E-02	2.70E-02
U45	3.93E-02	9.68E-02	1.13E-01	8.25E-02	4.46E-02
U46	6.11E-02	1.71E-01	1.90E-01	1.32E-01	6.95E-02
U47	7.62E-02	2.76E-01	2.94E-01	1.96E-01	1.01E-01
U48	8.05E-02	3.35E-01	3.68E-01	2.52E-01	1.34E-01
U49	6.51E-02	2.46E-01	3.02E-01	2.26E-01	1.29E-01
U50	4.32E-02	1.40E-01	1.85E-01	1.48E-01	8.87E-02
U51	2.20E-02	5.02E-02	6.29E-02	4.79E-02	2.70E-02
U52	3.30E-02	8.46E-02	1.03E-01	7.66E-02	4.25E-02
U53	4.23E-02	1.24E-01	1.48E-01	1.08E-01	5.89E-02
U54	4.88E-02	1.57E-01	1.88E-01	1.37E-01	7.46E-02
U55	4.63E-02	1.50E-01	1.88E-01	1.42E-01	8.08E-02
U56	3.53E-02	1.07E-01	1.40E-01	1.12E-01	6.61E-02
U57	1.80E-02	4.11E-02	5.21E-02	4.07E-02	2.33E-02
U58	2.39E-02	5.99E-02	7.53E-02	5.80E-02	3.32E-02
U59	2.86E-02	7.63E-02	9.68E-02	7.38E-02	4.18E-02
U60	2.94E-02	8.17E-02	1.05E-01	8.15E-02	4.65E-02
U61	2.56E-02	6.94E-02	9.23E-02	7.38E-02	4.34E-02

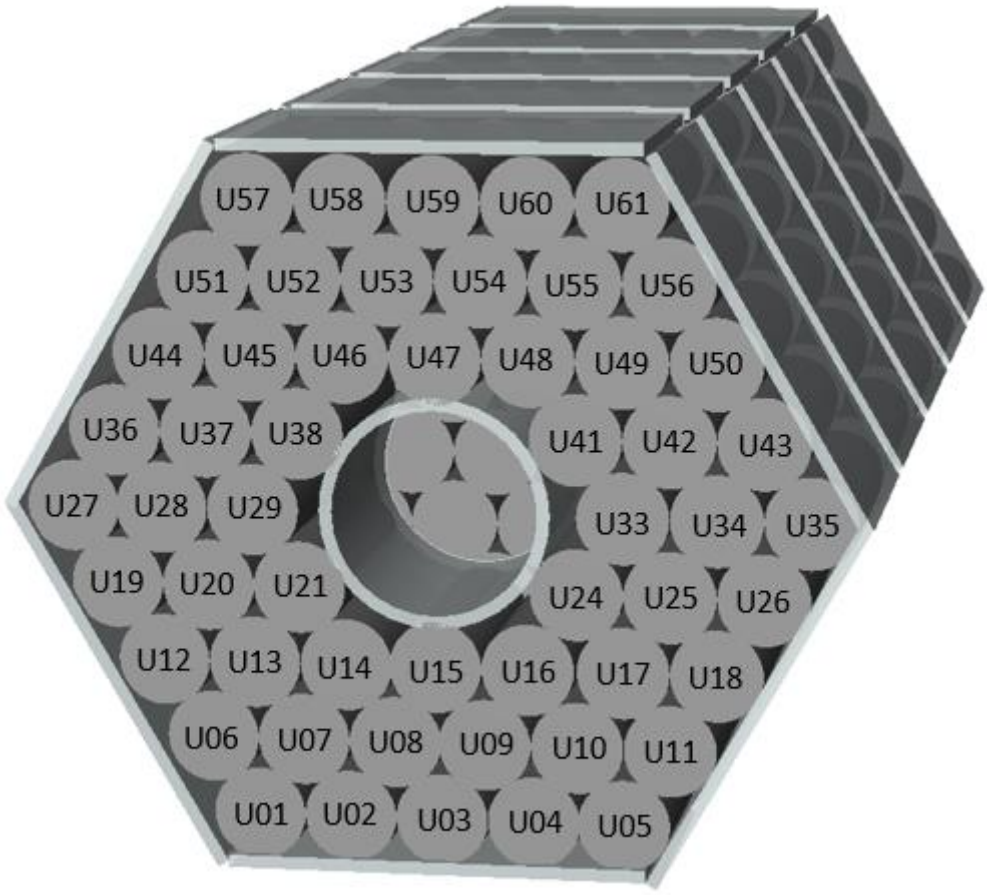

Fig.3.5. Marking of ^{nat}U cylinders of the QUINTA setup for determining the fission numbers.

In the Table A.2, there are given the cumulative reaction rates for residual radionuclides obtained from the experiment. As can be seen from the table, for sample 10Th biggest values of reaction rates for almost all residual nuclei, because of deuterons beam passes beside the 9Th sample and this sample was irradiated with secondary neutrons, and the smallest values of reaction rates for sample 12Th. ^{233}Pa is produced in the reaction ^{232}Th(n,γ)^{233}Th (β^- decay, $T_{1/2}$=22.3 min.) → ^{233}Pa (β^- decay, $T_{1/2}$=26.967 day → ^{233}U). Ratio of the weight of produced ^{233}U to ^{232}Th for sample 9Th is 1.39(4)E-12, for 10Th is 3.51(10)E-12, for 11Th is 2.39(8)E-12 and for 12Th equals 1.48(4)E-12. The obtained experimental results were compared with Monte Carlo simulations performed with the FLUKA code. Ratio of the experimental and calculated reaction rates for residual nuclei ^{233}Pa for the sample 9Th is 1.64(5), for 10Th is 1.75(5), for 11Th is 1.70(5) and for the 12Th is

1.78(5). For residual nuclei ^{231}Th, the ratio of the experimental and calculated reaction rates for sample 9Th is 1.68(19), for 10Th is 1.95(7), for 11Th is 2.32(14) and for the 12Th is 2.50(18). Ratio of the experimental and calculated cumulative reaction rates for such residual nuclei of fission reactions as ^{87}Kr, ^{88}Kr, ^{91}Sr, ^{92}Sr, ^{92}Y, ^{93}Y, ^{97}Zr, ^{103}Ru, ^{105}Ru, ^{105}Rh, ^{115}Cd, ^{128}Sb, ^{132}Te, ^{131}I, ^{132}I, ^{133}I, ^{135}I, ^{135}Xe, ^{140}Ba, ^{142}La, ^{143}Ce are in the range 1.4 – 2.8, for such residual nuclei as ^{96}Nb, ^{99}Mo, ^{113}Ag, ^{122}Sb, ^{124}Sb, ^{130}I, ^{135}Ce, ^{141}Ce are in the range 3.4 – 6.6. Ratio of the experimental and calculated total fission reaction rates for the sample 9Th is 2.69(39), for 10Th is 1.29(15), for 11Th is 1.78(19) and for the 12Th is 1.87(21). Calculations of fission reaction rates R(n,f) from the experimental data were carried out as follows. Cumulative yields Y of the fission products of ^{232}Th at a neutron energy of 14 MeV were taken from the TENDL-2011[98] library. The average values of the fission product R/Y ratios for the following nuclei: ^{85m}Kr, ^{87}Kr, ^{88}Kr, ^{91}Sr, ^{92}Y, ^{92}Sr, ^{93}Y, ^{95}Zr, ^{96}Nb, ^{97}Zr, ^{129}Sb, ^{131}I, ^{132}Te, ^{132}I, ^{132}Cs, ^{133}I, ^{134}I, ^{135}I, ^{135}Xe, ^{140}Ba, ^{141}Ce, ^{142}La and ^{143}Ce were found to be 5.57(80)E-26 for 9Th, 9.8(11)E-26 for 10Th, 6.91(73)E-26 for 11Th, and 3.50(39)E-26 for sample 12Th. These numbers are the fission reaction rates R(n,f) for ^{232}Th.

§ 3.5. Conclusions

QUINTA setup irradiated by deuterons with energy 6 GeV. Obtained experimental results were compared with the results of simulations by FLUKA code. Comparing the experimental and calculated data, we found agreement for residual nuclei ^{233}Pa, ^{231}Th and for several products of fission reactions such as ^{87}Kr, ^{88}Kr, ^{91}Sr, ^{92}Sr, ^{92}Y, ^{93}Y, ^{97}Zr, ^{99}Mo, ^{103}Ru, ^{105}Ru, ^{105}Rh, ^{115}Cd, ^{128}Sb, ^{132}Te, ^{131}I, ^{132}I, ^{133}I, ^{135}I, ^{135}Xe, ^{140}Ba, ^{142}La, ^{143}Ce. For other products of fission reactions ratio of the experimental and calculated cumulative reaction rates is above than 3. We are supposing, these ratios is depend on the yield of isotopes in fission reactions induced by high energy particles. Since for isomers, the models are not yet able to predict the ground state/metastable level(s) split.

CHAPTER IV. EXPERIMENTS ON THE NATURAL URANIUM ASSEMBLY WITH LEAD SHIELD

§ 4.1. Introduction

The ADS-related research has long been attracting attention of the international scientific community primarily due to societal concerns with the problem of the long-lived radioactive waste storage [63; p.336-367, 99] and the proposals of subcritical nuclear power plant concepts based on the uranium-thorium cycle, and controlled by high-energy particle accelerators (Accelerator Driven System(s)) [100, 101]. Such research has been actively conducted throughout the world for the last two decades at PNF (Poahng) [102; p.458], n-ToF (CERN) [103], MYRRHA (Belgium) [104] and «Energy + Transmutation» setup at JINR (Dubna) [23, 105-107]. The following programs are currently under development: SINQ (PSI) [108], KEK (Japan) [109], MYRRHA (Belgium), n-ToF (CERN), including other research programs at LANL (USA) [110]. The programs are focused on precise measurement of nuclear data and development of new materials in order to create prototypes of industrial ADS-systems.

During the past several years, such studies have been conducted with accelerated particle beams at Nuclotron of VBLHEP (Veksler and Baldin Laboratory of High Energy Physics) JINR (Dubna) in the frameworks of the international collaboration Energy plus Transmutation of Radioactive Waste. This program has carried out a large number of experiments with the subcritical uranium target "QUINTA" [65-72, 120-123], as well as the lead-graphite target "GAMMA-3" [20; p.85, 73; p.51-58]. Several experiments were conducted using a solid lead target "GENERATOR" [74-76] at the proton beam of JINR DLNP (Dzhelepov Laboratory of Nuclear Problems) Phasotron.

This chapter presents the experimental data and comparison with the calculations performed in the course of studies of ^{232}Th, ^{129}I, and ^{127}I interactions with secondary neutrons using the "QUINTA" target assembly at the deuteron

beams with energies 2, 4 and 8 GeV from the Nuclotron accelerator of the VBLHEP, JINR.

§ 4.2. Experiment

The natural uranium assembly with lead shield is presented in Fig.4.1. The assembly is surrounded by a lead shielding with a thickness of 10 cm and a weight of 2545 kg with a beam entrance window of dimensions 15 x 15 cm^2. There is a window measuring 15 x 5 cm^2 on the left side of lead shielding, near the third section, where the transmutation samples can be placed. The upper part of the lead assembly has a special hole for mounting and dismantling of detector samples as well as their installation inside the uranium assembly between sections.

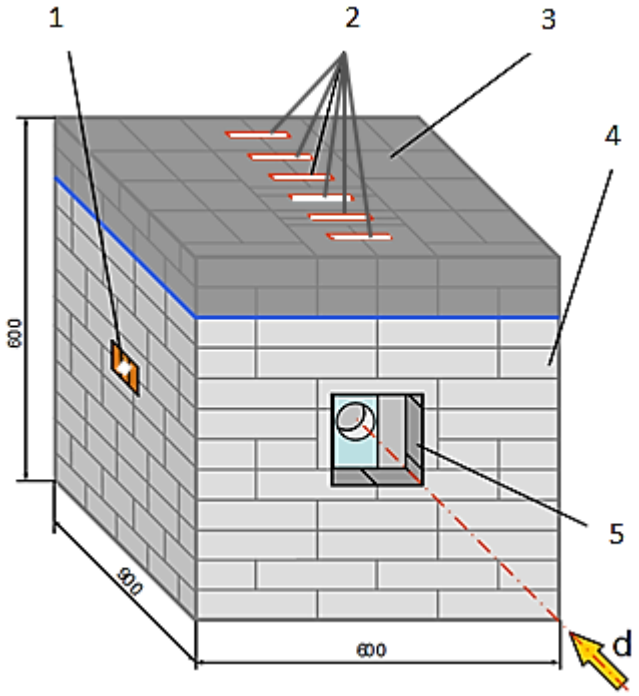

Fig.4.1. The general view of the "QUINTA" setup, where 1 – window for placement of the transmutation samples, 2 – hatches for mounting and dismantling of detector probes and installation of the samples inside the uranium assemblies between sections, 3 – lead cover assembly, 4 – the lead assembly, 5 – the 15x15-cm^2 beam input window.

In the experiments, the transmutation samples (^{127}I, ^{129}I, ^{nat}Th, ^{233}U, ^{235}U, ^{nat}U, ^{237}Np, ^{238}Pu, ^{239}Pu, and ^{241}Am) were placed inside the window 1 (see Fig. 4.1). Aluminum and copper foils were installed in front of the target to determine the integral flux of deuterons and the shape of the beam. A well-known method of activating aluminum foil through the reaction ^{27}Al(d,x)^{24}Na and copper foil through the reaction ^{nat}Cu(d,x)^{24}Na was used [65; p.20]. Table 4.1 shows the data on the conditions of irradiation and properties of the samples that were used in our studies (^{nat}Th, ^{129}I, and ^{127}I).

Table 4.1. Data on the conditions of irradiation and the properties of the samples.

Deuterons energy, GeV	2		4		8	
Irradiation time, min.	376		561		970	
Integral number of deuterons	2.90(7)E+13		2.63(8)E+13		8.77(40)E+12	
Coordinates of the center of beam, cm *	Xc	Yc	Xc	Yc	Xc	Yc
	1.5(2)	0.1(1)	1.8(1)	-0.3(1)	0.9(1)	0.1(1)
FWHM (full width at half maximum of the beam profile), cm *	$FWHM_X$	$FWHM_Y$	$FWHM_X$	$FWHM_Y$	$FWHM_X$	$FWHM_Y$
	2.0(1)	1.7(2)	1.5(2)	1.1(1)	1.0(1)	1.3(1)
Samples	Th-nat		Th-nat		Th-nat	
Mass, g.	0.975		1.000		0.249	
Diameter of samples, cm	1.3		1.3		1.3	
Samples	I-129	I-127	I-129	I-127	I-129	I-127
Mass (I-129), g.	0.591	-	0.339	-	0.218	-
Mass (I-127), g.	0.129	1.550	0.074	1.270	0.048	1.980
Mass (Na-23), g. **	0.118	0.290	0.067	0.230	0.043	0.360
Mass (Al-27), g. ***	17.6	-	17.6	-	17.6	-
Diameter of samples, cm	2.1	2.0	2.1	2.0	2.1	2.0

* The parameters of the deuteron beam were determined by fission reactions caused by deuterons in natural lead using the method of fission tracks. The lead-

mica sandwiches were placed before the first section of the QUINTA.

** ^{127}I and ^{129}I samples are constructed as NaI.

*** Container for radioactive ^{129}I.

After each session of irradiation the samples were transported to the DLNP YASNAPP-2 complex, where their γ-spectra were measured with three HPGe detectors manufactured by ORTEC (single detector efficiency is 33%, the energy resolution is 1.8 keV at line 1.33 MeV ^{60}Co) and CANBERRA (two detectors with efficiencies of 18% and 30%, the energy resolutions are 1.9 keV and 1.8 keV at the 1.33 MeV ^{60}Co line). For each sample, from 13 to 16 γ-spectra were measured with different time intervals and the cooling time of the first spectrum ranged from 79 to 157 min. Energy and efficiency calibration of the detectors was performed using a set of conventional radioactive sources (^{54}Mn, ^{57}Co, ^{60}Co, ^{88}Y, ^{113}Sn, ^{133}Ba, ^{137}Cs, ^{139}Ce, ^{152}Eu, ^{228}Th, ^{241}Am).

§ 4.3. Data analysis and calculations

The primary analysis of the measured γ-spectra was performed using the DEIMOS32 code [79; p.583-587]. The program allows determining the areas under the γ-peaks and their positions (channel number). After that, using a software package [80; p.57-61] the spectra were calibrated for energy, corrected for the detector efficiency and separate γ-lines of the product nuclei were identified as formed in the samples as a result of interactions with secondary neutrons. Experimental intensities of γ-transitions were corrected for the nuclear decay during the irradiation as well as for the self-absorption for the γ-rays measured, for the geometric dimensions of the samples, for the true coincidence summing, for the beam interruptions during irradiation and the variations in intensity of the deuteron beam (based on the on-line measurements with fast ionization chambers). All these procedures are described in detail in [23; p.159, 80; p.57-61, 82; p.53-64].

To determine the experimental values of reaction rates, equation (3.1) was

used. The values of reaction rates can also be calculated according to the following equation:

$$R(A_r, Z_r) = \int_{E_{thr}(A_r,Z_r)}^{\infty} \sigma(A_r, Z_r, E_n)\varphi(E_n)dE_n \quad (4.1)$$

where, $\sigma(A_r, Z_r, E_n)$ is the reaction cross section, and $\varphi(E_n)$ the neutron fluence. Calculations of reaction rates (Calc.1) for nuclear reactions on ^{232}Th, ^{129}I and ^{127}I isotopes were performed using the MARS15 code in the MCNP mode [111; p.50-60]. In the neutron energy range between 1 meV and 14 MeV, the corresponding reaction cross sections from ENDF/B-VI library were used. The reaction rates of neutrons above 14 MeV were simulated using the LAQGSM code version as implemented in the MARS15 code [112; p.496-501].

In addition, calculation of the neutron fluence (Calc.2) was carried out with MCNPX2.7 code [113] using the INCL4 (intranuclear cascade model) [114] and ABLA (fission-evaporation model) [115; p.635] models. For reaction (n,γ) in ^{232}Th, the reaction cross sections were calculated by the program TALYS1.6 [116], and for the (n,fission) reaction they were taken from the TENDL-2009 [117] nuclear data library. The values of the thorium fission cross sections up to 200 MeV, calculated by the program TALYS1.6 are in good agreement with the data from the TENDL-2009 and JEFF3.1.2 [118] library, as well as with the experimental data [119; p.230] (see Figure 4.2). Fig.4.3 shows the fluence of secondary neutrons at a deuteron energy of 2 GeV, calculated by the MARS15 and MCNPX-2.7 codes for the ^{232}Th sample. The reaction cross sections for (n,γ), (n,4n) and (n,6n) reactions in ^{129}I, up to 20 MeV were taken from the ENDF/B-VII library and from 20 to 1000 MeV were calculated using the TALYS1.6 program. The cross sections for (n,γ), (n,2n) and (n,4n) reactions in ^{127}I, up to 20 MeV were taken from ENDF/B-VI library, for energy range from 20 to 1000 MeV were calculated using the TALYS1.6 program.

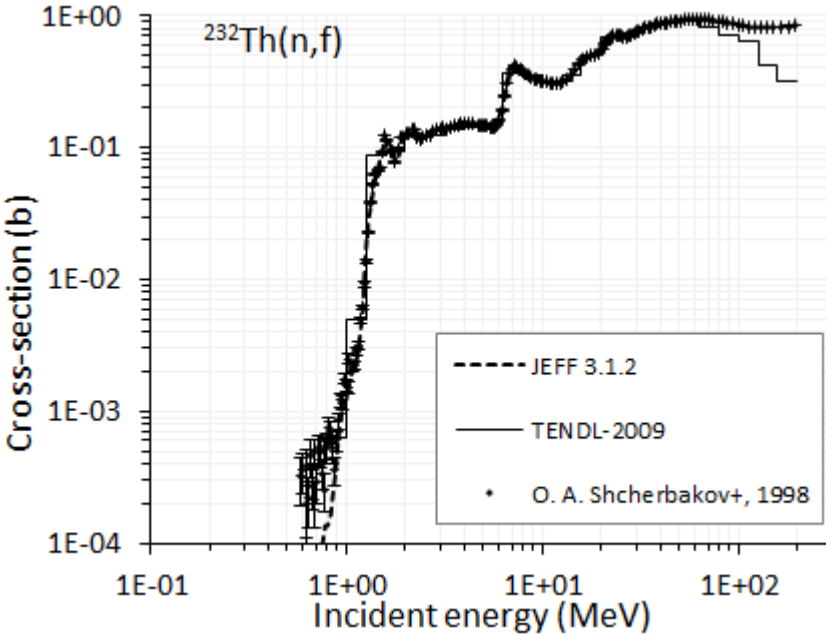

Fig.4.2. Comparison of the calculated fission cross sections of ^{232}Th with the experiment [119; p.230], as a function of the neutron energy.

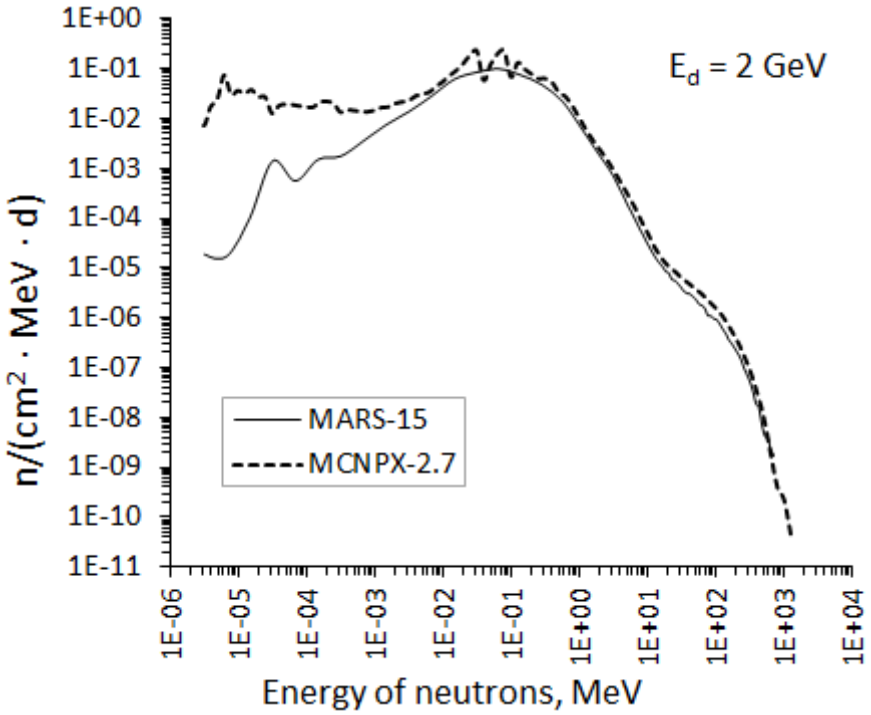

Fig.4.3. Fluence of secondary neutrons at a deuteron energy of 2 GeV, calculated using the codes MARS-15 and MCNPX-2.7 for the ^{232}Th sample.

§ 4.4. Results of reactions in ^{232}Th

Table 2 shows the results of neutron interactions in the ^{232}Th sample for all three beam energies and for all the measured nuclei (I_γ is the intensity of gamma rays (%), $T_{1/2}$(Exper) is the observed half-lives of the radionuclides, R is reaction rate, <R> is the average value of reaction rate (atoms^{-1} · deuteron^{-1})). The results show that with increasing deuteron energy the value of the reaction rates for almost all product nuclei increases too. Apparently, this growth is due to the increase of flux of secondary neutrons with increase of deuteron energy. Fig.4.4 shows the ratio of the reaction rates R(4 GeV) / R(2 GeV) and R(8 GeV) / R(2 GeV) for the several identified product nuclei of fission reactions with secondary neutrons at all three deuteron energies (2, 4, 8 GeV). Average values of the ratios R (4 GeV) / R (2 GeV) and R (8 GeV) / R (2 GeV) for the fission products of ^{232}Th are 2.19(9) and 4.72(27), respectively, and for the (n,γ) reaction the corresponding ratios are 1.95(8) and 4.71(25).

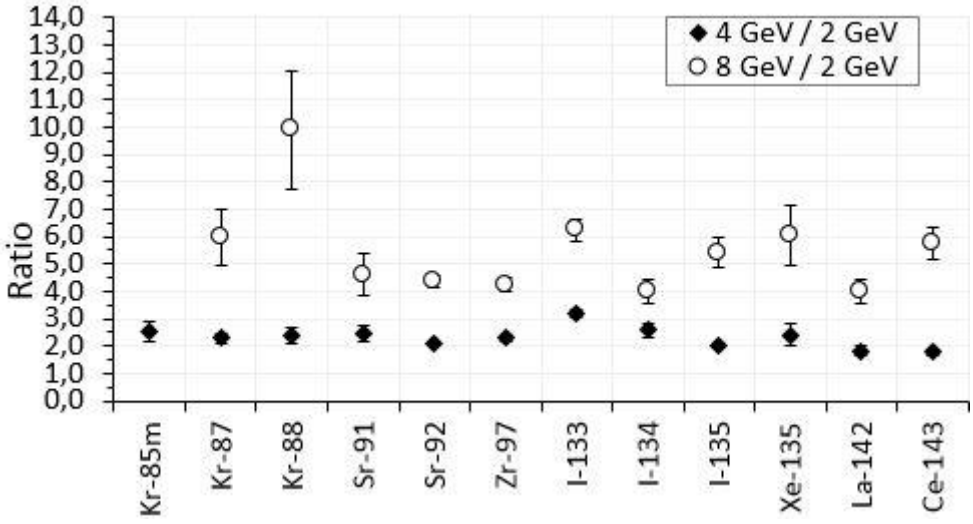

Fig.4.4. Several experimental values of the reaction rate ratios R(4 GeV) / R(2 GeV) and R(8 GeV) / R(2 GeV) for identified fission products of ^{232}Th irradiated by secondary neutrons at deuteron energies of 2, 4, and 8 GeV.

In Table B.1 there are presented the results for the following product nuclei: ^{85m}Kr, ^{87}Kr, ^{88}Kr, ^{91m}Y, ^{91}Sr, ^{92}Y, ^{92}Sr, ^{93}Y, ^{97}Nb, ^{97}Zr, ^{133}I, ^{134}I, ^{135}I, ^{135}Xe, ^{138}Cs,

^{142}La and ^{143}Ce – produced by fission of ^{232}Th; radionuclides: ^{66}Ga, ^{88}Y, ^{92m}Nb, ^{105}Ru, ^{115}Cd, ^{115m}In, ^{117}In ^{126}Sb, ^{128}Sb, ^{129}Sb, ^{132}Te and ^{132}I – products of the (n,spallation) reactions (the ratios of the reaction rates to cumulative yield R / Y for these radionuclides differs from that for fission products by a factor of 10-20). ^{233}Pa is produced in the reaction ^{232}Th(n,γ)^{233}Th (β^- decay, $T_{1/2}$=22.3 min.) → ^{233}Pa (β^- decay, $T_{1/2}$=26.967 day) → ^{233}U. Ratio of the weight of produced ^{233}U to ^{232}Th at 2 GeV is 2.90(17)E-13 at 4 GeV is 4.88(8)E-13 and at 8 GeV equals 3.93(18)E-13.

Fig.4.5 shows the experimental values of the (n,γ) and fission (n,f) reaction rates as a function of the deuteron energy in comparison with the calculations Calc.1 (MARS) and Calc.2 (MCNPX). In both cases, there is a linear increase in the reaction rate values with increasing deuteron energy.

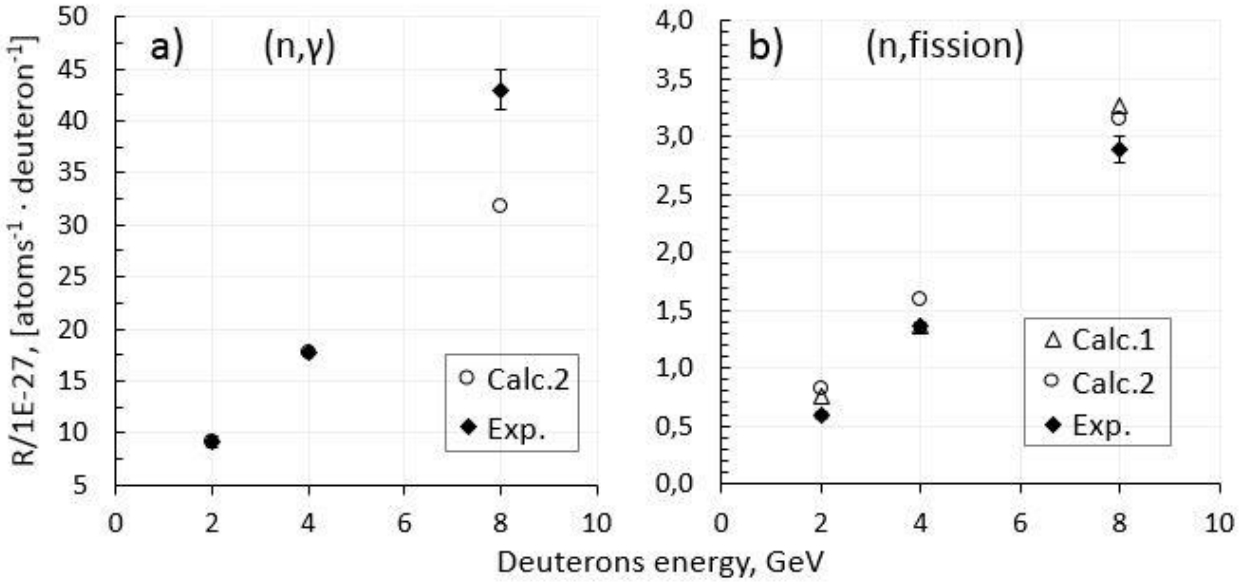

Fig.4.5. a) Comparison of experimental and calculated values of the (n,γ) reactions rate in ^{232}Th in interactions with secondary neutrons as a function of the deuteron energy (for 2 and 4 GeV, the calculated data are overlapped by experimental data). b) Comparison of experimental and calculated values for the fission (n,f) reaction rate in the interaction of ^{232}Th with secondary neutrons as a function of the deuteron energy (for 4 GeV, the calculated data Calc.1 is overlapped by experimental data).

The calculations of fission reaction rates R(n,f) from the experimental data were carried out as follows. The cumulative Y yield of fission products of ^{232}Th at a neutron energy of 0.4 MeV were taken from the JEFF3.1 library. The average values of the R/Y ratios for the following fission product nuclei: ^{85m}Kr, ^{87}Kr, ^{88}Kr, ^{91m}Y, ^{91}Sr, ^{92}Y, ^{92}Sr, ^{93}Y, ^{97}Nb, ^{97}Zr, ^{133}I, ^{134}I, ^{135}I, ^{135}Xe, ^{138}Cs, ^{142}La and ^{143}Ce were found to be 0.59(3)E-27 at 2 GeV, 1.36(4)E-27 at 4 GeV, and 2.89(12)E-27 at 8 GeV. These numbers are the rate of the fission reaction R(n,f) for ^{232}Th. The ratio (n,γ)/(n,f) for different deuteron energies are 15.5(23) at 2 GeV, 13.1(20) at 4 GeV, and 14.9(22) at 8 GeV. The calculated values (Calc.2.) for these ratios are 12.3 (2 GeV), 12.2 (4 GeV), and 11.2 (8 GeV).

§ 4.5. Results of reactions in ^{129}I

During the irradiation, samples ^{129}I (coated with aluminum, the weight of the Al shell is 17.6 g) and ^{127}I (in a shell of plexiglass, weighing 2.53 g) were installed on the side of section №3 of the uranium assembly (see Fig.4.1, point.1). In the ^{129}I samples, an impurity of the stable ^{127}I isotope was present. To account for the ^{127}I contribution, the ^{129}I samples were irradiated simultaneously with pure ^{127}I samples. In Table B.2 there are given values of the reaction rates for identified radionuclides in ^{129}I (NaI) samples. Na-22$^{a)}$ is the product of the ^{23}Na(n,2n)^{22}Na reaction. Na-22$^{b)}$ is the product of the ^{27}Al(n,α2n)^{22}Na reaction. Na-24$^{a)}$ is the product of the ^{23}Na(n,γ)^{24}Na reaction. Na-24$^{b)}$ is the product of the ^{27}Al(n,α)^{24}Na reaction. ^{22}Na was produced simultaneously in two reactions: ^{27}Al(n,α2n)^{22}Na (E_{thr}=23.35 MeV) and ^{23}Na(n,2n)^{22}Na (E_{thr}=12.96 MeV). ^{24}Na is generated in ^{27}Al(n,α)^{24}Na (E_{thr}=3.25 MeV) and ^{23}Na(n,γ)^{24}Na reactions. The fraction of ^{24}Na produced in the (n,γ) reaction at the deuteron energy of 2 GeV is 2.1 %, it is 0.9 % at 4 GeV, and 0.6 % at 8 GeV.

The ^{22}Na and ^{24}Na isotopes are mainly produced in ^{27}Al due to its large quantities. The contribution of ^{24}Na produced from ^{23}Na was calculated using the

values of reaction rates for ^{24}Na in ^{127}I sample. We assume that ^{82}Br is the product of the ^{81}Br(n,γ)^{82}Br reaction and the admixture of ^{81}Br is present in the ^{129}I sample composition. According to our estimates (Calc.2), the admixture of ^{81}Br may amount to not more than 1.5(5)% in the ^{129}I sample. ^{82}Br was not observed in the ^{127}I samples. ^{123}I, ^{124}I, and ^{126}I are the products of (n,7n), (n,6n) and (n,4n) reactions, respectively. ^{130}I is the product of (n,γ) reaction.

In Table B.3 there are given values of the reaction rates in ^{127}I for 2, 4, and 8-GeV deuteron beam energy. ^{7}Be is produced in the plexiglass (^{12}C and ^{16}O) shell of the samples. ^{22}Na and ^{24}Na are produced in (n,2n) and (n,γ) reactions on ^{23}Na. ^{118m}Sb, ^{120m}Sb and ^{122}Sb are products of (n,α6n) (E_{thr}=44.11 MeV), (n,α4n) (E_{thr}=27.42 MeV), and (n,α2n) (E_{thr}=11.23 MeV) reactions. The ^{119}Te, ^{121}Te and ^{123m}Te radionuclides are products of (n,t6n) (E_{thr}=57.56 MeV), (n,t4n) (E_{thr}=39.92 MeV), and (n,t2n) (E_{thr}=23.01 MeV) reaction, respectively. ^{120}I, ^{121}I, ^{123}I, ^{124}I, and ^{126}I are products of (n,8n) (E_{thr}=62.18 MeV), (n,7n) (E_{thr}=51.53 MeV), (n,5n) (E_{thr}=33.59 MeV), (n,4n) (E_{thr}=26.04 MeV), and (n,2n) (E_{thr}=9.22 MeV) reactions. ^{128}I is a product of (n,γ) reaction. In Fig.4.6 presented experimental values of the ratio of reaction rate R(4 GeV) / R(2 GeV) and R(8 GeV) / R(2 GeV) for ^{127}I (NaI) samples. Table 4.2 shows some results of comparing the experimental and calculated (Calc.1 and Calc.2) data in ^{127}I and ^{129}I.

The ratio of the weight of produced ^{130}I to ^{129}I under the conditions of the present experiment at 2 GeV is 1.40(3)E-13 at 4 GeV equals 2.94(6)E-13 and at 8 GeV is 1.69(4)E-13. But intensity of the deuteron beams at 2 GeV is 1.29(3)E+09, at 4 GeV is 7.81(24)E+08 and at 8 GeV is 1.51(7)E+08 deuteron/sec. If we calculate the transmutation for the conditions: 10 mA and irradiation for 30 days. It is: 2 GeV – 0.082(2)%; 4 GeV – 0.190(4)% and 8 GeV – 0.330(7)%. These calculations allow us to estimate the transmutation at high currents and irradiation time. According to Calc.1 and experimental data, 90(5)% of the transmutation ^{129}I is (n,γ) reaction at all three deuteron energies (2, 4, 8 GeV).

Table 4.3 gives detailed information on the determination of the neutron fluence and Fig.4.7 shows the experimental and calculated neutron fluence. For the

experimental determination of the neutron fluence, we used 80% of the experimental values of the reaction rate, because, Calc.2 shows that neutrons in the energy range ΔE add 80(5)% contribution to the reaction rate. Neutron fluence is determined by solving equation (2) and the values of the reaction cross sections calculated using the program TALYS1.6 for the energy range ΔE are averaged.

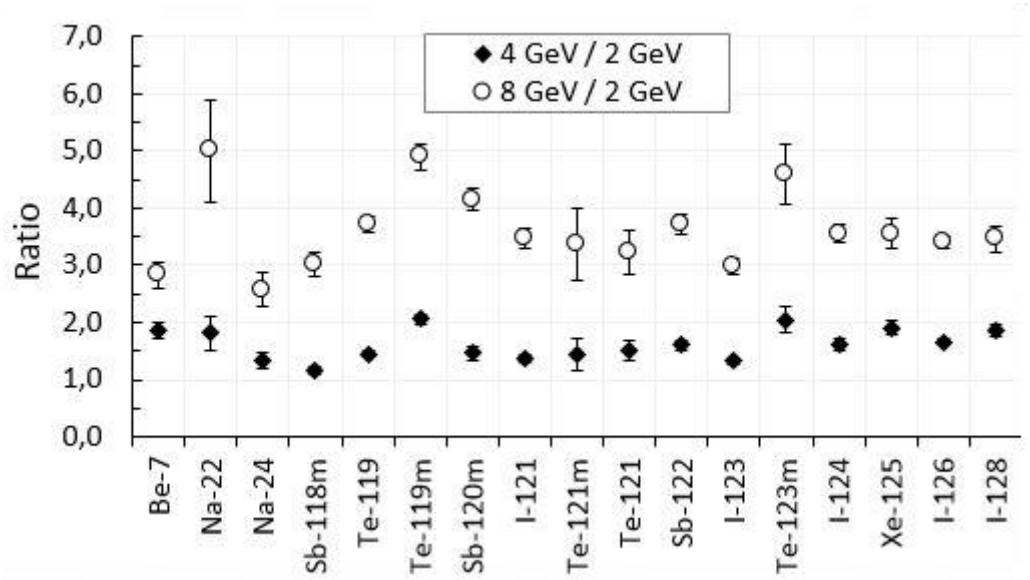

Fig.4.6. Experimental values of the reaction rate ratio R(4 GeV) / R(2 GeV) and R(8 GeV) / R(2 GeV) for ^{127}I (NaI) with secondary neutrons for product nuclei at deuteron energies 2, 4, 8 GeV.

Table 4.2. Comparison of the experimental results for the ^{127}I and ^{129}I samples with the calculations.

Nuclear reactions on ^{127}I and ^{129}I samples	**2 GeV**		**4 GeV**		**8 GeV**	
	Exp/Calc.1	**Exp/Calc.2**	**Exp/Calc.1**	**Exp/Calc.2**	**Exp/Calc.1**	**Exp/Calc.2**
^{127}I(n,γ)^{128}I		0.45(2)		0.59(2)		0.68(3)
^{127}I(n,2n)^{126}I	0.99(3)	0.59(2)	0.88(2)	0.59(2)	0.72(2)	0.54(2)
^{127}I(n,4n)^{124}I	1.17(5)	0.68(3)	1.00(8)	0.71(6)	0.90(5)	0.71(4)
^{129}I(n,γ)^{130}I		0.50(1)		0.58(1)		0.57(1)
^{129}I(n,4n)^{126}I	1.44(5)	0.73(3)	2.27(6)	1.48(4)	1.63(9)	1.23(7)
^{129}I(n,6n)^{124}I	1.98(20)	0.79(8)	2.38(17)	1.29(9)	1.35(24)	0.80(14)

Table 4.3. A detailed table for the determining of neutron fluence using the ^{127}I(n,xn) reactions. 0.8R – 80% of reaction rate R(exp.), σ – averaged values of the reaction cross sections for the energy range ΔE, F – fluence of neutrons (n/MeV·d·cm^2).

2 GeV				
Nuclear reactions	**0.8R**	**ΔE (MeV)**	**σ (b)**	**F**
^{127}I(n,8n)^{120}I				
^{127}I(n,7n)^{121}I	7.15(29)E-30	57 – 100	0.110	1.51(30)E-6
^{127}I(n,5n)^{123}I	3.16(13)E-29	38 – 73	0.249	3.63(73)E-6
^{127}I(n,4n)^{124}I	4.40(18)E-29	29 – 61	0.337	4.08(82)E-6
^{127}I(n,2n)^{126}I	1.68(6)E-28	10 – 44	0.621	8.0(16)E-6
4 GeV				
^{127}I(n,8n)^{120}I	7.20(64)E-30	66 – 120	0.050	2.65(53)E-6
^{127}I(n,7n)^{121}I	9.84(48)E-30	57 – 100	0.110	2.07(41)E-6
^{127}I(n,5n)^{123}I	4.18(22)E-29	38 – 73	0.249	4.80(96)E-6
^{127}I(n,4n)^{124}I	7.07(57)E-29	29 – 61	0.337	6.6(13)E-6
^{127}I(n,2n)^{126}I	2.80(7)E-28	10 – 44	0.621	1.33(26)E-5
8 GeV				
^{127}I(n,8n)^{120}I	1.73(14)E-29	66 – 120	0.050	6.4(13)E-6
^{127}I(n,7n)^{121}I	2.49(16)E-29	57 – 100	0.110	5.2(10)E-6
^{127}I(n,5n)^{123}I	9.44(56)E-29	38 – 73	0.249	1.08(22)E-5
^{127}I(n,4n)^{124}I	1.56(8)E-28	29 – 61	0.337	1.45(29)E-5
^{127}I(n,2n)^{126}I	5.74(16)E-28	10 – 44	0.621	2.72(54)E-5

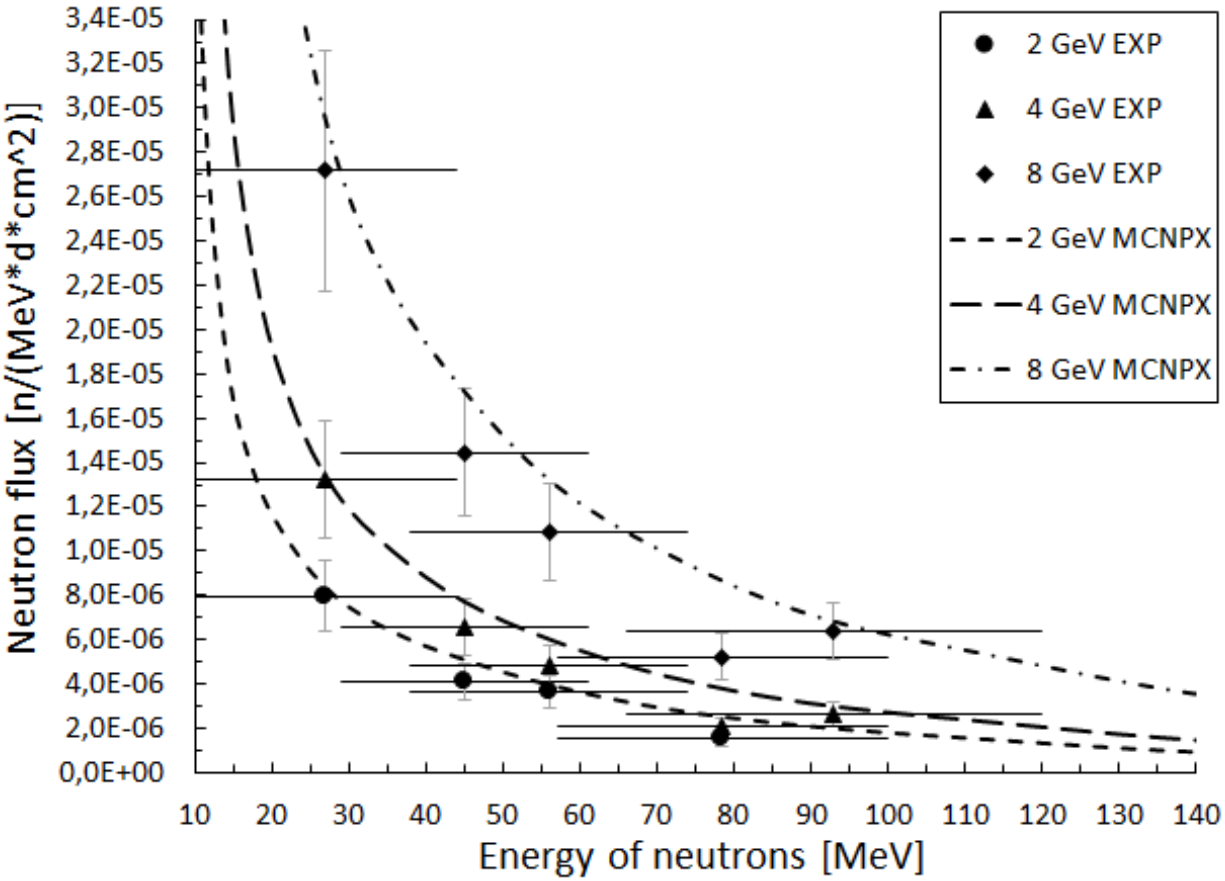

Fig.4.7. Experimental and calculated (MCNPX-2.7) values of neutron fluence.

§ 4.6. Conclusions

The QUINTA setup designed by the Energy plus Transmutation collaboration was used for the investigation of various fundamental aspects of Accelerator-Driven Systems concerning spallation and fission reactions, and transmutation of radioactive materials. The experimental data obtained in the study of the interaction of secondary neutrons with ^{232}Th, ^{129}I, ^{127}I nuclei at the QUINTA show a proportional increase in the values of reaction rate with increasing energy of deuterons, for almost all produced nuclei. The experimental results were compared with Monte Carlo simulations performed using the MCNPX2.7 and MARS15 codes. Ratios of the experimental and calculated rates of (n,γ), (n,xn) and (n,fission) reactions are in the range 0.5 – 2.4.

MAIN RESULTS AND CONCLUSIONS

According to the results of the research carried out on the theme of dissertation "Study of secondary neutron interactions with ^{232}Th, ^{129}I, and ^{127}I nuclei at the uranium assembly QUINTA irradiated by 2, 4, 6, and 8 GeV deuterons", the following conclusions are presented:

1. For the first time, an assembly from natural uranium was irradiated by deuterons with energy 6 GeV. Thorium samples were irradiated by secondary neutrons generated in the assembly. Obtained experimental results were compared with the results of simulations by FLUKA code. Comparing the experimental and calculated data, we found agreement for residual nuclei ^{233}Pa, ^{231}Th and for several products of fission reactions such as ^{87}Kr, ^{88}Kr, ^{91}Sr, ^{92}Sr, ^{92}Y, ^{93}Y, ^{97}Zr, ^{99}Mo, ^{103}Ru, ^{105}Ru, ^{105}Rh, ^{115}Cd, ^{128}Sb, ^{132}Te, ^{131}I, ^{132}I, ^{133}I, ^{135}I, ^{135}Xe, ^{140}Ba, ^{142}La, ^{143}Ce. For other products of fission reactions, the ratio of the experimental and calculated cumulative reaction rates is above than 3. We are supposing, these differences is depend on the yield of isotopes in fission reactions induced by high energy particles. But the ratios of the experimental and calculated total fission reaction rates for the thorium samples are in the range 1.29-2.69.
2. At the results of simulations is taken detailed information about number of fission reactions in the each natural uranium cylinders of QUINTA setup. The total number of fission reactions in the setup, generated by one 6 GeV deuteron is 51.3 and 14.9 fission of them generated with high energy (E > 20 MeV) particles.
3. For the first time, the natural uranium assembly with lead shield was irradiated by the deuteron beams with energies 2, 4 and 8 GeV. During the experiment, the ^{232}Th, ^{129}I, and ^{127}I samples were placed inside the window on the left side of the QUINTA setup. The experimental values of reaction rate for all measured nuclei in the ^{232}Th, ^{129}I, and ^{127}I samples irradiated by secondary neutrons at deuteron energies of 2, 4, and 8 GeV were obtained. The results show that with increasing deuteron energy the value of the reaction rates for almost all product nuclei increases too. Apparently, this growth is due to the increase of the flux of secondary neutrons with increase of deuteron energy.

4. The ratios of the experimental values of reaction rates to the calculated values for the (n,γ), (n,fission) reactions in ^{232}Th samples are in the range of 0.72-1.36, and for the (n,γ), (n,xn) reactions in ^{129}I and ^{127}I samples are in the interval 0.45-2.38.
5. For the first time, the neutron fluences in the energy range 10-120 MeV were determined using threshold (n,xn) reactions in ^{127}I samples. The experimental and calculated results agree quite well.
6. The ratio of the mass of the produced ^{130}I to the mass of ^{129}I was determined, in order to experimentally assess the possibility of transmutation by means of the ^{129}I(n,γ) reaction. The obtained data shows that it is unrealistic to transmute the products of fission reactions with currently available accelerators.

BIBLIOGRAPHY

1. APT Conceptual Design Report // LANL Report LA-UR-97-1329, April 1997.
2. Berthou V., Degueldre C., Magill J. Transmutation characteristics in thermal and fast neutron spectra: application to americium // Journal of Nuclear Materials. - Elsevier (Netherlands), 2003. –vol. 320 –p. 156–162.
3. Accelerator-driven Systems (ADS) and Fast Reactors (FR) in Advanced Nuclear Fuel Cycles – A Comparative Study // OECD/NEA report. - Austria, 2002. –p. 263-269.
4. Implications of partitioning and transmutation in radioactive waste management // IAEA-TECDOC. - Austria, 2004. –p. 100.
5. Status and Assessment Report on Actinide and Fission Product Partitioning and Transmutation // OECD/NEA report. - Austria, 1999. –p. 175.
6. Yang W.S., Kim Y., Hill R.N., Taiwo T.A., Khalil H.S. Long-Lived Fission Product Transmutation Studies // Nuclear Science and Engineering. - USA, 2004. -vol. 146 –p. 291-318.
7. Zamani M., et al., Experience gained during 10 years transmutation experiments in Dubna // Journal of Physics: Conference Series. - United Kingdom, 2006. –vol. 41 –p. 475.
8. Eriksson M., Accelerator-driven Systems: Safety and Kinetics // Doctoral Thesis, Department of Nuclear and Reactor Physics, Royal Institute of Technology. – Stockholm, 2005.
9. Adam J., et al. // Proceedings of the Conference on Nuclear Spectroscopy and Nuclear Structure. - Russia, 2001. –p. 201.
10. Balabekyan A.R., et al., Symmetric and asymmetric fission modes in proton-induced fission at 660 MeV of 238U // Physics of Atomic Nuclei. - Springer (USA), 2010. –vol. 73 –p. 1814.
11. Zavorka L., Transmutation of actinides using spallation reactions // Dissertation Thesis, Faculty of Nuclear Sciences and Physical Engineering, Czech Technical University in Prague. – Prague, 2015.

12. Majerle M., et al., MCNPX simulations of the experiments with relativistic protons directed to thick, lead targets // Nuclear Instruments and Methods in Physics Research A. - Elsevier (Netherlands), 2007. -vol. 580 –p. 110.
13. Adam J., et al., A Feasibility Study of Nonelastic Reactions in Thorium and Uranium by the Spallation Neutrons // JINR Preprint E15-2010-23. - Russia, 2010.
14. Manolopoulou M., et al., Proton and neutron production from GAMMA-2 spallation source irradiated by relativistic proton beams // Nuclear Instruments and Methods in Physics Research A. - Elsevier (Netherlands), -vol. 586 –p. 239.
15. Adam J., et al., Spallation neutron spectrum on a massive lead/paraffin target irradiated with 1 GeV protons // European Physical Journal A. - Springer (USA), 2005. –vol. 23 –p. 61.
16. Barashenkov V.S., Monte Carlo simulation of ionization and nuclear processes initiated by hadron and ion beams in media // Computer Physics Communications. - Elsevier (Netherlands), 2000. –vol. 126 –p. 28.
17. Wan J.S., et al., Transmutation of 129I and 237Np using spallation neutrons produced by 1.5, 3.7 and 7.4 GeV protons // Nuclear Instruments and Methods in Physics Research A. - Elsevier (Netherlands), 2001. –vol. 463 – p. 634.
18. Prael R.E., H. Lichtenstein, User Guide to LCS: The LAHET Code System // LA-UR-89-3014, Los Alamos National Laboratory. - USA, 1989.
19. Adam J., et al., Lead-Graphite Setup "Gamma-3" for the Study of Transmutation of Long-Lived Radionuclides at JINR LHEP Nuclotron Particle Beams // JINR Preprint P1-2010-102. - Russia, 2010.
20. Adam J., et al., A study of reaction rates of (n,f), (n,γ) and (n,2n) reactions in ^{nat}U and ^{232}Th by the neutron fluence produced in the graphite set-up (GAMMA-3) irradiated by 2.33 GeV deuteron beam // European Physical Journal A. - Springer (USA), 2011. -vol. 47 –p. 85.
21. Asquith N.L., et al., The spatial distribution of thermal and epithermal

neutrons in a graphite moderated spallation neutron field // Radiation Measurements. - Elsevier (Netherlands), 2014. –vol. 67 –p. 15.

22. Hashemi-Nezhad S.R., et al., Determination of natural uranium fission rate in fast spallation and fission neutron field: An experimental and Monte Carlo study // Nuclear Instruments and Methods in Physics Research A. - Elsevier (Netherlands), 2008. –vol. 591 –p. 517.
23. Adam J., et al., A study of nuclear transmutation of Th and ^{nat}U with neutrons produced in a Pb target and U blanket irradiated by 1.6 GeV deuterons // European Physical Journal A. - Springer (USA), 2010. –vol. 43 –p. 159.
24. Borger J.J., et al., Studies of the neutron field of the Energy plus Transmutation set-up under 4 GeV deuteron irradiation // Radiation Measurements. - Elsevier (Netherlands), 2011. –vol. 46 –p. 1765.
25. Krása A., et al., Neutron production in a Pb/U-setup irradiated with 0.7–2.5 GeV protons and deuterons // Nuclear Instruments and Methods in Physics Research A. - Elsevier (Netherlands), 2010. –vol. 615 –p. 70.
26. Hashemi-Nezhad S.R., et al., Determination of uranium fission rate in an arbitrary neutron field using fission track detectors // Radiation Measurements. - Elsevier (Netherlands), 2008. –vol. 43 –p. S204.
27. Borger J.J., et al., Spatial distribution of thorium fission rate in a fast spallation and fission neutron field: An experimental and Monte Carlo study // Nuclear Instruments and Methods in Physics Research A. - Elsevier (Netherlands), 2012. –vol. 664 –p. 103.
28. Batusov Yu.A., et al., Investigation of fast neutron spectra in the uranium assembly of the experimental setup “energy plus transmutation” in the JINR Nuclotron proton beam at an energy of 1.5 GeV // Radiation Measurements. - Elsevier (Netherlands), 2009. –vol. 44 –p. 917.
29. Capella A., Sukhatme U., Tan C.-I., Tran Thanh Van J., Dual Parton Model // Physics Reports. - Elsevier (Netherlands), 1994. –vol. 236 –p. 225.
30. Glauber R.J. and Matthiae G., High-energy scattering of protons by nuclei,

Nuclear Physics B. - Elsevier (Netherlands), 1970. –vol. 21 –p. 135.

31. Fasso A., Ferrari A., Roesler S., Sala P.R., Ballarini F., Ottolenghi A., Battistoni G., Cerutti F., Gadioli E., Garzelli M.V., Empl A., Ranft J., The physics models of FLUKA: status and recent developments // Computing in High Energy and Nuclear Physics, 24-28 March 2003. - La Jolla, California.
32. Gribov V.N., Interaction of gamma quanta and electrons with nuclei at high energies, Sovet Physics JETP. - USSR, 1970. –vol. 30 –p. 709.
33. Bertocchi L., Graphs and Glauber // Il Nuovo Cimento A. - Springer (USA), 1972. –vol. 11 –p. 45.
34. Gadioli E., Hodgson P.E., Pre-equilibrium Nuclear Reactions // Clarendon Press. - England, 1992.
35. Weisskopf V.F., Statistics and nuclear reactions // Physical Review. - USA, 1937. –vol. 52 –p. 295.
36. Serber R., Nuclear Reactions at High Energies // Physical Review. - USA, 1947. –vol. 72 –p. 1114.
37. Goldberger M., The Interaction of High Energy Neutrons and Hevy Nuclei // Physical Review. - USA, 1948. –vol. 74 –p. 1269.
38. Metropolis N., Bibins R., Storm M., Monte Carlo Calculations on Intranuclear Cascades. I. Low-Energy Studies // Physical Review. - USA, 1958. –vol. 110 –p. 185.
39. Guthrie M.P., Alsmiller R.G., Bertini H.W., Calculation of the capture of negative pions in light elements and comparison with experiments pertaining to cancer radiotherapy // Nuclear Instruments and Methods. - Elsevier (Netherlands), 1968. –vol. 66 –p. 29.
40. Griffin J.J., Statistical Model of Intermediate Structure // Physical Review Letters. - USA, 1966. –vol. 17 –p. 478-481.
41. Agostinelli S., et al., Geant4 – a simulation toolkit // Nuclear Instruments and Methods in Physics Research A. - Elsevier (Netherlands), 2003. –vol. 506 –p. 250.
42. Geant4: Physics Reference Manual (2016).

43. Alsmiller R.G., Alsmiller F.S., Hermann O.W., The high-energy transport code HETC88 and comparisons with experimental data // Nuclear Instruments and Methods in Physics Research A. - Elsevier (Netherlands), 1990. –vol. 295 –p. 337–343.
44. Titarenko Yu.E., et al., Experimental and Computer Simulations Study of Radionuclide Production in Heavy Materials Irradiated by Intermediate Energy Protons // arXiv:nucl-ex/9908012, LANL Report LA-UR-99-4489. - USA, 1999.
45. Letaw J.R., et al., Proton-nucleus total inelastic cross sections - an empirical formula for E greater than 10 MeV // The Astrophysical Journal Supplement Series. - IOP Publishing, United Kingdom, 1983. –vol. 51 –p. 271.
46. Letaw J.R., et al., Comparison of distributed reacceleration and leaky-box models of cosmic-ray abundances (Z = 3-28) // The Astrophysical Journal Supplement Series. - IOP Publishing, United Kingdom, 1993. –vol. 414 –p. 601.
47. Pearlstein S., Medium-energy nuclear data libraries: a case study, neutron- and proton-induced reactions in 56Fe // The Astrophysical Journal Supplement Series. - IOP Publishing, United Kingdom, 1989. –vol. 346 –p. 1049-1060.
48. Barashenkov V.S., Toneev V.D., High Energy interactions of particles and nuclei with nuclei // Atomizdat. - Moscow, 1972.
49. Griffin J.J., Energy dependence of average direct reaction cross sections and partial nuclear level densities // Physics Letters B. - Elsevier (Netherlands), 1967. –vol. 24 –p. 5-7.
50. Ribansky I., et al., Pre-equilibrium decay and the exciton model // Nuclear Physics A. - Elsevier (Netherlands), 1973. –vol. 205 –p. 545-560.
51. Kalbach C., Exciton Number Dependence of the Griffin Model Two-Body Matrix Element // Zeitschrift für Physik A. - Springer (USA), 1978. –vol. 287 –p. 319-322.
52. Fong P., Statistical Theory of Fission // Gordon and Breach. - New York,

1969.

53. Dostrovsky I., Zraenkel Z., Friedlander G., Monte Carlo Calculations of Nuclear Evaporation Processes. III. Applications to Low-Energy Reactions // Physical Review. - USA, 1959. –vol. 116 –p. 683-702.
54. Dostrovsky I., Fraenkel Z., Rabinowitz P., Monte Carlo Calculations of Nuclear Evaporation Processes. V. Emission of Particles Heavier Than He^4 // Physical Review. - USA, 1960. –vol. 118 –p. 791.
55. Grypeos M.E., Lalazissis G.A., Massen S.E., Panos C.P., The 'cosh' or symmetrized Woods-Saxon nuclear potential // Journal of Physics G. - IOP Publishing, United Kingdom, 1991. –vol. 17 –p. 1093.
56. Elton L.R.B., Nuclear Sizes // Oxford University Press. - Oxford, 1961.
57. DeShalit A., Feshbach H., Theoretical Nuclear Physics, Vol. 1: Nuclear Structure // USA, 1974.
58. Boudard A., et al., New potentialities of the Liège intranuclear cascade model for reactions induced by nucleons and light charged particles // Physical Review C. - USA, 2013. –vol. 87 –p. 014606.
59. Mancusi D., et al., Extension of the Liège intranuclear-cascade model to reactions induced by light nuclei // Physical Review C. - USA, 2014. –vol. 90 –p. 054602.
60. ENDF/B-VI: Cross Section Evaluation Working Group, ENDF/B-VI Summary Document, Report BNL-NCS-17541 (ENDF-201), edited by P.F. Rose, National Nuclear Data Center, Brookhaven National Laboratory, Upton. - NY, USA, 1991.
61. Grand P., Takahashi H., Breeding nuclear fuels with accelerators – replacement for breeder reactors // Nuclear Instruments and Methods in Physics Research B. - Elsevier (Netherlands), 1985. –vol.10/11 –p. 454–459.
62. Jameson R.A., Lawrence G.P., Bowman C.D., Accelerator-driven transmutation technology for incinerating radioactive waste and for advanced application to power production // Nuclear Instruments and Methods in Physics Research B. - Elsevier (Netherlands), 1992. –vol. 68 –p.

474–480.

63. Bowman C.D., Arthur E.D., Lisowski P.W., Lawrence G.P., Jensen R.J., Anderson J.L., Blind B., Cappiello M., Davidson J.W., England T.R., Engel L.N., Haight R.C., Hughes III H.G., Ireland J.R., Krakowski R.A., LaBauve R.J., Letellier B.C., Perry R.T., Russell G.J., Staudhammer K.P., Versamis G., Wilson W.B., Nuclear energy generation and waste transmutation using an accelerator-driven intense thermal neutron source // Nuclear Instruments and Methods in Physics Research A. - Elsevier (Netherlands), 1992. –vol. 320 –p. 336–367.
64. Carminati F., Klapisch R., Revol J.P., Roche Ch., Rubio J.A., Rubbia C., An energy amplifier for cleaner and inexhaustible nuclear energy production driven by a particle beam accelerator // Tech. rep. CERN/AT/93-47. - Switzerland, 1993.
65. Коллаборация «Энергия и трансмутация радиоактивных отходов». Исследование пространственных распределений реакций деления и радиационного захвата нейтронов в массивной урановой мишени, облучаемой дейтронами с энергией 1-8 ГэВ (установка «Квинта») // Препринт ОИЯИ, Р1-2012-147. - Дубна, 2012, 20 с.
66. Asquith N.L., Hashemi-Nezhad S.R., Tyutyunnikov S., Kadykov M., Chilap V., Adam J., Furman W., Activation of ^{197}Au and ^{209}Bi in a fast spectrum sub-critical assembly composed of 500 kg natural uranium irradiated with 1 and 4 GeV deuterons // Annals of Nuclear Energy. - Elsevier (Netherlands), 2014. –vol. 63 –p. 742–750.
67. Furman W.I., Adam J., Baldin A., et al., Recent results of the study of ADS with 500 kg natural uranium target assembly QUINTA irradiated by deuterons with energies from 1 to 8 GeV at JINR NUCLOTRON // Proceedings of Science, XXI International Baldin Seminar on High Energy Physics Problems, September 10-15, 2012, Dubna, PoS (Baldin ISHEP XXI) 086.
68. Zavorka L., Adam J., Furman W.I., et al., A Summary of the Experimental

Results on Reactions in the Uranium Samples Irradiated with a Deuteron Beam of Energies up to 8 GeV at the QUINTA Target // Proceedings of Science, XXI International Baldin Seminar on High Energy Physics Problems, September 10-15, 2012, Dubna, PoS (Baldin ISHEP XXI) 089.

69. Suchopár M., Wagner V., Vrzalová I., et al., Monte-Carlo simulations of natural uranium setups irradiated with relativistic deuterons by means of MCNPX code // Proceedings of Science, XXI International Baldin Seminar on High Energy Physics Problems, September 10-15, 2012, Dubna, PoS (Baldin ISHEP XXI) 091.
70. Zavorka L., Adam J., Artiushenko M., Baldin A.A., Brudanin V.B., Bukhal O., Caloun P., Chilap V.V., Furman W.I., Husak K., Kadykov M.G., Katovsky K., Khushvaktov J., Marin I.I., Pronskikh V.S., Solnyshkin A.A., Sotnikov V., Stegailov V.I., Suchopar M., Svoboda O., Tsoupko-Sitnikov V.M., Tyutyunnikov S.I., Voronko V., Vrzalova J., Wagner V., Zhivkov P., Zhuk I., Validation of Monte Carlo simulation of neutron production in a spallation experiment // Annals of Nuclear Energy. - Elsevier (Netherlands), 2015. –vol. 80 –p. 178–187.
71. Zavorka L., Adam J., Baldin A.A., Caloun P., Chilap V.V., Furman W.I., Kadykov M.G., Khushvaktov J., Pronskikh V.S., Solnyshkin A.A., Sotnikov V., Stegailov V.I., Suchopar M., Tsoupko-Sitnikov V.M., Tyutyunnikov S.I., Voronko V., Vrzalova J., Neutron-induced transmutation reactions in ^{237}Np, ^{238}Pu, and ^{239}Pu at the massive uranium spallation target // Nuclear Instruments and Methods in Physics Research B. - Elsevier (Netherlands), 2015. –vol. 349 –p. 31–38.
72. Suchopár M., Wagner V., Svoboda O., Vrzalová J., Chudoba P., Kugler A., Adam J., Závorka L., Baldin A., Furman W., Kadykov M., Khushvaktov J., Solnyshkin A., Tsoupko-Sitnikov V., Tyutyunnikov S., Cross-section studies of relativistic deuteron reactions on copper by activation method // Nuclear Instruments and Methods in Physics Research B. - Elsevier (Netherlands), 2015. –vol. 344 –p. 63–69.

73. Asquith N.L., Hashemi-Nezhad S.R., Westmeier W., Zhuk I., Tyutyunnikov S., Adam J., Study of ^{232}Th(n,γ) and ^{232}Th(n,f) reaction rates in a graphite moderated spallation neutron field produced by 1.6 GeV deuterons on lead target // Nuclear Instruments and Methods in Physics Research B. - Elsevier (Netherlands), 2015. –vol. 344 –p. 51–58.
74. Majerle M., Adam J., Čaloun P., Gustov S.A., Henzl V., Henzlová D., Kalinnikov V.G., Krivopustov M.I., Krása A., Křížek F., Kugler A., Mirokhin I.V., Solnyshkin A.A., Tsoupko-Sitnikov V.M., Wagner V., Spallation experiment on thick lead target: analysis of experimental data with Monte Carlo codes // Preprint JINR, E15-2008-94. - Russia, 2008.
75. Adam J., Balabekyan A., Brandt R., et al., Investigation of the formation of residual nuclei in reactions induced by 660 MeV protons interacting with the radioactive ^{237}Np, ^{241}Am and ^{129}I targets // Journal of Nuclear Science and Technology. - Japan, 2002. –vol. 39 –p. 272-275.
76. Henzl V., Henzlova D., Kugler A., Wagner V., Adam J., Caloun P., Kalinnikov V.G., Krivopustov M.I., Pavliouk A.V., Stegajlov V.I., Tsoupko-Sitnikov V.M., Westmeier W., Transmutation of ^{129}I with high energy neutrons produced in spallation reactions induced by protons in massive target // Journal of Nuclear Science and Technology. - Japan, 2002. –vol. 39 –p. 1248-1251.
77. Böhlen T.T., Cerutti F., Chin M.P.W., Fassò A., Ferrari A., Ortega P.G., Mairani A., Sala P.R., Smirnov G., Vlachoudis V., The FLUKA Code: Developments and Challenges for High Energy and Medical Applications // Nuclear Data Sheets. - Elsevier (Netherlands), 2014. –vol. 120 –p. 211-214.
78. Ferrari A., Sala P.R., Fasso` A., Ranft J., FLUKA: a multi-particle transport code, CERN-2005-10 (2005), INFN/TC_05/11, SLAC-R-773. - Switzerland, 2005.
79. Frana J., Program DEIMOS32 for gamma-ray spectra evaluation // Journal of Radioanalytical and Nuclear Chemistry. - Springer (USA), 2003. –vol. 257 –p. 583-587.

80. Адам И., Пронских В.С., Балабекян А.Р., Калинников В.Г., Мразек Я., Приемышев А.Н., Франа Я., Система программ и дополнения к методу активационного анализа для определения сечений ядерных реакций, // Измерительная техника. 2001. №1. P.57-61. // Препринт ОИЯИ. P10-2000-28. – Дубна.
81. Sudár S., “TRUECOINC”, a software utility for calculation of the true coincidence correction // IAEA-TECDOC-1275, p. 37–48. - Austria, 2002.
82. Адам И., Балабекян А., Барашенков В.С., и др., Исследование образования продуктов протон-ядерных реакций в мишени ^{129}I при энергии протонов 660 МэВ // Письма в ЭЧАЯ. 2004. Т.1. № 4(121). С. 53-64.
83. Ferrari A., Sala P.R., A new model for hadronic interactions at intermediate energies for the FLUKA code // Proc. MC93 Int. Conf. on Monte Carlo Simulation in High Energy and Nuclear Physics, Tallahassee (Florida), 22-26 February 1993. Ed. by Dragovitsch P., Linn S.L., Burbank M., World Scientific. - Singapore 1994, p. 277-288.
84. Ferrari A., Sala P.R., The Physics of High Energy Reactions // Proc. Workshop on Nuclear Reaction Data and Nuclear Reactors Physics, Design and safety International Centre for Theoretical Physics. - Miramare-Trieste, Italy, 15 April - 17 May 1996.
85. Ferrari A., Ranft J., Roesler S., Sala P.R., The production of residual nuclei in peripheral high energy nucleus-nucleus interactions // Zeitschrift für Physik C. - Springer (USA), 1996. –vol. 71 –p. 75-86.
86. Ferrari A., Ranft J., Roesler S., Sala P.R., Cascade particles, nuclear evaporation, and residual nuclei in high energy hadron-nucleus interactions // Zeitschrift für Physik C. - Springer (USA), 1996. –vol. 70 –p. 413-426.
87. Nakamura K., et al. (Particle Data Group) // Journal of Physics G. - IOP Publishing, United Kingdom, 2010. –vol. 37 –p. 075021.
88. Möhring H.J., Hadron-nucleus inelastic cross-sections for use in hadron cascade calculations at high energies // CERN TIS-RP/116. - Switzerland,

1983.

89. Qing-biao Shen, Systematics of intermediate energy proton nonelastic and neutron total cross section // IAEA Report INDC(CPR)-020. - Austria, 1991.
90. Prael R.E., Ferrari A., Tripathi R.K., Polanski A., Comparison of nucleon cross section parameterization methods for medium and high energies // Proc. 4th Workshop on Simulating Accelerator Radiation Environments (SARE4), 14-16 September 1998. - Knoxville (USA).
91. Prael R.E., Ferrari A., Tripathi R.K., Polanski A., Plots supplemental to: "Comparison of nucleon cross section parameterization methods for medium and high energies" // Los Alamos report LA-UR-98-5843. - USA, 1998.
92. Sorge H., Stöcker H., Greiner W., Poincarè invariant Hamiltonian dynamics: Modelling multi-hadronic interactions in a phase space approach // Annals of Physics. - Elsevier (Netherlands), 1989. –vol. 192 –p. 266-306.
93. Sorge H., Stöcker H., Greiner W., Relativistic quantum molecular dynamics approach to nuclear collisions at ultrarelativistic energies // Nuclear Physics A. - Elsevier (Netherlands), 1989. –vol. 498 –p. 567-576.
94. Sorge H., Flavor production in Pb(160A GeV) on Pb collisions: Effect of color ropes and hadronic rescattering // Physical Review C. - USA, 1995. –vol. 52 –p. 3291-3314.
95. Cavinato M., Fabrici E., Gadioli E., Gadioli Erba E., Galbiati E., Monte Carlo calculations using the Boltzmann Master Equation theory of nuclear reactions // Physics Letters B. - Elsevier (Netherlands), 1996. –vol. 382 –p. 1-5.
96. Cavinato M., Fabrici E., Gadioli E., Gadioli Erba E., Riva G., Monte Carlo calculations of heavy ion cross-sections based on the Boltzmann Master equation theory // Nuclear Physics A. - Elsevier (Netherlands), 2000. –vol. 679 –p. 753-764.
97. Cerutti F., Battistoni G., Capezzali G., Colleoni P., Ferrari A., Gadioli E., Mairani A., Pepe A., Low energy nucleus-nucleus reactions: the BME

approach and its interface with FLUKA // Proc. 11th International Conference on Nuclear Reaction Mechanisms. - Varenna (Italy) June 12-16, 2006.

98. TENDL-2011, Nuclear data library www.talys.eu/.
99. Janssen A.J., Transmutation of fission products in reactors and Accelerator-Driven Systems // ECN-R-94-001. - Netherlands, 1994.
100. Rubbia C., Rubio J.A., et al. Conceptual design of a fast neutron operated high power energy amplifier // CERN/AT/95-44 (ET). - Switzerland, 1995.
101. Thorium Fuel Cycle – Potential Benefits and Challenges // IAEA-TECDOC-1450. - Austria, 2005.
102. Kim G.N., et al., Measurement of photoneutron spectrum at Pohang Neutron Facility // Nuclear Instruments and Methods A. - Elsevier (Netherlands), 2002. –vol. 485 –p. 458.
103. https://ntof-exp.web.cern.ch/ntof-exp/
104. http://sckcen.be/en/Technology_future/MYRRHA
105. Krivopustov M.I., Pavlyuk A.V., Malakhov A.I., et al. About the first experiment on investigation of ^{129}I, ^{237}Np, ^{238}Pu and ^{239}Pu transmutation at the Nuclotron 2.52 GeV deuteron beam in neutron field generated in U/Pb assembly “Energy plus Transmutation” // Journal of Radioanalytical and Nuclear Chemistry. - Springer (USA), 2009. –vol. 279 –p. 567–584 // Preprint JINR E1-2007-7. - Dubna. 2007.
106. Adam J., Katovsky K., Balabekyan A., et al. Transmutation of ^{129}I, ^{237}Np, ^{238}Pu, ^{239}Pu and ^{241}Am Using Neutrons Produced in Target-Blanket System “Energy plus Transmutation” by relativistic Protons // Pramana Journal of Physics. - India, 2007. –vol.68 –p. 201-212.
107. Adam J., Katovsky K., Balabekyan A., et al. Transmutation of ^{129}I, ^{237}Np, ^{239}Pu and ^{241}Am Using Neutrons Produced in Pb-Target with ^{nat}U Blanket System “Energy plus Transmutation” Bombarded by 2.0 GeV Relativistic Protons // Proc. of the International Conference on Nuclear Data and technology. - USA, 2005. –vol.2 –p. 1560-1562.

108. https://www.psi.ch/sinq/

109. https://www.kek.jp/en/index.html

110. http://lansce.lanl.gov/facilities/index.php

111. Mokhov N.V., et al., Technical Report FERMILAB-CONF-12-635-APC, 2012; Mokhov N.V., et al., Fermilab Report Fermilab-FN-628, 1995; Mokhov N.V., et al., AIP Conf. Proc. 896, 2007. P.50-60; https://mars.fnal.gov/

112. Mokhov N., Aarnio P., Eidelman Yu., Gudima K., Konobeev A., Pronskikh V., Rakhno I., Striganov S., Tropin I., MARS15 code developments driven by the intensity frontier needs // Progress in Nuclear Science and Technology. - USA, 2014. –vol. 4 –p. 496-501. // FERMILAB-CONF-12-635-APC.

113. Pelowitz D.P., MCNPX User's Manual: Version 2.5.0, Technical Report, LA-CP- 05-0369. - Los Alamos National Laboratory and University of California, 2005.

114. Boudard A., Cugnon J., Leray S., Volant C., Intranuclear cascade model for a comprehensive description of spallation reaction data // Physical Review C. - USA, 2002. –vol.66, 044615.

115. Junghans A.R., et al. Projectile-fragment yields as a probe for the collective enhancement in the nuclear level density // Nuclear Physics A. - Elsevier (Netherlands), 1998. –vol. 629 –p. 635.

116. Koning A., Hilaire S., Goriely S., TALYS-1.6 User Manual: Technical Report, NL-1755 ZG. - Netherlands, 2013.

117. TENDL-2009, Nuclear data library http://www.talys.eu/tendl-2009/

118. JEFF3.1.2, Nuclear data library https://www.oecd-nea.org/dbforms/data/eva/evatapes/jeff_31/JEFF312/.

119. Shcherbakov O.A., Donets A.Y., Evdokimov A.V., Fomichev A.V., Fukahori T., Hasegawa A., Laptev A.B., Maslov V.M., Petrov G.A., Tuboltsev Y.V., Vorobiev A.S., Neutron-Induced Fission of ^{233}U, ^{238}U, ^{232}Th, ^{239}Pu, ^{237}Np, ^{nat}Pb and ^{209}Bi Relative to ^{235}U in the Energy Range 1-200 MeV // Journal of Nuclear Science and Technology. - Japan, 2002. –vol. 39 –p. 230.

120. Khushvaktov J., Adam J., Baldin A.A., Chilap V.V., Furman V.I., Sagimbaeva F., Solnyshkin A.A., Stegailov V.I., Tichy P., Tsoupko-Sitnikov V.M., Tyutyunnikov S.I., Vespalec R., Vrzalova J., Yuldashev B.S., Wagner V., Zavorka L., Zeman M. Interactions of secondary particles with thorium samples in the setup QUINTA irradiated with 6 GeV deuterons //Nuclear Instruments and Methods in Physics Research B. - Elsevier, 2016. vol.381. pp. 84-89.
121. Adam J., Chilap V.V., Furman V.I., Kadykov M.G., Khushvaktov J., Pronskikh V.S., Solnyshkin A.A., Stegailov V.I., Suchopar M., Tsoupko-Sitnikov V.M., Tyutyunnikov S.I., Vrzalova J., Wagner V., Zavorka L. Study of secondary neutron interactions with ^{232}Th, ^{129}I, and ^{127}I nuclei with the uranium assembly “QUINTA” at 2, 4, and 8 GeV deuteron beams of the JINR Nuclotron accelerator //Applied Radiation and Isotopes. - Elsevier, 2016. vol.107. pp. 225-233.
122. Khushvaktov J.H., Adam J., Baldin A.A., Furman W.I., Gustov S.A., Kish Yu.V., Solnyshkin A.A., Stegailov V.I., Svoboda J., Tichy P., Tsoupko-Sitnikov V.M., Tyutyunnikov S.I., Vespalec R., Vrzalova J., Wagner V., Yuldashev B.S., Zavorka L., Zeman M. Monte Carlo simulations and experimental results on neutron production in the uranium spallation target QUINTA irradiated with 660 MeV protons //Applied Radiation and Isotopes. - Elsevier, 2018. vol.137. pp. 102-107.
123. Adam J., Baldin A.A., Chilap V., Furman W., Katovsky K., Khushvaktov J., Kumar V., Pronskikh V., Mar’in I., Solnyshkin A., Suchopar M., Tsupko-Sitnikov V., Tyutyunnikov S., Vrzalova J., Wagner V., Zavorka L. Measurement of the high energy neutron flux on the surface of the natural uranium target assembly QUINTA irradiated by deuterons of 4 and 8 GeV energy //Physics Procedia. - Elsevier, 2015. vol.80. pp. 94-97.
124. Balabekyan A.R., Demekhina N.A., Karapetyan G.S., Drnoyan D.R., Zhemenik V.I., Adam J., Zavorka L., Solnyshkin A.A., Tsoupko-Sitnikov V.M., Khushvaktov J., Karayan L., Guimarães V., Deppman A., Garcia F.

Target residues formed in the 4.4 GeV deuteron-induced reaction on gold //Physical Review C. - American Physical Society (USA), 2014. vol. 90. id. 054612.

Appendix A.

Table A.1.

Experimental obtained cumulative reaction rates for residual radionuclides.

Residual nuclei	**Reaction rate (atom^{-1} deuteron^{-1})**			
	9Th	**10Th**	**11Th**	**12Th**
Be-7		9.0(11)E-27		
Na-22		7.5(16)E-27		
Na-24	1.47(5)E-27	1.00(2)E-27	3.78(22)E-28	1.25(18)E-28
Mg-28	6.44(48)E-28			
S-38	2.73(61)E-28			
Ar-41			5.00(71)E-28	
K-42	6.11(95)E-28			
K-43	2.09(9)E-27	4.01(5)E-28	2.84(25)E-28	1.08(4)E-27
Sc-43		7.8(14)E-28		
Ca-47		2.07(31)E-28		
Sc-47		5.51(52)E-28		
Sc-48	3.71(25)E-28			
V-48		1.05(18)E-27		
Mn-52		1.90(49)E-27		
Mn-56	1.33(25)E-27			
Ni-56		7.8(36)E-28		
Fe-59		7.5(11)E-28		
Ga-66	9.7(27)E-28	1.22(22)E-27		3.48(43)E-28
Ge-66				1.57(28)E-27
Zn-69m	3.07(18)E-28	3.03(16)E-28	2.22(15)E-28	7.9(11)E-29
As-70		1.50(27)E-27	1.65(29)E-27	
Zn-71m		2.39(24)E-28		
As-71	1.97(19)E-28			
As-72		1.84(70)E-27	6.2(11)E-28	
Ga-72		8.8(19)E-28	1.02(13)E-28	
Ga-73		1.12(19)E-27		
Se-73		1.87(29)E-28		
As-74	7.3(10)E-28	2.10(36)E-27		

As-76		9.77(68)E-28		
Br-76		6.17(96)E-28	2.97(27)E-28	
Ge-77		1.01(14)E-27	4.46(62)E-28	1.43(33)E-28
As-78	7.8(13)E-28			
Rb-81		3.91(29)E-28		
Br-82		9.61(34)E-28	6.78(65)E-28	
Rb-82m		6.87(63)E-28		
Rb-83	2.95(35)E-27	1.47(30)E-27		
Sr-85	1.45(12)E-27			
Kr-85m	2.09(8)E-27	3.92(61)E-27	3.01(28)E-27	1.30(9)E-27
Y-85m		6.1(19)E-28		
Rb-86		1.12(37)E-27		
Y-86		4.08(42)E-28		
Zr-86	4.80(28)E-28	4.48(44)E-28	2.42(16)E-28	
Kr-87			3.08(32)E-27	1.29(12)E-27
Y-87			4.66(89)E-28	
Y-87m	1.22(9)E-27	1.07(5)E-27	5.43(63)E-28	2.55(20)E-28
Sr-87m		1.28(38)E-28		
Kr-88	2.64(57)E-27	4.60(18)E-27	3.04(29)E-27	1.67(17)E-27
Y-88		1.45(18)E-27		
Nb-89m		4.22(88)E-28		
Nb-90	4.02(34)E-28	1.12(3)E-27		
Y-90m	1.06(10)E-27		6.44(65)E-28	2.46(17)E-28
Y-91m		1.29(5)E-26		
Sr-91	2.96(17)E-27	5.90(27)E-27	4.42(17)E-27	2.06(11)E-27
Sr-92	2.86(18)E-27	5.17(16)E-27	3.61(21)E-27	1.80(13)E-27
Y-92	4.66(38)E-27	9.66(70)E-27	6.45(61)E-27	3.21(82)E-27
Y-93	4.95(66)E-27	5.76(40)E-27	5.41(31)E-27	2.08(18)E-27
Mo-93m	3.46(58)E-28	2.72(81)E-28		
Tc-94	3.51(46)E-28			
Tc-94m		1.28(19)E-27		
Ru-94		2.21(30)E-27		
Zr-95		7.47(61)E-27	4.90(32)E-27	
Nb-95		2.87(51)E-27		

Tc-95		5.1(13)E-28		
Ru-95		3.66(27)E-27		
Nb-96	7.96(96)E-28	1.39(14)E-27	8.37(55)E-28	3.96(40)E-28
Tc-96		5.7(10)E-28		
Zr-97	2.36(11)E-27	5.09(16)E-27	3.41(14)E-27	1.69(6)E-27
Nb-97		4.94(17)E-27		
Nb-98m		1.71(22)E-27		
Tc-99m		1.21(5)E-27		
Mo-99	3.48(37)E-27		4.31(30)E-27	2.04(12)E-27
Rh-99		2.83(15)E-27		
Rh-99m		4.5(11)E-28		
Rh-100	4.54(27)E-28	4.62(57)E-28		
Rh-101m	9.87(56)E-28	7.9(12)E-28		
Pd-101		1.40(16)E-27		
Ru-103	3.12(14)E-27	7.35(42)E-27	4.11(17)E-27	1.94(12)E-27
Ru-105	2.95(13)E-27	5.16(11)E-27	3.65(14)E-27	1.57(13)E-27
Rh-105	2.84(21)E-27	5.89(23)E-27	3.82(28)E-27	1.80(12)E-27
In-108		9.0(24)E-28		
Ag-110m		6.2(33)E-27	2.65(28)E-27	
In-110			1.70(16)E-27	
Pd-111m		1.42(6)E-27	9.2(15)E-28	
Ag-111		5.76(72)E-27		
Cd-111m		3.91(28)E-27		
In-111	8.3(12)E-28	6.23(22)E-28	2.67(22)E-28	1.48(43)E-28
Ag-112		6.3(19)E-27		
Ag-113		6.28(71)E-27	4.93(54)E-27	2.26(23)E-27
Sn-113		1.46(34)E-27		
Cd-115	1.55(7)E-27		2.44(16)E-27	1.17(7)E-27
In-115m		1.24(39)E-27		
In-116m		3.94(54)E-27		
Sb-116		6.76(86)E-28		
Sb-116m			1.20(15)E-27	
Te-116		2.15(21)E-27		
Cd-117		9.72(94)E-28	9.21(85)E-28	3.94(52)E-28

Cd-117m		1.56(11)E-27	1.23(15)E-27	
Sb-117	3.65(32)E-27	6.6(11)E-27	3.42(21)E-27	
Sn-117m	1.03(18)E-27			
Sb-118m	3.17(30)E-27	4.50(99)E-28	2.19(25)E-28	1.47(24)E-28
Te-119	4.42(61)E-28	3.00(24)E-28	2.11(20)E-28	
Te-119m		3.04(38)E-28		
Sb-120m		6.13(69)E-28	4.49(62)E-28	1.78(30)E-28
I-120m		2.26(72)E-27		
Te-121		7.04(90)E-28		
Te-121m		3.03(36)E-27		
I-121		7.44(67)E-28		
Sb-122	4.63(70)E-28	7.88(75)E-28	5.01(93)E-28	
Xe-122		2.40(25)E-27		
Te-123m		2.43(91)E-27		
I-123		2.80(28)E-27		
Xe-123		1.09(13)E-27		
Sb-124		1.71(32)E-27		8.7(22)E-28
I-124		7.8(20)E-28	3.99(40)E-28	
Xe-125	1.52(9)E-27	6.78(32)E-28	3.82(23)E-28	1.58(21)E-28
Sb-126		9.16(44)E-28		
I-126		2.17(22)E-27		
Sb-127		1.16(10)E-27		
Xe-127	9.52(91)E-28	1.16(6)E-27	8.2(16)E-28	
Cs-127		1.50(13)E-27	7.6(13)E-27	
Sb-128	3.27(61)E-28	5.65(53)E-28	5.22(55)E-28	3.03(36)E-28
Ba-128		6.3(30)E-28		
Cs-129	2.28(11)E-27			
Sb-129	4.64(65)E-27	1.15(7)E-27	6.95(69)E-28	
Ba-129		1.35(36)E-27		
I-130	2.60(29)E-28		5.16(95)E-28	2.67(28)E-28
I-131		2.56(22)E-27	2.23(17)E-27	9.92(60)E-28
Te-132	1.42(17)E-27	2.32(11)E-27	1.90(8)E-27	9.13(90)E-28
I-132	8.1(12)E-28	2.23(61)E-27	1.37(17)E-27	
Cs-132	1.75(12)E-28	2.85(45)E-27	2.46(14)E-27	1.43(23)E-27

La-132		6.39(99)E-28	4.10(58)E-28	1.19(38)E-28
Ce-132		5.76(44)E-28	2.95(56)E-28	
I-133	1.70(7)E-27	3.16(28)E-27	2.48(9)E-27	1.33(5)E-27
La-133		1.12(23)E-26		
I-134		1.02(15)E-26	6.2(10)E-27	3.96(25)E-27
I-135	1.84(17)E-27	3.39(14)E-27	2.24(10)E-27	1.17(9)E-27
Xe-135	2.29(45)E-27	3.77(43)E-27	3.29(69)E-27	1.64(35)E-27
Cs-135m		1.54(21)E-27		
La-135		8.8(19)E-27		
Ce-135	1.45(13)E-27	4.70(51)E-28	1.30(19)E-27	6.38(93)E-28
Cs-136		4.59(24)E-28		
Cs-138		6.6(10)E-27		
Pr-138m		2.77(69)E-28		
Ba-139				2.24(36)E-27
Ba-140	3.44(58)E-27	6.33(48)E-27	3.65(48)E-27	2.98(60)E-27
La-140	3.92(69)E-28	1.15(30)E-27	5.25(80)E-28	3.91(77)E-28
Ce-141		6.07(50)E-27	6.30(40)E-27	
La-142	2.26(21)E-27		2.92(23)E-27	1.19(11)E-28
Ce-143	2.10(9)E-27	3.50(6)E-27	3.07(11)E-27	1.57(7)E-27
Eu-145		6.7(16)E-28		
Eu-146		1.02(12)E-27		
Eu-147		3.41(48)E-27		
Gd-149	1.52(47)E-27	1.14(16)E-27		
Tb-152		6.61(50)E-28	2.76(48)E-28	
Dy-152	7.37(65)E-28	3.98(31)E-28	2.38(52)E-28	
Dy-155	8.90(44)E-28	6.66(22)E-28	3.60(37)E-28	1.43(24)E-28
Dy-157		8.35(23)E-28	4.61(35)E-28	1.86(27)E-28
Eu-157	9.3(33)E-28			
Er-161	1.44(17)E-27	1.11(7)E-27		3.28(62)E-28
Tm-167		1.08(21)E-27		
Tm-168		1.34(24)E-27	2.38(47)E-27	
Lu-170		2.52(42)E-27		
Hf-170	1.08(8)E-28	1.18(21)E-27	5.05(67)E-28	
Hf-173		1.09(8)E-27	6.60(66)E-28	2.68(44)E-28

Ta-173		2.89(29)E-27		
Ta-174		1.89(20)E-27		
Ta-175			4.43(34)E-27	
Yb-175		1.99(55)E-27		
Hf-175		1.39(36)E-27		
Ta-176	9.6(27)E-28	1.17(12)E-27		
Ta-178m	1.21(17)E-28	1.21(11)E-27		
Re-181		1.13(9)E-27		
Os-182		1.14(17)E-27	8.61(66)E-28	
Re-182	3.23(29)E-27			
Re-183		3.81(20)E-27		
Os-183m		5.35(43)E-28		
Ta-185		3.27(73)E-27		
Os-185		1.21(10)E-27		
Ir-186		1.58(19)E-27	9.8(12)E-28	
Ir-186m			1.50(18)E-27	
Pt-186			3.45(71)E-28	
W-187		1.95(70)E-27		
Ir-188		1.17(27)E-27		
Pt-188		1.07(52)E-27		
Pt-191		1.53(29)E-27	1.30(33)E-27	
Au-191		2.01(27)E-27		
Hg-191m		7.3(25)E-28		
Au-192	1.76(22)E-27		1.6(11)E-27	
Hg-192	7.93(70)E-28	6.98(47)E-28	5.77(76)E-28	2.28(31)E-28
Au-193		3.88(54)E-27		
Hg-193		1.50(42)E-27		
Hg-193m		2.73(39)E-28		
Tl-194m		1.27(33)E-27		
Ir-196m		5.83(89)E-28		
Au-196		5.9(19)E-28		
Tl-196	9.14(83)E-28	1.18(13)E-27	4.96(51)E-28	2.20(32)E-28
Tl-198	1.38(18)E-27	1.46(22)E-27		2.98(65)E-28
Tl-198m		8.6(26)E-28		

Pb-198		6.8(21)E-28		
Pb-199	2.87(64)E-27			
Tl-200	7.5(14)E-28		5.07(83)E-28	
Pb-200	5.15(65)E-28	6.92(46)E-28	3.72(34)E-28	1.74(41)E-28
Pb-201		8.22(33)E-28	4.74(33)E-28	2.11(22)E-28
Pb-202m		6.2(14)E-28	6.22(75)E-28	
Bi-202		1.07(19)E-27		
Po-202	4.50(57)E-27			
Hg-203		1.30(20)E-27		
Bi-203		6.02(79)E-28		
Po-204	4.21(31)E-27			
Bi-204	9.47(53)E-28	1.47(9)E-27	1.02(6)E-27	4.34(31)E-28
Bi-205		1.30(18)E-27		
Po-205		1.65(42)E-27		
Bi-206		8.8(12)E-28		
Po-207	9.8(15)E-28	1.55(14)E-27	8.8(15)E-28	2.88(60)E-28
At-208			5.2(12)E-28	
At-209	1.21(57)E-27	1.87(5)E-27	1.14(10)E-27	5.10(45)E-28
At-210		1.24(9)E-27	7.74(58)E-28	2.89(23)E-28
Rn-211	4.82(74)E-28	8.74(39)E-28		3.69(41)E-28
Bi-213		3.56(23)E-27		
Ac-224		2.99(38)E-27		8.78(69)E-28
Ac-226	1.82(21)E-27	3.31(7)E-27	2.57(29)E-27	1.01(6)E-27
Th-227		4.08(49)E-27		
Th-231	3.73(42)E-26	7.04(26)E-26	4.85(29)E-26	2.91(21)E-26
Pa-233	7.22(23)E-26	1.82(5)E-25	1.24(4)E-25	7.66(23)E-26

Appendix B.

Table B.1.

Values of the production reaction rates (atoms^{-1} · deuteron^{-1}) by secondary neutron on ^{232}Th at 2, 4, and 8 GeV deuteron energies. (*) denotes the presence of an admixture of another nuclide.

Isotope	I_γ	**2 GeV**		**4 GeV**		**8 GeV**	
γ-Energy [keV]	[%]	**$T_{1/2}$(Library)** $T_{1/2}$(Exper.)	**<R>** R	**$T_{1/2}$(Library)** $T_{1/2}$(Exper.)	**<R>** R	**$T_{1/2}$(Library)** $T_{1/2}$(Exper.)	**<R>** R
Ga-66				**9.49(7) h**		**9.49(7) h**	
1039.231	37			12.6(20) h	**2.97(69)E-29**	6(5) h	**1.16(26)E-28**
Kr-85m		**4.48(1) h**		**4.48(1) h**			
151.159	75		**2.19(31)E-29**				
304.870	14			3.2(11) h	**5.52(85)E-29**		
Kr-87		**76.3(6) m**		**76.3(6) m**		**76.3(6) m**	
402.586	49.6	1.08(12) h	**4.52(43)E-29**	1.29(19) h	**1.04(7)E-28**	1.7(7) h	**2.70(69)E-28**
Kr-88		**2.84(3) h**	**3.64(28)E-29**	**2.84(3) h**	**8.7(13)E-29**	**2.84(3) h**	
196.301	26	2.3(4) h	3.67(32)E-29				
1529.770	10.9			3.9(1) h	1.20(12)E-28		**3.6(13)E-28**
2195.842	13.2		3.91(76)E-29		7.3(10)E-29		
2392.110	34.6	2.5(22) h	3.11(82)E-29	2.11(22) h	8.11(92)E-29		
Y-88				**106.65(4) d**		**106.65(4) d**	
898.042	93.7						

1836.063	99.2				**3.30(40)E-28**		**1.22(20)E-27**
Y-91m		**49.71(4) m**		**49.71(4) m**		**49.71(4) m**	
555.570	95		**2.80(68)E-29**		**1.61(9)E-28**		**1.74(27)E-28**
Sr-91		**9.63(5) h**	**4.20(96)E-29**	**9.63(5) h**	**1.02(2)E-28**	**9.63(5) h**	**1.93(20)E-28**
652.900	8			14(10) h	1.18(11)E-28		
749.800	23.6	10.8(10) h	4.97(24)E-29	9.1(7) h	1.01(4)E-28		2.09(31)E-28
1024.300	33	8.8(15) h	3.00(30)E-29	9.9(4) h 7	1.01(3)E-28	9.1(16) h	1.83(26)E-28
Sr-92		**2.71(1) h**		**2.71(1) h**		**2.71(1) h**	
1383.930	90	2.62(10) h	**4.16(14)E-29**	2.68(11) h	**8.79(32)E-29**	2.74(27) h	**1.81(13)E-28**
Y-92				**3.54(1) h**	**1.58(14)E-28**	**3.54(1) h**	**5.0(12)E-28**
934.460	13.9				1.63(36)E-28		4.8(15)E-28
1405.280	4.8			5.1(12) h	1.42(14)E-28		5.3(18)E-28
Nb-92m				**10.15(2) d**		**10.15(2) d**	
934.460	99				**2.43(19)E-28**		**3.17(69)E-28**
Y-93		**10.18(8) h**					
266.900	7.3	9(3) h	**4.82(62)E-29**				
Zr-97		**16.91(5) h**		**16.91(5) h**		**16.91(5) h**	
743.360	93	14.7(8) h	**2.97(14)E-29**	15.7(6) h	**6.76(18)E-29**	17.2(24) h	**1.26(9)E-28**
Nb-97				**72.1(7) m**			
658.080	98				**6.89(46)E-29**		
Ru-105		**4.44(2) h**		**4.44(2) h**	**2.67(28)E-29**	**4.44(2) h**	
469.370	17.5				2.14(82)E-29		

724.210	47	9(6) h	**1.17(11)E-29**	5.7(26) h	2.74(30)E-29		**8.9(22)E-29**
Cd-115				**53.46(1) h**		**53.46(1) h**	
336.240	45.9						
527.900	27.5			1.7(5) d	**3.88(62)E-29**		**1.98(65)E-28**
In-115m		**4.87(1) h**					
336.240	45.8	4.4(20) h	**8.8(15)E-30**				
In-117		**43.2(3) m**	**2.49(30)E-29**	**43.2(3) m**		**43.2(3) m**	
158.562	87		2.30(49)E-29				
553.000	100		2.61(38)E-29		**7.26(95)E-29**	26.5(1) m	**1.04(27)E-28**
Sb-126				**12.46(3) d**	**6.51(69)E-29**	**12.46(3) d**	**5.11(90)E-28**
414.810	83.3						
666.331	100				5.4(15)E-29		5.9(10)E-28
695.030	100				6.82(78)E-29		4.1(12)E-28
Sn-127						**91.1(5) m**	
1114.300	39					2.08(1) h	**7.8(23)E-29**
Sb-128		**9.01(3) h**		**9.01(3) h**		**9.01(3) h**	**1.02(15)E-28**
314.120	61						0.66(34)E-28
526.570	45			4.5(22) h	**3.81(29)E-29**		1.10(31)E-28
743.220	100	14.7(8) h	**3.96(17)E-29**		7.62(81)E-29*		1.11(19)E-28
Sb-129				**4.40(1) h**			
812.800	43			6(4) h	**8.2(16)E-30**		
Te-132				**3.20(1) d**		**3.20(1) d**	

228.160	88				**4.64(94)E-29**		**1.46(38)E-28**
I-132				**2.29(1) h**	**1.95(63)E-29**		
667.718	99				1.63(93)E-29		
954.550	17.6				2.22(86)E-29		
I-133		**20.8(1) h**		**20.8(1) h**		**20.8(1) h**	
529.872	87	1.06(15) d	**2.05(13)E-29**	21.2(2) h	**6.52(20)E-29**	1.24(15) d	**1.28(9)E-28**
I-134		**52.5(2) m**		**52.5(2) m**	**2.04(12)E-28**	**52.5(2) m**	**3.17(33)E-28**
847.025	95.4	1.15(7) h	**7.95(97)E-29**	1.06(2) h	1.84(21)E-28	1.33(19) h	3.02(66)E-28
884.090	64.9			1.11(7) h	1.95(23)E-28		3.15(39)E-28
1072.550	14.9			1.12(2) h	2.32(25)E-28		4.1(16)E-28
1136.160	9.1				2.34(39)E-28		
I-135		**6.57(2) h**	**3.53(22)E-29**	**6.57(2) h**	**7.10(24)E-29**	**6.57(2) h**	**1.91(26)E-28**
1131.511	22.7	6.8(8) h	3.83(25)E-29	5.7(6) h	7.64(57)E-29	12.9(1) h	1.94(28)E-28
1260.409	28.9	7(5) h	3.38(18)E-29	6.7(4) h	6.95(28)E-29	7(2) h	1.68(73)E-28
1791.196	7.8			8.1(16) h	7.27(70)E-29		
Xe-135		**9.14(2) h**		**9.14(2) h**		**9.14(2) h**	
249.770	90	16.8(21) h	**3.23(60)E-29**	16.8(19) h	**7.8(12)E-29**	20(3) h	**1.95(34)E-28**
Cs-138				**33.4(2) m**		**33.4(2) m**	
1435.795	76.3				**1.45(15)E-28**		**2.25(48)E-28**
La-142		**91.1(5) m**		**91.1(5) m**	**8.50(89)E-29**	**91.1(5) m**	
641.285	47	1.86(19) h	**4.64(34)E-29**	1.9(5) h	9.4(14)E-29	2.08(1) h	**1.85(27)E-28**
894.900	8.3			3.46(2) h	8.8(17)E-29		

2397.800	13.3				7.3(15)E-29		
Ce-143		**1.38(2) d**		**1.38(2) d**		**1.38(2) d**	
293.266	42.8	1.68(3) d	**4.38(29)E-29**	1.50(18) d	**7.81(35)E-29**	3.1(7) d	**2.51(35)E-28**
Pa-233		**26.97(1) d**		**26.97(1) d**		**26.97(1) d**	
312.170	38.6	17.8(16) d	**9.12(55)E-27**		**1.78(3)E-26**		**4.30(20)E-26**

Table B.2.

Values of the reaction rates (atoms^{-1} · deuteron^{-1}) on ^{129}I (NaI) at 2, 4, and 8-GeV deuterons.

(*) denotes mixing due to other nuclide.

Isotope γ-Energy [keV]	I_γ [%]	**2 GeV**		**4 GeV**		**8 GeV**	
		$T_{1/2}$(Library) $T_{1/2}$(Exper.)	**<R>** R	**$T_{1/2}$(Library)** $T_{1/2}$(Exper.)	**<R>** R	**$T_{1/2}$(Library)** $T_{1/2}$(Exper.)	**<R>** R
Na-22[a)]		**2.60(1) y**		**2.60(1) y**		**2.60(1) y**	
1274.530	99.94		**5.6(34)E-29**		**1.01(23)E-28**		**2.79(20)E-28**
Na-22[b)]		**2.60(1) y**		**2.60(1) y**		**2.60(1) y**	
1274.530	99.94		**8.1(49)E-30**		**5.7(13)E-30**		**6.42(46)E-28**
Na-24[a)]		**14.96(1) h**	**7.22(43)E-29**	**14.96(1) h**	**9.60(79)E-29**	**14.96(1) h**	**1.85(14)E-28**
1368.633	100	15.02(3) h		15.6(4) h		15.0(4) h	
2754.028	99.94	15.05(3) h		15.6(5) h		14.9(5) h	
Na-24[b)]		**14.96(1) h**	**2.72(16)E-29**	**14.96(1) h**	**4.83(40)E-29**	**14.96(1) h**	**9.47(74)E-29**

1368.633	100	15.02(3) h		15.6(4) h		15.0(4) h	
2754.028	99.94	15.05(3) h		15.6(5) h		14.9(5) h	
Br-82		**35.30(2) h**	**6.21(9)E-29**	**35.30(2) h**	**6.93(12)E-28**	**35.30(2) h**	**1.22(5)E-27**
554.348	70.8	1.08(5) d*	8.33(91)E-29	1.45(5) d	7.44(21)E-28	1.25(5) d	1.29(11)E-27
619.106	43.4	1.42(3) d	5.92(15)E-29	1.58(6) d	6.57(24)E-28	1.33(5) d	1.14(7)E-27
698.374	28.5	1.44(4) d	6.15(17)E-29	1.68(7) d	6.88(34)E-28	1.74(20) d	1.54(9)E-27
776.517	83.5	1.45(2) d	6.17(11)E-29	1.56(6) d	6.60(24)E-28	1.39(4) d	1.21(5)E-27
827.828	24	1.45(5) d	6.41(19)E-29	1.53(7) d	6.76(27)E-28	1.41(2) d	1.07(9)E-27
1044.002	27.2	1.48(5) d	6.42(20)E-29	1.52(6) d	7.13(28)E-28	1.7(3) d	1.24(12)E-27
1317.473	26.5	1.54(5) d	6.51(20)E-29	1.61(7) d	7.05(30)E-28	1.32(11) d	1.24(9)E-27
1474.880	16.3	1.45(6) d	6.14(20)E-29	1.58(6) d	6.94(28)E-28	1.36(12) d	1.18(8)E-27
I-123		**13.27(8) h**		**13.27(8) h**			
158.970	83	12.3(6) h	**1.16(7)E-29**	10(3) h	**3.08(38)E-29**		
I-124		**4.18(2) d**	**2.46(25)E-29**	**4.18(2) d**		**4.18(2) d**	
602.729	63	3.9(7) d	2.34(15)E-29	5.9(13) d	**6.15(43)E-29**	5.0(17) d	**8.6(15)E-29**
1690.983	10.9	4.1(19) d	2.97(31)E-29				
I-126		**13.11(5) d**	**6.35(22)E-29**	**13.11(5) d**	**2.02(5)E-28**	**13.11(5) d**	**3.68(20)E-28**
388.633	34.1		6.58(20)E-29	27(12) d	2.06(7)E-28		3.85(22)E-28
666.331	33.1		6.14(25)E-29	26(12) d	1.98(7)E-28		3.46(24)E-28
753.819	4.2	17(7) d	5.42(66)E-29				
I-130		**12.36(3) h**	**5.58(6)E-27**	**12.36(3) h**	**1.17(2)E-26**	**12.36(3) h**	**2.02(3)E-26**
418.010	34.2	12.47(2) h	5.54(9)E-27	12.8(4) h	1.15(5)E-26	12.27(29) h	2.01(7)E-26

457.720	0.2	10.1(18) h	5.51(49)E-27				
536.090	99	12.44(2) h	5.48(7)E-27	12.8(4) h	1.14(5)E-26	12.2(4) h	1.99(7)E-26
539.100	1.4	12.49(17) h	5.68(12)E-27	12.43(27) h	1.24(3)E-26	13.2(9) h	2.16(13)E-26
553.900	0.7	1.08(5) d*	11.9(20)E-27*				
586.050	1.7	12.51(12) h	5.54(11)E-27	12.9(5) h	1.14(3)E-26	12.5(7) h	1.91(9)E-26
603.500	0.6	13.8(5) h	6.59(20)E-27	13.4(18) h	1.24(10)E-26	2.37(15) d*	2.35(24)E-26
668.540	96	12.45(2) h	5.48(8)E-27	12.9(4) h	1.14(4)E-26	12.3(5) h	1.98(7)E-26
685.990	1.1	12.53(16) h	5.26(12)E-27	13.1(5) h	1.07(4)E-26	12.9(18) h	2.09(14)E-26
739.480	82	12.42(2) h	5.50(8)E-27	12.9(4) h	1.17(4)E-26	12.1(4) h	1.99(7)E-26
800.230	0.1	11.6(19) h	5.31(54)E-27				
808.290	0.2	13.0(6) h	5.66(26)E-27	14.9(20) h	1.05(9)E-26		
877.350	0.2	11.5(10) h	6.02(44)E-27				
967.020	0.9	12.47(24) h	5.41(13)E-27	13.3(8) h	1.17(6)E-26		2.42(26)E-26
1096.480	0.5	1.5(5) d	5.50(16)E-27	13.7(11) h	1.28(8)E-26		2.52(38)E-26
1122.150	0.2	12.7(10) h	5.13(28)E-27	16.4(25) h	1.38(19)E-26		
1157.470	11.3	12.37(4) h	5.68(9)E-27	13.1(5) h	1.15(4)E-26	11.8(4) h	2.03(7)E-26
1222.560	0.2	12.5(8) h	6.67(32)E-27				
1272.120	0.7	12.65(24) h	5.90(13)E-27	13.6(7) h	1.26(6)E-26	10(4) h	2.50(32)E-26
1403.900	0.3	12.3(3) h	6.11(18)E-27	14.1(20) h	1.18(13)E-26		

Table B.3.

Values of the reaction rates (atoms^{-1} · deuteron^{-1}) on ^{127}I (NaI) at 2, 4, and 8-GeV deuterons.

(*) denotes mixing due to other nuclide.

Isotope	I_γ	**2 GeV**		**4 GeV**		**8 GeV**	
γ-Energy [keV]	[%]	**$T_{1/2}$(Library)** $T_{1/2}$(Exper.)	**<R>** R	**$T_{1/2}$(Library)** $T_{1/2}$(Exper.)	**<R>** R	**$T_{1/2}$(Library)** $T_{1/2}$(Exper.)	**<R>** R
Be-7		**53.12(7) d**		**53.12(7) d**		**53.12(7) d**	
477.595	10.5	38(15) d	**3.68(30)E-29**	25(12) d	**6.81(47)E-29**		**1.04(9)E-28**
Na-22		**2.60(1) y**		**2.60(1) y**		**2.60(1) y**	
1274.530	99.94		**5.58(51)E-29**		**1.01(24)E-28**		**2.79(75)E-28**
Na-24		**14.96(1) h**	**7.22(66)E-29**	**14.96(1) h**	**9.6(11)E-29**	**14.96(1) h**	**1.85(26)E-28**
1368.633	100	15.18(18) h	7.04(15)E-29	15.21(10) h	9.40(24)E-29	15.17(14) h	1.79(5)E-28
2754.028	99.94	15.31(21) h	9.65(58)E-29	14.86(10) h	1.39(9)E-28	14.76(19) h	2.93(19)E-28
Ag-108m						**418(21) y**	**4.40(85)E-30**
433.937	90						4.2(12)E-30
614.276	89.8						4.6(12)E-30
722.907	90.8						11.2(20)E-30*
In-111		**2.80(1) d**	**6.54(31)E-31**				
171.280	90	2.8(4) d	6.30(42)E-31				
245.395	94	2.5(4) d	6.86(48)E-31				

Sb-118m		**5.00(2) h**	**2.12(10)E-30**	**5.00(2) h**	**2.47(21)E-30**	**5.00(2) h**	**6.37(58)E-30**
253.678	99	5.09(25) h	1.99(8)E-30	5.1(4) h	2.26(15)E-30	5.0(4) h	5.77(32)E-30
1050.650	97	5.8(7) h	2.32(15)E-30	4.6(7) h	2.90(23)E-30	4.7(4) h	7.57(56)E-30
1229.680	100	5.1(4) h	2.25(12)E-30	8.3(14) h	2.88(38)E-30	6.2(8) h	7.30(69)E-30
Te-119		**16.03(5) h**		**16.03(5) h**		**16.03(5) h**	
644.010	84	19.0(6) h	**2.77(11)E-30**	16.9(7) h	**4.01(12)E-30**	15.5(6) h	**1.03(3)E-29**
Te-119m		**4.70(4) d**	**2.80(8)E-30**	**4.70(4) d**	**5.76(32)E-30**	**4.70(4) d**	**1.37(9)E-29**
153.590	66	4.9(4) d	2.83(9)E-30	4.1(6) d	5.73(49)E-30	3.92(23) d	1.32(6)E-29
1212.730	66	5.4(7) d	2.69(16)E-30		5.77(42)E-30	4.6(8) d	1.54(11)E-29
I-120				**81.0(6) m**		**81.0(6) m**	
560.440	73			1.32(2) h	**9.00(80)E-30**	1.40(14) h	**2.16(18)E-29**
Sb-120m		**5.76(2) d**	**2.13(10)E-30**	**5.76(2) d**	**3.13(36)E-30**	**5.76(2) d**	**8.82(42)E-30**
197.300	87	12.3(21) d	2.17(19)E-30	5.5(7) d	3.05(37)E-30	5.6(5) d	8.53(59)E-30
1023.100	99.4	9(4) d	2.11(20)E-30	1.6(10) d	3.9(12)E-30	5.4(5) d	9.03(63)E-30
1171.300	100	5.4(13) d	2.12(15)E-30			5.0(15) d	9.6(16)E-30
I-121		**2.12(1) h**		**2.12(1) h**		**2.12(1) h**	
212.189	84	2.14(9) h	**8.94(36)E-30**	2.05(10) h	**1.23(6)E-29**	1.99(9) h	**3.11(20)E-29**
Te-121m		**154(7) d**		**154(7) d**		**154(7) d**	
212.189	81		**6.2(13)E-30**		**8.9(16)E-30**		**2.08(35)E-29**
Te-121		**16.78(35) d**	**1.06(21)E-29**	**16.78(35) d**		**16.78(35) d**	**3.42(15)E-29**
507.591	17.7	23(8) d	2.02(18)E-29			13(5) d	5.80(47)E-29*
573.139	80.3	22.7(10) d	1.02(4)E-29	19.3(13) d	**1.60(8)E-29**	16.6(19) d	3.42(15)E-29

Sb-122		**2.72(1) d**		**2.72(1) d**		**2.72(1) d**	
564.119	71	2.64(23) d	**1.96(9)E-30**	2.4(3) d	**3.13(15)E-30**	2.89(22) d	**7.30(37)E-30**
I-123		**13.27(8) h**		**13.27(8) h**		**13.27(8) h**	
158.970	83	13.0(6) h	**3.95(16)E-29**	12.3(6) h	**5.22(28)E-29**	12.5(7) h	**1.18(7)E-28**
Te-123m		**119.7(1) d**		**119.7(1) d**		**119.7(1) d**	
158.970	84		**7.7(10)E-30**		**1.57(15)E-29**		**3.53(35)E-29**
I-124		**4.18(2) d**	**5.50(22)E-29**	**4.18(2) d**	**8.84(71)E-29**	**4.18(2) d**	**1.95(10)E-28**
602.729	63	4.18(15) d	5.23(13)E-29	4.13(5) d	8.59(25)E-29	3.96(9) d	1.87(4)E-28
722.786	10.3	4.14(22) d	5.67(18)E-29	17(7) d	1.61(11)E-28	5.1(11) d	3.20(34)E-28
1325.512	1.6	3.4(10) d	4.65(51)E-29	4.8(28) d	7.80(75)E-29	3.4(3) d	1.86(14)E-28
1509.470	3.1			5.5(7) d	1.03(16)E-28	4.5(5) d	3.03(31)E-28
1690.983	10.9	4.6(4) d	6.13(22)E-29	4.9(3) d	8.68(46)E-29	4.07(17) d	2.19(7)E-28
Xe-125		**16.9(2) h**	**7.64(47)E-31**	**16.9(2) h**	**1.45(10)E-30**	**16.9(2) h**	**2.71(23)E-30**
188.418	54	17.1(26) h	7.62(54)E-31	15.3(23) h	1.43(10)E-30	20(6) h	2.64(24)E-30
243.378	30	1.8(5) d	7.70(95)E-31		1.70(33)E-30		3.27(69)E-30
I-126		**13.11(5) d**	**2.10(7)E-28**	**13.11(5) d**	**3.50(9)E-28**	**13.11(5) d**	**7.17(20)E-28**
388.633	34.1	13.3(6) d	2.06(4)E-28	12.37(16) d	3.49(8)E-28	10.7(5) d	7.10(11)E-28
491.243	2.8	12.8(6) d	2.35(6)E-28	11.8(6) d	3.96(13)E-28	11.1(11) d	8.07(28)E-28
666.331	33.1	13.8(7) d	2.00(4)E-28	11.98(29) d	3.41(5)E-28	10.8(6) d	6.90(11)E-28
753.819	4.2	14.0(7) d	2.15(5)E-28	11.5(6) d	3.77(14)E-28	11.0(11) d	7.86(20)E-28
879.876	0.7	15(4) d	1.59(18)E-28	12.8(18) d	3.19(20)E-28	9.1(12) d	6.57(57)E-28
I-128		**24.99(2) m**		**24.99(2) m**		**24.99(2) m**	**3.77(29)E-26**

442.901	17	25.2(1) m	**1.09(6)E-26**	25.06(2) m	**2.04(12)E-26**	24.90(2) m	3.57(21)E-26
526.557	1.6					24.68(2) m	4.19(30)E-26